Ecological Research Series

MATHEMATICAL MODELING OF PHYTOPLANKTON IN LAKE ONTARIO

1. Model Development and Verification

MATHEMATICAL MODELING OF PHYTOPLANKTON IN LAKE ONTARIO

1. MODEL DEVELOPMENT AND VERIFICATION

By

Robert V. Thomann
Dominic M. Di Toro
Richard P. Winfield
Donald J. O'Connor
Manhattan College, Riverdale, New York

Project Officer

ABSTRACT

The basic mathematical structure for describing the dynamics of phytoplankton in Lake Ontario is presented in this report. Data on chlorophyll and principle nutrients are reviewed and summarized and the mathematical modeling strategy is detailed.

The modeling strategy begins with the construction of a horizontally completely mixed lake with vertical layers, Lake 1. This spatially simplified model is used to develop the interactions and kinetic behavior of the various components of each subsystem. A more detailed, three-dimensional model is then used to describe open lake and nearshore variations in phytoplankton biomass. Ten biological and chemical variables are used in both models and include four trophic levels above the phytoplankton, chlorophyll a as a measure of phytoplankton biomass, two phosphorus components and three nitrogen components. For Lake 1, using three vertical segments, a total of 30 simultaneous nonlinear differential equations must be solved while for the three-dimensional model, using 67 segments a total of 670 equations are solved. In both cases, the models are run for a period of one year or longer.

Under reasonable sets of model parameters as reported in the literature, the Lake 1 model output compared favorably with observed data on the dependent variables. Spring growth and peak chlorophyll concentrations are related primarily to increasing light and temperature. The model indicates that growth ceases due to phosphorus limitation. Zooplankton grazing and subsequent recycling of nutrients due to excretion and plankton endogenous respiration result in a late summer increase in phytoplankton biomass. Both nitrogen and phosphorus are then limiting resulting in a broad fall peak in phytoplankton biomass. A decline then results from low temperatures due to fall overturn.

The results, to date, indicate that the mathematical model of phytoplankton in Lake Ontario as developed herein is a reasonable first approximation to observed data. As such, the model can form a basis for preliminary estimates of the effects of nutrient reduction programs on Lake Ontario.

CONTENTS

LIST OF TABLES

LIST OF FIGURES

ACKNOWLEDGMENTS

CHAPTER 1

CONCLUSIONS

The dynamic behavior of lake-wide phytoplankton and associated nutrients can be adequately modeled with a simplified model. Such a model is horizontally well-mixed, but is vertically stratified and, therefore, represents an average open lake condition for Lake Ontario.

The phytoplankton modeling structure used in previous estuarine and delta applications is therefore also appropriate for describing phytoplankton biomass in lakes.

Analytical studies of the one-dimensional vertical phytoplankton biomass equation indicate that when the biomass is increasing, then asymptotically the log growth rate of the population will approach a value independent of depths. Data for four bodies of water including Lake Ontario support this theoretical prediction.

Detailed verification analyses using four years of data on Lake Ontario indicate that the spring growth phase and peak phytoplankton biomass are primarily controlled by increasing light and temperature and phosphorus limitation. The mid-summer minimum in phytoplankton is estimated to be due primarily to zooplankton grazing and nitrogen limitation. The broad fall peak in phytoplankton is a complex interaction of nutrient regeneration (up to five times the external nutrient inputs), subsequent nutrient limitation and then the fall overturn. Both nitrogen and phosphorus are important nutrients in this dynamic succession.

It is estimated that a period of 10-20 years may be necessary for the whole of Lake Ontario to reach a new level of dynamic equilibrium in phytoplankton biomass after a nutrient reduction program is instituted.

It is also concluded that a sufficient verification base for the lake-wide model has been established to permit the use of the model for preliminary simulations of the effects of various levels of nutrient reduction.

CHAPTER 2

RECOMMENDATIONS

Preliminary emphasis in this report is on the scientific foundation and validity of the model, principally the Lake 3 model. It is recommended that simulations and projections of the effects of nutrient reductions be carried out, first, in the Lake 1 model and then explored at a greater level of detail in the three-dimensional Lake 3 model. These projections should be long term and attempt to delineate the time required to reach a new dynamic equilibrium in Lake Ontario.

A detailed examination of the behavior of the Lake 3 model is warranted especially in view of the importance of nearshore versus open-lake problems. The three-dimensional nature of this model requires a significantly greater effort for verification purposes and for understanding the response of the Lake 3 model under different environmental conditions of flow and nearshore temperature and waste discharge.

Following the analysis of Lake 3 model responses, it is recommended that simulations be made of nutrient reduction programs. Such simulations should be carried out to determine the expected phytoplankton biomass and the time to reach that level for the different regions of Lake Ontario.

It is also recommended that the modeling structure of Lake 1 be expanded to include phytoplankton species dependence and a more flexible food web arrangement for the higher trophic levels. The primary data source would be the data collected as part of the International Field Year for the Great Lakes (IFYGL) effort.

CHAPTER 3

INTRODUCTION

3.1 PURPOSE OF RESEARCH

The overall purpose of this research is to structure a mathematical modeling framework of the major features of eutrophication in large lakes. Lake Ontario, the subject of intensive field work as part of the IFYGL is used as the problem setting (Figure 1). The overall objectives of the research include:

1. Determination of important interactions in lake eutrophication.

2. Analysis of lake water quality and biological responses to natural and man-made inputs.

3. Formation of a basis for estimating the direction of change to be expected under remedial environmental control actions.

The problems of impairment of the quality of lake systems are magnified for "large lakes" such as the Great Lakes. The size of these lakes is such as to preclude any immediate improvement in quality after control actions are taken. Further, it is much more difficult to obtain reliable data on water quality, biological structure and hydrodynamic circulation, again because of the difficulty of sampling large lake systems. The general circulation itself may not be adequately known in relation to climatological and hydrological factors. In the biological area, measures of phytoplankton populations are temporally and spatially dependent and reflect complex interactions with nutrients, such as nitrogen and phosphorus, and upper trophic level predation. This report reviews work accomplished to date on development of a mathematical model of phytoplankton in Lake Ontario that hopefully will form a reasonable basis for estimating the effects of nutrient removal programs.

3.2 SCOPE OF RESEARCH

The scope of this research is, therefore, lake-wide and attention is directed primarily to the behavior of the phytoplankton for the lakes as a whole. The smallest scale considered in the more advanced model (Lake 3) is on the order of 10-40 km. Detailed nearshore behavior on a scale less than this is not a part of this research. Furthermore, this research is concerned with phytoplankton dynamics as described on a time scale of weeks to months. Therefore, the seasonal progression of the phytoplankton throughout a year and from year-to-year is the time scale of interest. Short-term fluctuations, in the order of hours or days, are not described herein.

Finally, the modeling structure developed as part of this research is aimed at the phytoplankton biomass as a measure of eutrophication and associated water quality. Attached algae, such as *Cladophora*, are not modeled. Particular emphasis is placed on the interaction of the passive phytoplankton biomass (as characterized by the concentration of chlorophyll) with the nutrients, principally nitrogen and phosphorus and the grazing by herbivorous zooplankton and higher order trophic levels.
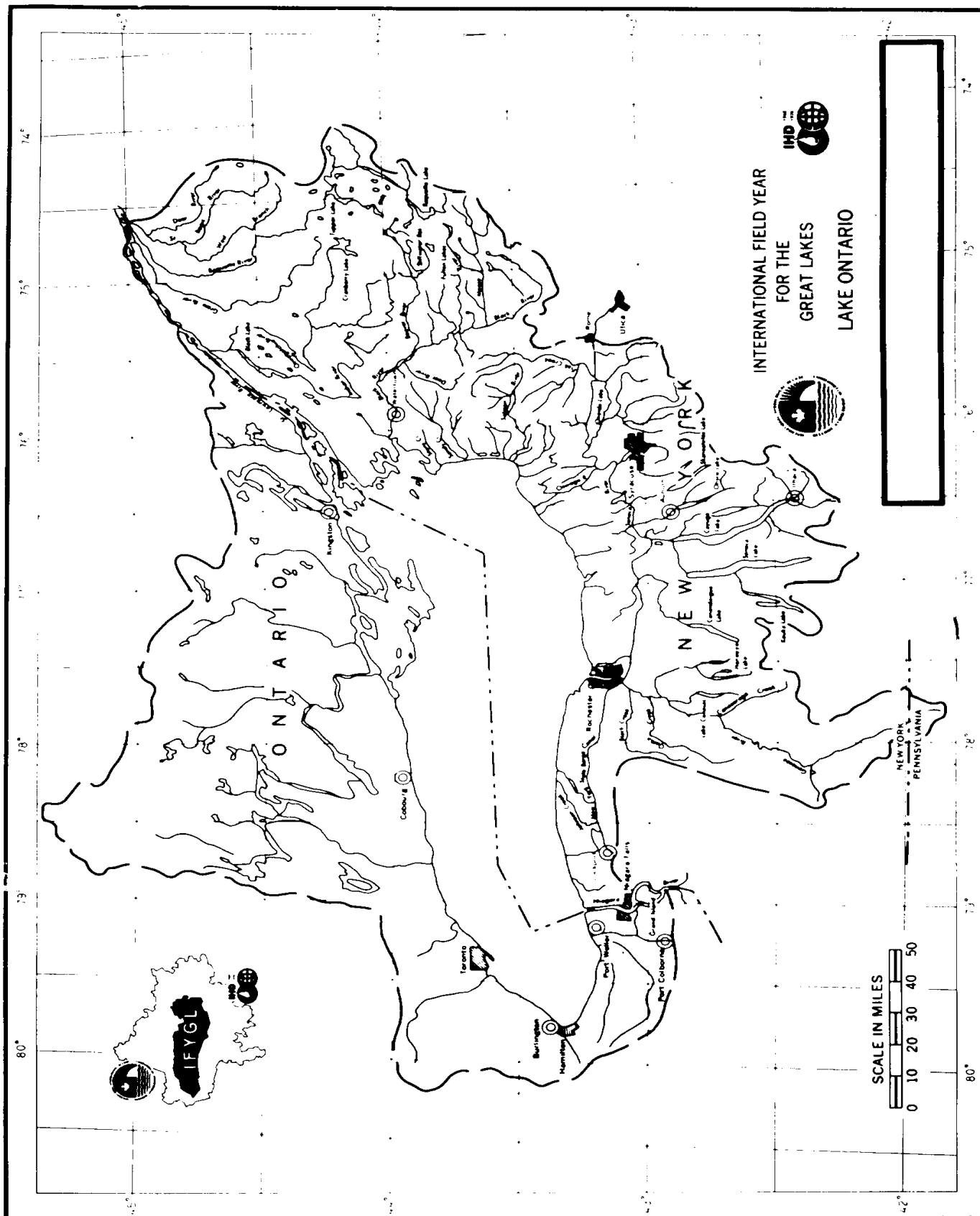
Figure 1. General basin map of Lake Ontario.

The primary thrust of the research is to provide a more rational and scientifically defensible structure for environmental decision-making on the efficacy of nutrient control and removal programs. As such, there are various levels of detail that could be explored. The goal is to include the "right" level of detail that explains the observed data, provides a basis for prediction, but is not too inordinately complex.

This report summarizes work performed to date on model development and strategy, data reduction and compilation, sensitivity analyses and verification analyses. Simulations of conditions under varying levels of nutrient reduction are not included in this report and will be part of a separate document.

CHAPTER 4

LAKE ONTARIO - BACKGROUND

With the Niagara River, the outflow of Lake Erie and, hence, the cumulation of all the upper Great Lakes outflow as its principle source of inflow and the St. Lawrence River its outflow, Lake Ontario is the last in the chain of Laurentian Great Lakes. Lake Ontario's narrow and deep rock basin was formed by the action of glacial corrosion (Hutchinson, 1957).

4.1 MORPHOMETRY

Lake Ontario is the smallest of the Great Lakes in terms of surface area, 19,477 km^2 (7,520 mi^2), with a drainage area of 90,132 km^2 (34,880 mi^2) (Beeton and Chandler, 1963). The mean depth of Lake Ontario, 90 meters (296 feet), is second only to Lake Superior for the Great Lakes and can be considered one of its most Important physical features (Beeton and Chandler, 1963; Canada Centre for Inland Waters, personal communication). Lake Ontario's volume is 1,669 km^3 (401 mi^3), with a maximum depth of 244 meters (801 feet) (Canada Centre for Inland Waters, 1974; Canadian Hydrographic Service, 1970). The lake's elevation above sea level is 74.01 meters (242.8 feet) (Canadian Hydrographic Service, 1970) which makes its depth of crypto-depression to be 170 meters (558 feet). Lake Ontario's length is 307 km (191 mi), with a maximum width of 87 km (54 mi) (Canadian Hydrographic Service, 1970). The lake's shoreline length is 1,380 km (858 mi) (Beeton and Chandler, 1963). The variation of volume and area with depth is illustrated in Appendix A (Figures A-1 and A-2).

4.2 HYDROLOGY

The Niagara River is the major source of inflow for Lake Ontario, being the cumulative outflow of the other Great Lakes. The average flow of the Niagara River is 195,000 cfs (International Joint Commission, 1969), and accounts for 84 percent of the flow discharged via the St. Lawrence River, as can be seen in Table 1. The average annual precipitation on Lake Ontario's water surface is 83.28 cm (32.79 in) and the average annual evaporation is 71 cm (28 in) (Great Lakes Basin Commission, 1971).

Table 1. Flow Budget

Source	Flow (cfs)	% of Discharge
Major Tributaries		
Niagara River	195,000	84.1
Twelve Mile Creek	6,400	2.8
Oswego River	6,200	2.7
Trent River Region	4,200	1.8
Black River	3,800	1.6
Genesse River	2,700	1.2
Welland Canal	1,200	0.5
Other Tributaries	5,900	2.5
Other Sources Precipitation - Evaporation and Other)	6,600	2.8
Discharge St. Lawrence River	232,000	

The thermal bar development which precedes the development of the full thermocline begins in late April or early May in Lake Ontario (International Joint Commission, 1969). The offshore movement of the thermal bar is such that within 17 to 28 days the nearshore ring of stratified water covers over half the area of the lake. The average depth of the thermocline is 17 meters (55.8 feet), with its dissipation beginning in late September (International Joint Commission, 1969). The hydraulic detention time of Lake Ontario (volume divided by flow) is 8.1 years, and is significant in that it gives some indication of the response time of the lake (see Chapter 6).

4.3 NUTRIENT INPUTS

Nitrogen and phosphorus are the nutrients used in the present configuration of the model, though silica will most likely be incorporated in the future. The only nutrient loading information available at the beginning of this project was for total nitrogen and phosphorus. Loading information for the individual forms of the nutrients (ammonia, orthophosphate, etc.) similar to those used in the model's nutrient systems, would be of great utility.

Nutrient loads for Lake Ontario are shown in Table 2. These reflect the total loads from the various sources (industrial, municipal and tributary) and were obtained by the International Joint Commission (IJC). These loads are broken down to individual waste discharges in the IJC's excellent 1969 three-volume publication (IJC, 1969). Table 2 indicates that the Niagara River accounts for over one-half of Lake Ontario's nutrient load. Table 3 gives the loading information as it was incorporated into the Lake 1 model. It can be noted that the loads are also shown as equivalent boundary concentrations, for an average inflow of 232,000 cfs. The inorganic form of the nutrients were set at the lake's winter concentrations with the remaining load inputted in the non-living organic form.

4.4 AVAILABLE LAKE DATA

The bulk of the data used for this investigation was obtained from three sources:

1. Limnological Data Reports, Lake Ontario, 1966-1969. Canada Centre for Inland Waters (CCIW) (CCIW, 1969).

2. STORET, U.S. Environmental Protection Agency (USEPA).

3. Report to the International Joint Commission on the Pollution of Lake Ontario and the International Section of the St. Lawrence River (IJC, 1969).

These sources were supplemented with other data available in the literature. The Limnological Data Reports (LDR) of CCIW comprise the largest single source of Lake Ontario survey data available. CCIW's cruises not only had adequate dense spatial grids (see Figure 2 for a typical grid) but also comprised good temporal coverage for the years surveyed (Table 4).

STORET, the USEPA's water quality storage and retrieval system is the prime residence of all United States collected water quality data. The pre-IFYGL STORET database consisted mainly of data from three 1965 synoptic cruises. The temporal coverage by these cruises was not sufficient to be of direct use for verification analysis. The data were, therefore, considered only as supplemental to the basic data set. STORET's utility is for storage and analysis of IFYGL data and as a database for tributary nutrient concentration data. It was, therefore, decided to use the data contained in the LDR as a verification database for the preliminary models and the STORET data as a verification database for the more advanced models.

Due to the magnitude of data in the LDR, a data reduction mechanism had to be implemented. The main criterion for the data reduction was compatibility with model output so as to facilitate comparison. Considerable effort was expanded on this task, with the principal product being

Table 2. Nutrient Loadings

Source	Nitrogen			Phosphorus		
	lbs/day	kg/day	%	lbs/day	kg/day	%
Niagara	522,200	236,900	59	42,200	19,100	56
Tributaries	191,000	86,600	22	15,600	7,100	21
Municipal	72,600	32,900	8	16,200	7,300	22
Industrial	97,300	44,100	11	1,000	500	1
Total	883,100	400,500		75,000	34,000	

Table 3. Nutrient Load Distribution

System	Nutrient Load		As Boundary Concentration
	lbs/day	kg/day	mg/l
<u>Nitrogen</u>			
Non-Living Organic N	551,400	250,100	0.443
Ammonia N	18,800	8,500	0.015
Nitrate N	312,900	141,900	0.250
<u>Phosphorus</u>			
Non-Living Organic P	57,100	25,900	0.457
Inorganic P	17,900	8,100	0.0143
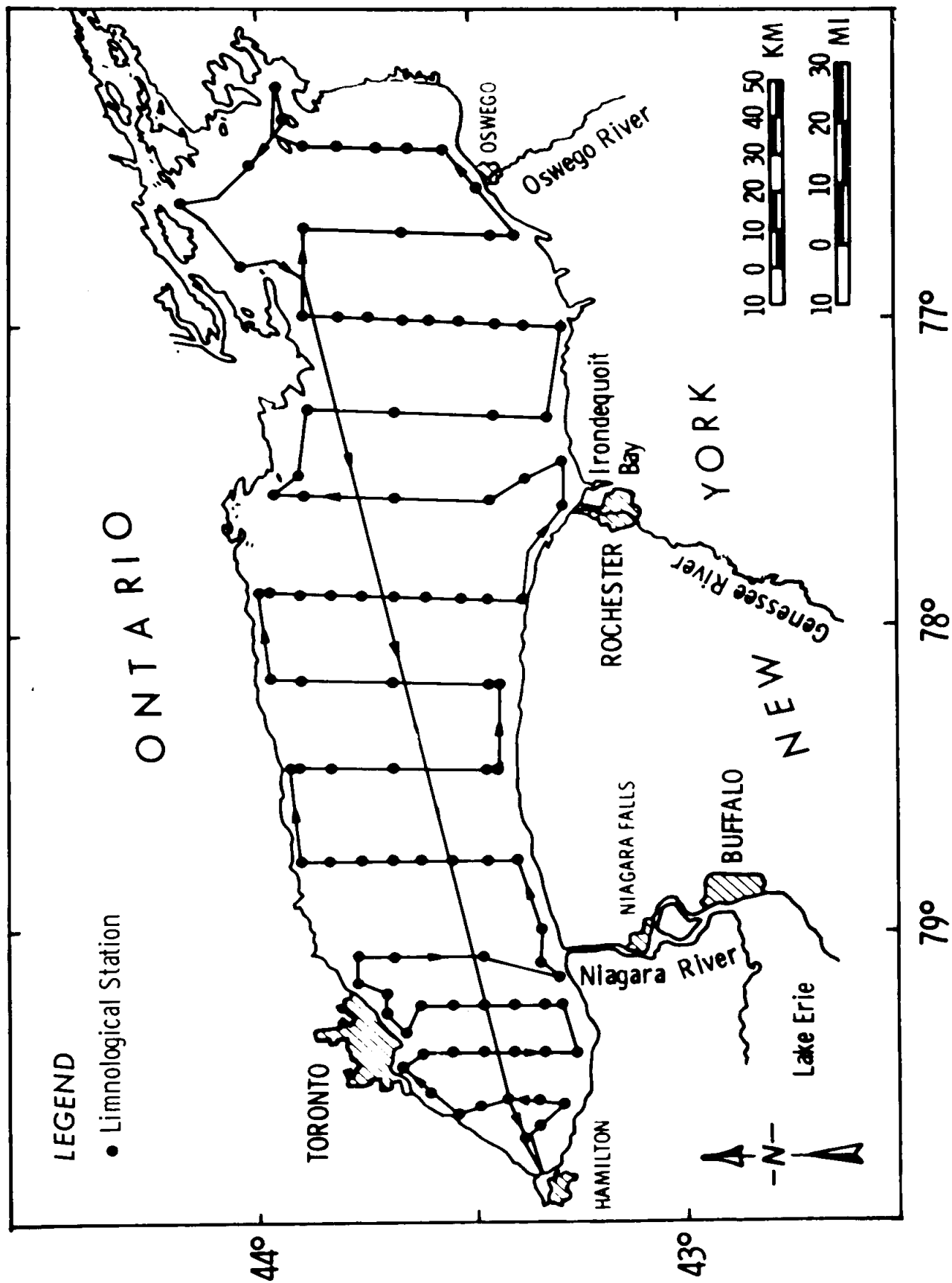
Figure 2. Typical CCIW cruise tracks, April 1969.

Table 4. CCIW Limnological Data Report Summary (Number of Cruises With Adequate Spatial Definition)

	1966 (June-Sept)	1967 (June-Nov)	1968 (April-Nov)	1969 (April-Dec)
Nitrogen:				
Organic or Kjeldahl-N	-	11	-	-
Ammonia Nitrogen	-	10	5	9
Nitrate Nitrogen	4	10	6	9
Phosphorus:				
Total Phosphate	-	4	5	8
Reactive Phosphate	5	10	6	9
Temperature	9	11	9	9
Chlorophyll *a*	-	11	6	9

main lake means and standard deviation for the relevant variables at individual sample depths. Main lake statistics were obtained, since this is what the Lake 1 and 2 models were designed to represent. Stations which had sounding depths of greater than 50 meters were considered main lake stations. Data were also reduced for depth intervals corresponding to segment depth for some years. Main lake, nearshore or entire lake reductions can be computed using the present software. Also, latitude-longitude blocks can be specified to give more refined spatial definition to the data retrievals. Therefore, Lake 3 comparison data is readily obtained with this option. Figure 3 is a sample output of the data reduction.

The Lake 1 model was designed to aid in the understanding of the principal mechanism which underlie the process of eutrophication. A key criterion in evaluating the validity of a model is to compare the model's output to the data observed in the field. Analysis of the field data of the water quality parameters under consideration revealed temporal patterns that were observed year-after-year. These patterns can be seen in the summary data plots used fo the evaluation of model output (see Chapter 6). Therefore, it is apparent that data accumulation and reduction are key steps in the modeling framework, for only when these are completed can the validity of the model be determined.
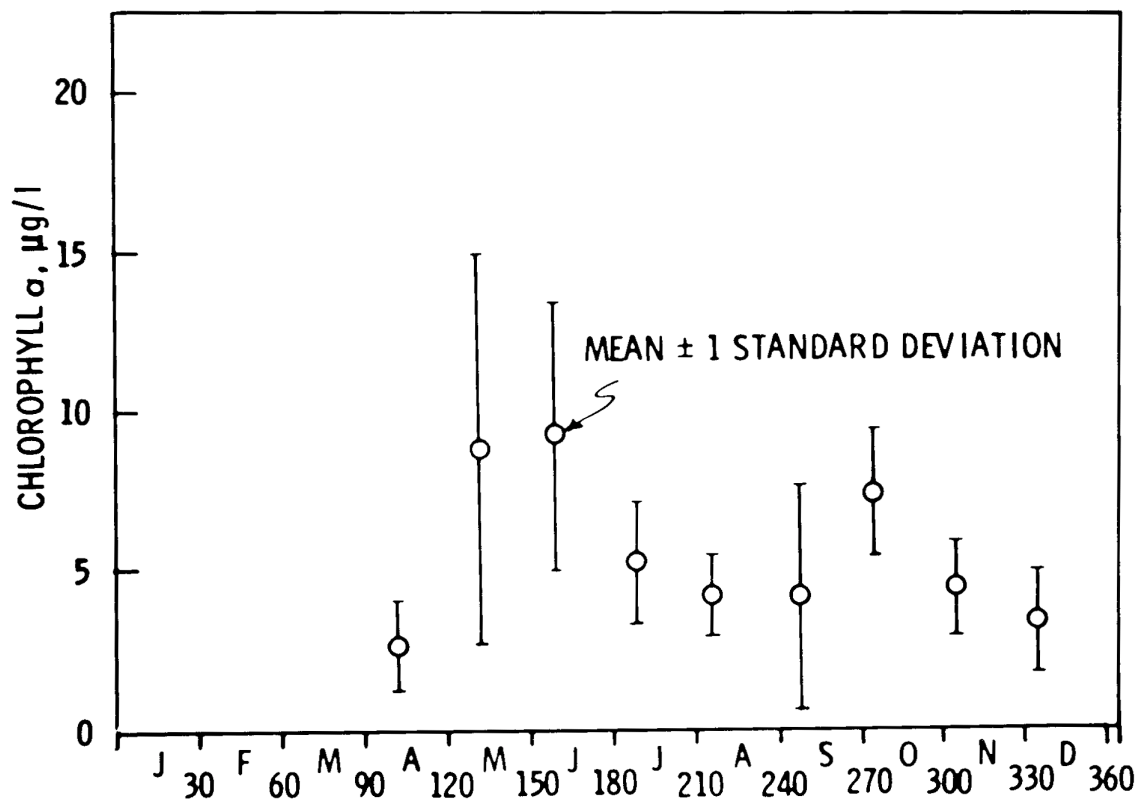
Figure 3. Typical output from data reduction - main lake average at 1 meter.

CHAPTER 5

LAKE ONTARIO - MODEL STRUCTURE

5.1 THEORETICAL BACKGROUND

The basic theory used for the Lake Ontario model makes use of previous model structures (Di Toro *et al.*, 1971; Hydroscience, Inc., 1973; Thomann *et al.*, 1974) and essentially represents a mass balance around each ecological or nutrient compartment and around physical space.

The basic structure consists of three parts:

1. Transport and dispersion sub-system,
2. Biological sub-system, and
3. Chemical sub-system.

The latter two sub-systems represent the kinetic behavior or the extent and complexity of interactions between relevant variables while the first system represents the physical processes of water movement and mixing. The theory of each of the sub-systems is presently developed to a different degree with the transport and dispersion theory developed to a more advanced degree than the biological and chemical systems.

The general equation which results from applying the principle of the conservation of mass is:

$$\frac{\partial s_k}{\partial t} = -\frac{\partial}{\partial x}(us_k) - \frac{\partial}{\partial y}(vs_k) - \frac{\partial}{\partial z}(ws_k)$$

$$+ \frac{\partial}{\partial x}(E_x \frac{\partial s_k}{\partial x}) + \frac{\partial}{\partial y}(E_y \frac{\partial s_k}{\partial y})$$

$$+ \frac{\partial}{\partial z}(E_z \frac{\partial s_k}{\partial z}) \pm S_k(x,y,z,t,s_l,s_k) \pm w_k(x,y,z,t);$$

$$
\begin{aligned}
k &= l...m \\
l &= l...m \\
k &\neq l
\end{aligned}
\tag{1}
$$

where s_k is the kth dependent variable (biological or chemical), u, v, w are the velocity components in the x, y and z directions, respectively, E_x. E_y and E_z are the dispersion coefficients in each respective spatial direction, S_k represents the kinetic interactions between the k variables and W is the direct inputs of the substance, s_k. It should be noted that Equation (1) as written, does not include any interaction between the variables s_k and the transport and dispersion regime. Thus, the physical system is separable, in the sense that it can be externally supplied and once determined, it can be used for all variables. In vector form Equation (1) is:

$$\frac{\partial s_k}{\partial t} = (V \cdot [E](Vs_k) - V \cdot \vec{U}s_k) \pm S_k \pm W_k \tag{2}$$

where [E] is a diagonal matrix of dispensing coefficients, (s_k) is a column vector, U is the velocity vector and

$$\nabla \equiv \frac{\partial}{\partial t}\vec{i} + \frac{\partial}{\partial y}\vec{j} + \frac{\partial}{\partial z}\vec{k}$$

In Equation (2), the first term in parenthesis on the right hand side represents the dispersive and advective field in three dimensions, as given by the general circulation. In this work, it is assumed that the circulation is "known", either through observation or from output from a hydrodynamic model. The inputted circulation can be validated by utilizing Equation (2) for a tracer such as dye or water temperature to compare computed results to observed data. Water temperature has been used in some of this work and the results of that analysis are given in Chapter 8. Primary interest, therefore, centers about the reaction kinetics, their function forms and numerical values.

A finite difference approximation to Equation (2) is necessary in order to apply the equation to an actual water body. Thus, if the lake is divided into a series of finite completely mixed volumes, n in number and each with volume V_j, then it can be shown that

$$[V]\frac{d(s)_k}{dt} = [A](s)_k \pm (S)_k \pm (W)_k \qquad (3)$$

where [V] is an n x n diagonal matrix of volumes, $(s)_k$ is an n x 1 vector of the variables s_k, [A] is an n x n matrix of advection and dispersion terms; $(S)_k$ is an n x 1 vector of kinetic interactions and $(W)_k$ is an n x 1 vector of inputs of variable s_k. For m interacting variables and n physical locations, Equation (3) indicates that a total of m x n equations must be solved. In general, the equations are both linear and nonlinear.

When one recognizes that initially up to 10-15 interacting variables can be specified and that 50-100 initial spatial segments may be required, it is obvious that the computer program and data preparation necessary to obtain solutions are of a substantial magnitude. Accordingly, prudent practice would dictate a modeling strategy that

allows one to proceed sequentially from simple models to the more complex. Such a strategy is utilized in this work and is illustrated in Figure 4.

As indicated, two parallel paths are being followed. The upper path involves the gathering of data on the lake geomorphology and transport and dispersion structure. The model used is a single variable model of water temperature or chloride both representing tracer variables that can be used to validate various sectors of the inputted circulation. A three-dimensional grid of 67 segments is employed.

The emphasis in the lower parallel path is on the sub-system kinetics with spatial detail held to a minimum. The lake is assumed to be horizontally completely mixed and is divided into a series of vertical layers. Attention is specifically directed to the interactions between phytoplankton, zooplankton, and water chemistry. Two models, Lake 1 and Lake 2 are explored in this path.

The synthesis of the spatial definition of transport and mixing with the kinetic interactions is accomplished in Lake 3. This model, a coarse grid model, is three-dimensional and incorporates the major kinetic features of the Lake 1 and 2 models. With 67 segments and ten variables, a total of 670 equations or "compartments" must be solved. Future expansion calls for an approximate order of magnitude increase in the number of compartments to 5000.

In this report, primary emphasis is placed on the Lake 1 model. As such, a detailed review of the kinetics employed in the models is given below for the biological and chemical sub-systems. The systems diagram for the Lake 1 model is shown in Figure 5. The Lake 2 model includes those variables for Lake 1 and also includes a representation of the carbon cycle.

13
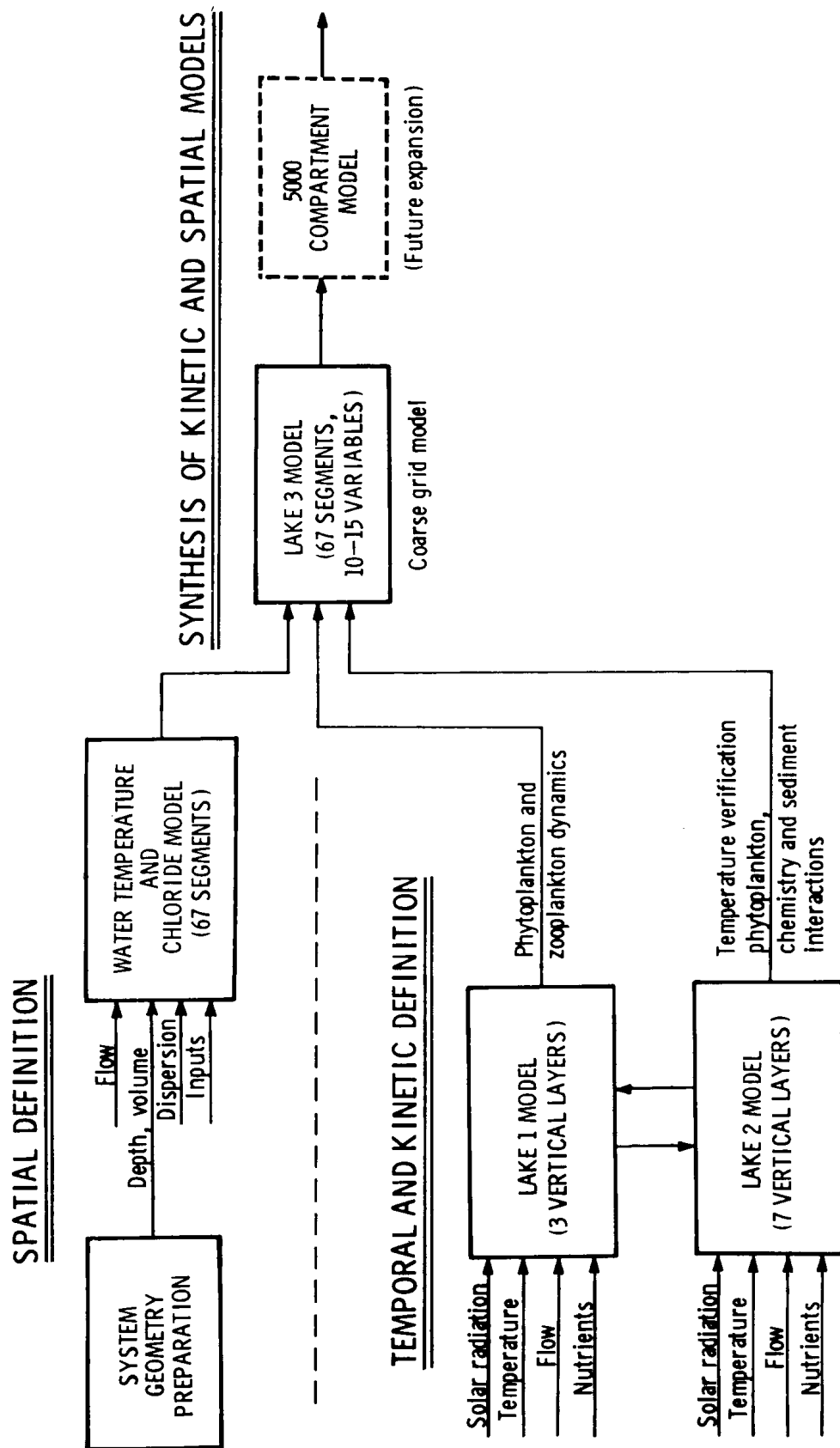
Figure 4. Eutrophication modeling strategy.
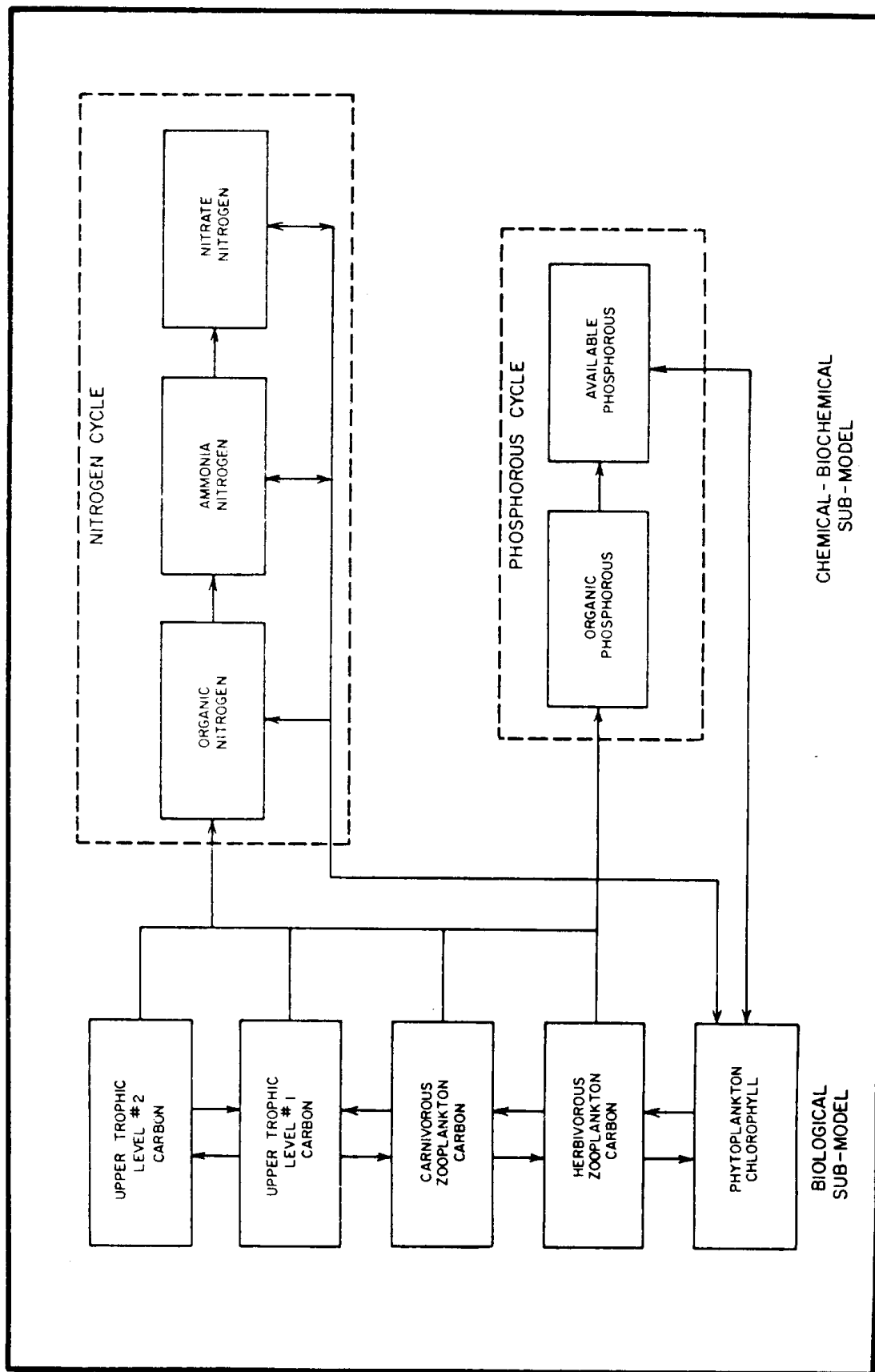
Figure 5. System diagram - Lake 1 model.

5.2 PHYTOPLANKTON CHLOROPHYLL

The basic kinetic interactions, for phytoplankton chlorophyll (a measure of biomass), is given for a single volume, j, as

$$S_{p_j} = V_j (G_p - D_p)_j P_j - V_j \frac{w_{ji}}{H_j} P_j + V_i \frac{w_{ij}}{H_i} P_i \qquad (4)$$

where P is the phytoplankton chlorophyll (µg/l), G_p and D_p are the growth and death rate (1/day), respectively, and w_{ji} and w_{ij} are the sinking velocities of the phytoplankton between segments j and i.

5.2.1 Phytoplankton Growth Rate

The growth rate expression is similar to that developed previously (Di Toro *et al.*, 1971) and as used in this work is given by

$$G_{pj} = G_1 (G_{max}, T) \cdot [I(I_a, I_s, k_e, P, H)]$$

$$\cdot ([N' K_{mn}, N_2, N_3)] [(K_{mp}, P_2)])$$

$$= \text{(temperature effect)} \bullet \text{(light effect)} \bullet$$
$$\text{(nutrient effect)} \qquad (5)$$

where G_{max} is the maximum growth rate, T is water temperature, I_s is light intensity at G_{max}, I_a is incoming solar radiation, k_e is the extinction coefficient, H is the depth of the segment, k_{mn} is the half-saturation constant for total inorganic nitrogen, N', N_2 is ammonia nitrogen, N_3 is nitrate nitrogen, K_{mp} is the half-saturation constant for phosphorus and p_2 is the available phosphorus. The temperature is given by Eppley (1972) as:

$$G_1 (T) G_{max} (1.066)^T \qquad (6)$$

where Eppley reports G_{max} at 0.587 (1/day). This form permits phytoplankton growth at low temperatures and at 20°C, results in a growth rate of 2.1/day.

The function form for the light effect is as given in previous work (Di Toro *et al.*, 1971) and incorporates vertical extinction of solar radiation and self-shading effects.

The form is

$$I = \frac{2.718f}{k_e H} (e^{-\alpha_1} - e^{-\alpha_0}) \qquad (7)$$

where $k_e = k'_e + 0.0088P + 0.054P^{0.66}$

$$\alpha_1 = \frac{I_a}{I_s} e^{-k_e H}$$

$$\alpha_0 = \frac{I_a}{I_s}$$

and k'_e is the light extinction coefficient at zero chlorophyll and f is the photoperiod. All pertinent variables are functions of j, the segment location.

The nutrient effect makes use of product Michaelis-Menten kinetics and is given by

$$N'_P = \frac{N_2 + N_3}{k_{mn} + (N_2 + N_3)} \cdot \frac{p_2}{k_{mp} + p_2} \qquad (8)$$

The range of values for k_{mn} and k_{mp}, the half-saturation constants for nitrogen and phosphorus, respectively, has been documented previously (Di Toro *et al.*, 1971). More recent work (Caperon and Meyer, 1972; Hendrey and Welch, 1973) tends to support the original range; namely k_{mn} in the range 5-50 µg N/l and k_{mp} in the range 1-10 µg/l. There is an obvious species dependence of this constant as well as a possible dependence on the eutrophic state of the lake. In the Lake 1 model, k_{mn} is used at 25 µg N/l and k_{mp} of 1 and 10 µg P/l is used as a range.

At the present time, silica limitation is not used in this model. Goering *et al.* (1973) and Paasche (1973) have estimated the half-saturation value for silica at about .02 - .08 mg Si/l for marine species. Under peak growing conditions in Lake Ontario, surface silica values are about 0.1-0.2 mg Si/l which tends to indicate that silica may not have a significant effect on the growth rate. Work is in progress, however, to include this nutrient since at the lower concentration and higher Michaelis levels, it could be important.

The complete growth rate expression, G_{pj} is then given by the product of Equations (6), (7), and (8). Although there is no *a priori* reason for using a product formulation, various experiments (see Equation (1)) have tended to support the approach. Another expression has been proposed on the grounds that Equation (5) is too severe in reducing growth due to the product term. The alternate construct is Equation (9):

$$G^`_p = G_1 \cdot \frac{3}{1/I + 1/N^` + 1/p} \tag{9}$$

or in general

$$G^`_p = G_i \cdot \frac{k}{\sum_i 1/\mu_i} \tag{10}$$

where k is a normalization factor and μ_i represent the general reduction factors. In general, from Equation (5) to Equation (10):

$$G^`_p > G_p$$

the extent of the inequality depending on μ_i. Undoubtedly then, Equation (5) will result in increased growth at least at some times; however, due to the coupling to the nutrient pool, such increased growth will in turn be more severe in its impact on the nutrients. Equation (10), therefore, appears to be less severe than Equation (5), but only with respect to phytoplankton growth. In the final analysis, the validity of any of these formulations rests on the ability to reproduce observed data, barring any real theoretical reasoning. This has been done at least for the product nutrient terms in early work by Ketchum (1934) (cited in Di Toro *et al.*, 1971) and more recently by Di Toro (1974a) for the flask experiments. The Lake 1 model was modified to test the sensitivity of the solutions to Equation (5) or Equation (10) and to determine which expression seems to be more appropriate. The results of the comparison are discussed more fully below.

It can also be noted that the cross growth rate of the phytoplankton biomass, $G_{pj} P_j$ is equivalent to the daily average productivity in the jth segment. Thus,

$$v_j = a_{cc} G_{pj} P_j H_j \tag{11}$$

where v_j is the average rate of carbon fixation (mg C m^2-day) and a_{cc} is the carbon to chlorophyll ratio (range 20-100 mg C/mg Chlor).

5.2.2 Phytoplankton Death Rate

The expression for the death rate of the phytoplankton includes two primary effects: endogenous respiration and predation by herbivorous zooplankton. The death rate is given by

$$D_{pj} = K_2 (1.08)^{T-20} + C_g z_j \tag{12}$$

where K_2 is a constant (1/day), C_g is the grazing rate of the herbivorous zooplankton (liters/day - mg zooplankton carbon) and z is the carbon concentration of the herbivorous zooplankton. As noted below for the zooplankton observed in Lake Ontario, a filtering rate of .03 - .06 liters mg C-day-°C appears appropriate and at 20°C, represents about 2-6 ml filtered per individual per day.

5.2.3 Phytoplankton Sinking

In Equation (4), the sinking of phytoplankton from one segment to another segment can be a potentially significant sink or source of phytoplankton and associated nutrients. This phenomena is a complex one incorporating vertical turbulence effects, the density structure and the physiological state of different species of phytoplankton. For example, the generation of gelatinous sheaths by phytoplankton has been shown to be of importance in settling (Hutchinson, 1967) and apparently the settling velocity of nutrient rich cells is somewhat less than cells that are nutritionally deficient (Yentsch, 1962). Published values of the sinking velocity of phytoplankton, mostly in quiescent laboratory conditions, range from 0.07-18 meters/day. In some instances the settling velocity is zero or negative.

Burns and Pashley (1974) have investigated the settling velocity profile of particulate organic carbon in Lake Ontario with an ingenious in situ measuring device. Their results show a general decrease in settling velocity with depth and a marked seasonal variation of settling velocity. For example, on July 19, 1972, the settling velocity in the thermocline (about 10 m) was estimated at about -0.3 m/day, while at 50 meters depth, the settling velocity was about +1.3 m/day. But in March 1973, the velocity profile was all positive ranging from 0.9 m/day at 20 meters to 0.1 m/day at 140 meters. Overall, the values given by Burns and Pashley (1974) varied between -0.4 and +2.0 m/day. These results and others tend to indicate that the settling velocity should be related in some ways to the state of the phytoplankton biomass (e.g., actively growing versus declining phase) and/or vertical velocity variations. In this work, however, the vertical settling velocity has been treated as a constant. As such, this effect is only approximately modeled and accordingly, the settling velocity has been treated as a constant over a range from .05 m/day to 0.5 m/day. The sensitivity of the results to the phytoplankton settling velocity is discussed below.

5.2.4 Zooplankton Carbon

The measure of the herbivorous zooplankton populations $z^{(1)}$ is taken as the carbon content of the biomass and all sources of food for $z^{(1)}$ are the phytoplankton chlorophyll. The general expression for a single volume j is therefore:

$$S_{z_j}^{(1)} = v_j (G_z^{(1)} - D_z^{(1)})_j z_j^{(1)} \tag{13}$$

where $G^{(1)}_z$ and $D^{(1)}_z$ are the growth and death rates respectively of $z^{(1)}_z$. The form of $G^{(1)}_z$ is

$$G_z^{(1)} = a_{zp} C_{gzp} K_g \frac{P}{K_g + P} \tag{14}$$

where a_{zp} is the zooplankton carbon to phytoplankton chlorophyll efficiency, C_{gzp} is the grazing rate of the herbivorous zooplankton and K_g is the half-saturation concentration of phytoplankton at which the growth of $z^{(1)}$ is half of maximum growth. This latter effect reflects the limiting growth of zooplankton at higher phytoplankton populations.

The mortality of the herbivorous zooplankton is given by two terms: endogenous respiration and grazing by the next highest trophic level.

Therefore,

$$D_z^{(1)} = K_z^{(1)}(T) + C_{g21}(T) z^{(2)} \tag{15}$$

where $K^{(1)}_z$ is the endogenous respiration rate as a function of temperature (1/day-°C), C_{g21} is the grazing rate (liters/day mg C-°C) and $z^{(2)}$ is the next highest trophic level, designated by superscript (2).

Expressions for all trophic levels above the herbivorous zooplankton arranged in a linear food chain are similar to Equations (13) and (14). Thus:

18

$$S_{z_j}^{(1)} = v_j (G_z^{(2)} - D_{z_j}^{(2)} z_j^{(2)}) \tag{16}$$

where $\qquad G_z^{(2)} = a_z C_{g21} z^{(1)}$

$$\tag{17}$$

and $\qquad D_z^{(2)} = K_z^{(2)}(T) + C_{g21}(T) z^{(3)}$

These expressions are an obvious oversimplification of a complex food web and reflect only a "linear" type of food chain (see Figure 5). Indeed the effect of the zooplankton on the phytoplankton as formulated above is to always decrease the population, yet it has been shown (Porter, 1973) that zooplankton can also increase phytoplankton population or have no effect. The mechanism for an increase in the population is apparently through the passage of gelatinous green algae through the zooplankton gut with subsequent breakup of the colonies and regrowth after excretion. The smaller species are generally decreased in numbers by zooplankton grazing, specifically smaller diatoms and *Asterionella formosa*, which are characteristics of Lake Ontario.

The zooplankton of Lake Ontario are dominated by the crustaceans specifically of the order Copepoda and Cladocera. Most hauls are made over 0-50 meter depth range. Principal copepod species given by Patalas (1969) are *Cyclops bicuspidatus* and *Tropocyclops prasinus* and of the cladocerans: *Daphnia retrocurva* and *Bosmina longirostris*. In Patalas' work in 1969, these four species accounted for 91% of the total zooplankton and averaged about 60/liter from June-October.

Others (Glooschenko *et al.*, 1972; McNaught and Buzzard, 1973; Watson and Carpenter, 1974) generally showed values in similar range, and in some cases, up to a maximum of almost 200/liter. For use in biomass computations, conversions must be made to equivalent carbon. Such conversion depends on age and

accompanying weight of the animal and can, therefore, vary over a wide range. Watson and Carpenter (1974) in their conversions used weights of species to arrive at total biomass and equivalently averaged about 2.8 µg dry weight/ind. The results using an average of 40% carbon by dry weight show peak values generally in August at lakewide averages of between 0.07-0.12 mg carbon/liter.

At the average dry weight of about 1-5 µg/ind grazing rates of about 0.8-2 ml/ind-day are appropriate (Di Toro *et al.*, 1971; Kibby, 1971). Indeed the rate for *Bosmina longirostris*, a dominant species in Lake Ontario has been given as 1-3 ml/ind-day (Hutchinson, 1967). Grazing rates expressed in liters per mg zooplankton carbon per day have been assumed to be linearly related to temperature and have been used in the range of .03-.06 (1/mg C-day-°C) corresponding to the reported grazing ranges at 20°C.

5.3 NITROGEN SYSTEM

The basic equations for the nitrogen sub-system follow previous work (Hydroscience, Inc., 1973; Thomann *et al.*, 1974) and include non-living organic nitrogen, N_1, ammonia nitrogen, N_2 and nitrate nitrogen, N_3. The equation for the source-sink term for organic nitrogen is:

$$S_{N_{i,j}} = \frac{a_1}{a_c} \Sigma D_z Z + \frac{a_1}{a_c} P_j$$

$$(1 - \frac{a_{zp} K_g}{K_g + P_j}) C_{gzp} z^1 \tag{18}$$

$$+ a_1 D_p P - K_1(T) N_1$$

where a_1 is nitrogen-to-chlorophyll ratio, and a_c is the carbon-to-chlorophyll ratio and K_1 is the overall decay of N_1.

The first and third terms represent organic nitrogen released through endogenous respiration by the zooplankton and

19

phytoplankton, respectively; and the second term represents the organic nitrogen of the grazed but unassimilated phytoplankton. The last term represents the decomposition, settling and other effects that contribute to the decay of organic nitrogen.

For ammonia,

$$S_{N_{2,j}} = K_{12}(T) N_2 - K_{22}(T) N_2 - a_1 \alpha G_P P \quad (19)$$

where K_{12} is the rate of production of ammonia from organic nitrogen, K_{22} is the rate of oxidation of ammonia to nitrate, and α is a preference factor given by

$$\alpha = \frac{N_2}{N_2 + N_3} \quad (20)$$

or is alternately set equal to one-half for an "indifferent" uptake of nitrogen. The last term represents the uptake of ammonia for phytoplankton growth. For nitrate,

$$S_{N_{3,j}} = K_{23} N_2 - a_1 (1 - \alpha) G_P P \quad (21)$$

where $K_{23} = K_{22}$, the production of nitrate by ammonia oxidation.

5.4 PHOSPHORUS SYSTEM

The equations for the phosphorus cycle used in the models are as previously developed (Hydroscience, Inc., 1973; Thomann *et al.*, 1974) and include non-living organic phosphorus and phosphorus available for phytoplankton growth. For organic phosphorus, the equation for the source and sink for p_1 is:

$$S_{p_{i,j}} = \frac{a_p}{a_c} \Sigma D_z Z + \frac{a_p}{a_c} P_j$$

$$(1 - \frac{a_{zp} K_g}{K_g + P_j}) C_g z^{(1)} - K_1 p_1 \quad (22)$$

where a_p is the phosphorus-to-chlorophyll ratio and K_1 represents a general decay of organic forms.

For the inorganic phosphorus, assumed as phosphorus available to the phytoplankton, the source-sink equation for p_2 is:

$$S_{p_{2,j}} = K_{12}(T) p_1 - a_p G_P p - K_{22}(T) P_2 \quad (23)$$

where K_{12} represents the rate of decomposition of organic phosphorus to forms available for phytoplankton utilization and K_{22} represents an overall loss of inorganic phosphorus.

5.5 CHEMICAL MODELS - DISSOLVED CARBON DIOXIDE

The inclusion of chemical reactions into models of Great Lakes water quality, by contrast to the biochemical and biological reactions considered above, poses a new set of problems by virtue of the rapid rates and the highly nonlinear forms of the governing reactions. Nevertheless, it appears that the problems can be handled nicely within the context of conservation of mass equations.

The investigation of purely chemical equilibrium models has been underway for quite some time. An altogether satisfactory presentation of these results is available (Stumm and Morgan, 1970). Application of certain models to the Great Lakes water chemistry has been undertaken by Kramer (1964, 1967) in a series of important papers. From this work, it is clear that the biological reactions affect the chemical systems primarily via the assimilation of dissolved carbon dioxide

20

during phytoplankton growth. From the point of view of the eutrophication problem, at issue are the purely chemical reactions which phosphorus undergoes; for example, precipitation or dissolution of phosphate minerals. These reactions may be of practical importance in terms of the overall dynamics of the phosphorus in the lakes. The other chemically active phytoplankton nutrient, silica, may also be affected by purely chemical reactions involving the alumino-silicate minerals. Thus, there are possible practical consequences of these purely chemical reactions so that their inclusion, at least on a preliminary basis, is warranted.

The presentation given below is based on the carbon dioxide - bicarbonate - carbonate equilibria primarily because of its importance as the major buffer system of the lakes, and because it can serve as a prototype for all other such reactions. In fact, the procedure is the same for the inclusion of all such reactions within the context of conservation of mass equations.

5.5.1 Equilibrium Analysis

The carbonate equilibria is treated in the conventional way (Stumm and Morgan, 1970; Trussell and Thomas, 1971). The major species considered are aqueous or dissolved $[CO_2]$ (the concentration of hydrated CO_2 being small, bicarbonate $[HCO_3^-]$, and carbonate $[CO_3^=]$ ions, together with the hydrogen $[H^+]$ and hydroxyl $[OH^-]$ ions. At first glance one is tempted to write mass balance equations for each of these species. However, this is complicated by the fact that they undergo reversible ionization reactions, e.g., $CO_2 + H_2O = H^+ + HCO_3^-$ which occur very rapidly relative to the time scales of mixing and gas transfer (Kern, 1960). In fact, it is clear that the individual species are each extremely reactive so that a direct mass balance formation results in equations which are nonlinear and numerically quite badly behaved.

The very fact that the ionization reactions are rapid leads to a much more tractable formulation in terms of quantities which are conservative relative to the ionization reactions. A formal mathematical discussion is given subsequently. However, it is easy to see the principle involved. Consider the total inorganic carbon concentrations.

$$C_T = [CO_2] + [HCO_3^-] + [CO_3^=] \qquad (24)$$

It is clear that any reversible ionization reaction will not affect the C_T of the system (we assume no carbonate precipitation are forming or dissolving). Thus, a mass balance equation for C_T can ignore the ionization reactions since they are neither sources nor sinks of C_T.

The electroneutrality requirement can be used to obtain a second conservative quantity. Let $\{M\}$ and $\{L\}$ be the concentration in equivalents of the metal ions and ligands, e.g., N_a^+, K^+, C_a^{++}, ..., and Cl^-, $SO_4^=$, ..., which are present and assumed not to react appreciably with the carbonate or hydrogen-hydroxide species. Then, it is clear that a charge balance equation:

$$\{M\} - \{L\} = [HCO_3^-] + 2[CO_3^=] + [OH^-] - [H^+] \qquad (25)$$

is unaffected by ionization reactions so that the quantity called alkalinity

$$[Alk] = \{M\} - \{L\} \qquad (26)$$

is also conservative in the sense that a mass balance equation for Alk need not consider ionization sources or sinks. It can be shown there are no other independent conservative quantities for this system, the other common conservative quantities (Stumm and Morgan, 1970) are linear combinations of C_T and A.

If C_T and Alk are known, the concentration of all the species being considered is easily obtained. In fact, using the equilibrium equations (Stumm and Morgan, 1970; Trussell and Thomas, 1971)

$$[H^+][OH^-] = K_W$$

$$[H^+][HCO_3^-] = K_1[CO_2] \qquad (27)$$

$$[H^+][CO_3^=] = K_2[HCO_3^-]$$

it is true that (Trussell and Thomas, 1971)

$$Alk = \alpha(H)\,C_T + \gamma(H) \qquad (28)$$

where

$$\alpha(H) = \frac{1 + 2K_2/[H^+]}{1 + [H^+]/K_1 + K_2/[H^+]} \qquad (29)$$

and

$$\gamma(H) = K_W/[H^+] - [H^+] \qquad (30)$$

It does not seem to have been noticed that if the alkalinity concentration is large relative to γ (H) = [OH⁻] - [H⁺], which is the common situation then, Equation (28) becomes

$$\frac{Alk}{C_T} = \alpha(H) \qquad (31)$$

so that only the ratio of alkalinity to total inorganic carbon is important in determining the resulting pH whenever Alk = Alk + [H⁺] - [OH⁻]. Using tabulated values of K_1 and K_2 for pore water, Figure 6 illustrates the pH, Alk/C_T relationship as a function of temperature. These figures are most useful since they represent the carbonate equilibria completely as a function of the ratio of the critical conservation quantities. Taken together with the conventional log concentration plot of the species versus pH, they provide a complete picture of the behavior of the equilibria.

The equations which govern the distribution of Alk and C_T are available as mass balances, independent of the ionization reactions. For example, in a one-dimensional vertical model the equations would be

$$\frac{\partial [Alk]}{\partial t} - \frac{1}{A}\frac{\partial}{\partial z}\left(EA\frac{\partial [Alk]}{\partial z}\right) = S_{Alk} \qquad (32)$$

$$\frac{\partial [C_T]}{\partial t} - \frac{1}{A}\frac{\partial}{\partial z}\left(EA\frac{\partial [C_T]}{\partial t}\right) = S_{C_T} \qquad (33)$$

with a zero mass flux boundary condition at z = 0 for alkalinity and an air-water exchange condition for C_T:

$$- EA\frac{\partial [C_T]}{\partial z} = K_L\left(CO_2(g) - CO_2(aq)\right) \qquad (34)$$

representing the exchange of carbon dioxide. The difficulty in solving these equations is due to this nonlinear boundary condition since CO_2 (aq) is a nonlinear function of the dependent variables of the problem: [Alk] and [C_T], so that a numerical procedure is required.

The internal sources and sinks of alkalinity and inorganic carbon are due to biological reactions. For example, the nitrification reaction (if bacterial synthesis is ignored) can be represented as:

$$NH_4^+ + 1\,1/2\,O_2 \rightarrow NO_3 + H_2O + 2H^+ \qquad (35)$$
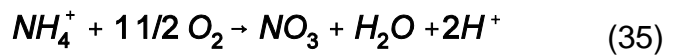
so that as ammonia is oxidized to nitrate, alkalinity is consumed (i.e., H⁺ is produced) and a term representing this sink of alkalinity would be included in the expression of S_{alk}.

Similarly as phytoplankton grow they utilize inorganic carbon and this sink would be included in S_{CT}. These mass balance equations would then be solved in conjunction with the equations for the other species of interest.
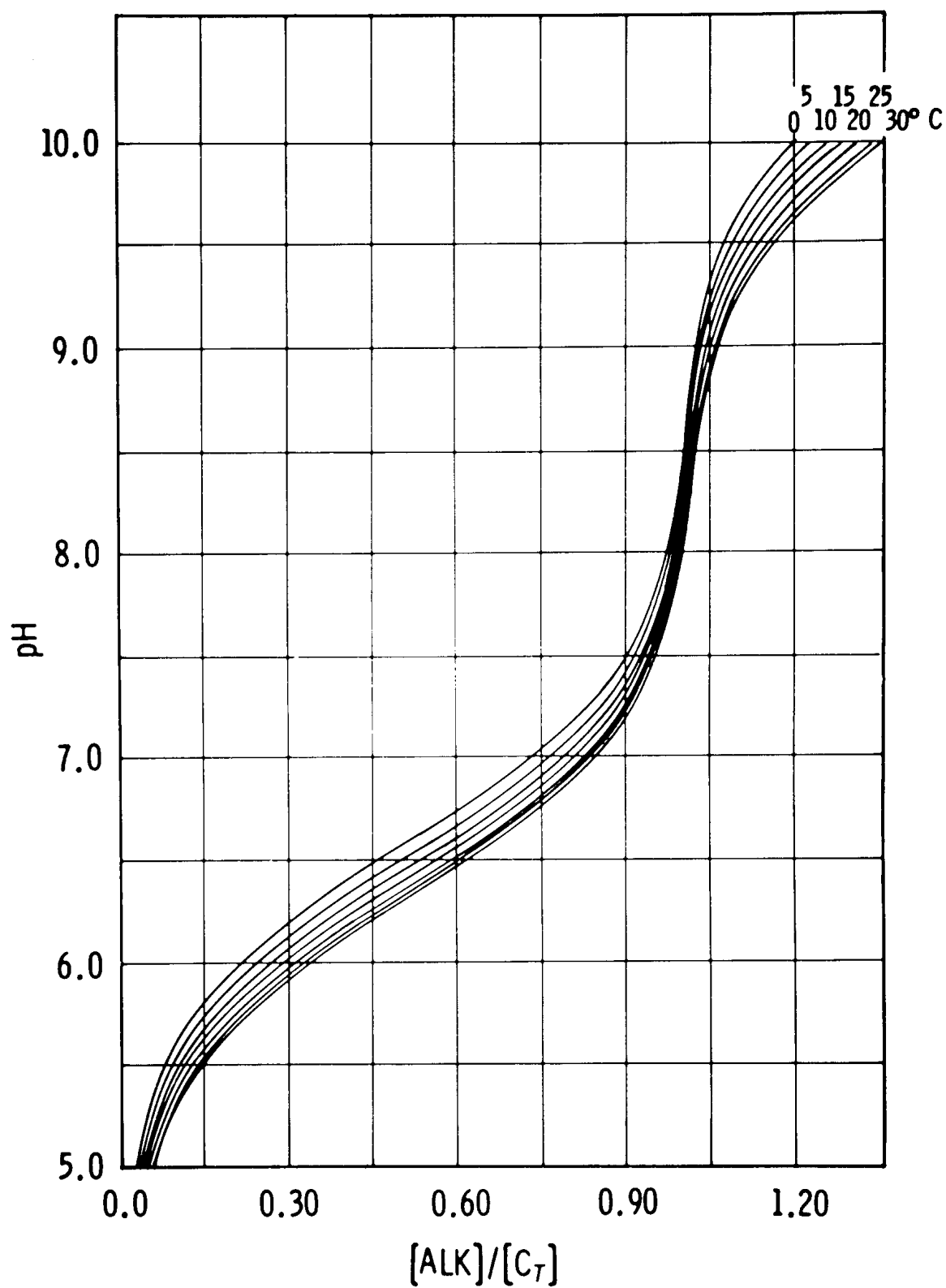
Figure 6. Relationship of pH and the ratio, Alk/C_T.

5.5.2 Linear Approximation

It is clear that mass balance equations which ignore the ionization reactions are only correct if the dependent variable is a conservative quantity relative to these reactions. Consider the conservative quantity $[C_T] - [Alk] = [CO_2 - Acidity]$. Clearly it is conservative since it is the difference of conservative quantities. From Equations (24), (25) and (26), it is the case that

$$[CO_2 - Acy] = [CO_2] + [H^+] - [CO_3^=] - [OH^-] \qquad (36)$$

But this equation implies that over a certain range of pH and C_T, the major component of CO_2-acidity is $[CO_2]$ itself. Figure 7 presents the % error in the approximation $[CO_2\text{-}Acy] = [CO_2]$. The chemical reasoning which leads to the same conclusion begins with the observation that in the above pH range, the alkalinity is primarily bicarbonate ion. If a source introduces only carbon dioxide, this does not change the alkalinity; therefore, the concentration of bicarbonate remains constant. Hence, the introduced CO_2 does not ionize to HCO_3^- and H^+ but rather remains as CO_2. Hence, ionization reactions can be ignored. Thus, from Equations (32) and (33) the mass balance equation for CO_2-acidity is

$$\frac{\partial [CO_2 - Acy]}{\partial t} - \frac{1}{A}\frac{\partial}{\partial z}\left(EA\,\frac{\partial [CO_2 - Acy]}{\partial z}\right)$$
$$= S_{C_T} - S_{Alk} \qquad (37)$$

and the reaeration source of $[CO_2\text{-}Acy]$ can be approximated as $K_L\,([CO_2]_{sat} - [CO_2\text{-}Acy])$ so that within the errors in Figure 7, the equation for $[CO_2$-acidity] is linear. Since the alkalinity equation is also linear, simple analytical solutions are available and superposition can be applied to buildup a solution when many sources and sinks are active. This is in contrast to the nonlinear C_T equation which must be solved with all source and sinks at once, a situation which is quite inconvenient.

Unfortunately, this linear region does not include the pH range typically encountered in the Great Lakes so that this simplification is not available. However, for more acid situations this simplification provides a useful and direct avenue for the solution of the inorganic carbon - alkalinity mass balance equation.

5.5.3 Temperature Dependence of the Equilibrium Constants

The equilibrium constants of the dissolved carbon system are rather strong functions of temperature so that this effect must be taken into account. The implementation of this dependency poses no serious problem since standard curves fitting techniques can be applied to the experimental data. However, such an approach backs a certain elegance and generality. It turns out, however, that for the temperature ranges encountered in natural waters there is an entirely satisfactory solution available based on the thermodynamic constants of the reactions.

It is well-known that the equilibrium constant, K, of a reversible reaction is related to the change in Gibbs free energy of the reaction at standard state, ΔG_r° via the equation:

$$\ln K = \frac{\Delta G_r^\circ}{RT} \qquad (38)$$

where

$$\Delta G_r^\circ = \sum_{products} \Delta G_f^\circ - \sum_{reactants} \Delta G_f^\circ$$

$\Delta G_f^\circ = $ *the Gibbs free energy of formation*

P $\quad=$ universal gas constant

T $\quad=$ temperature °K
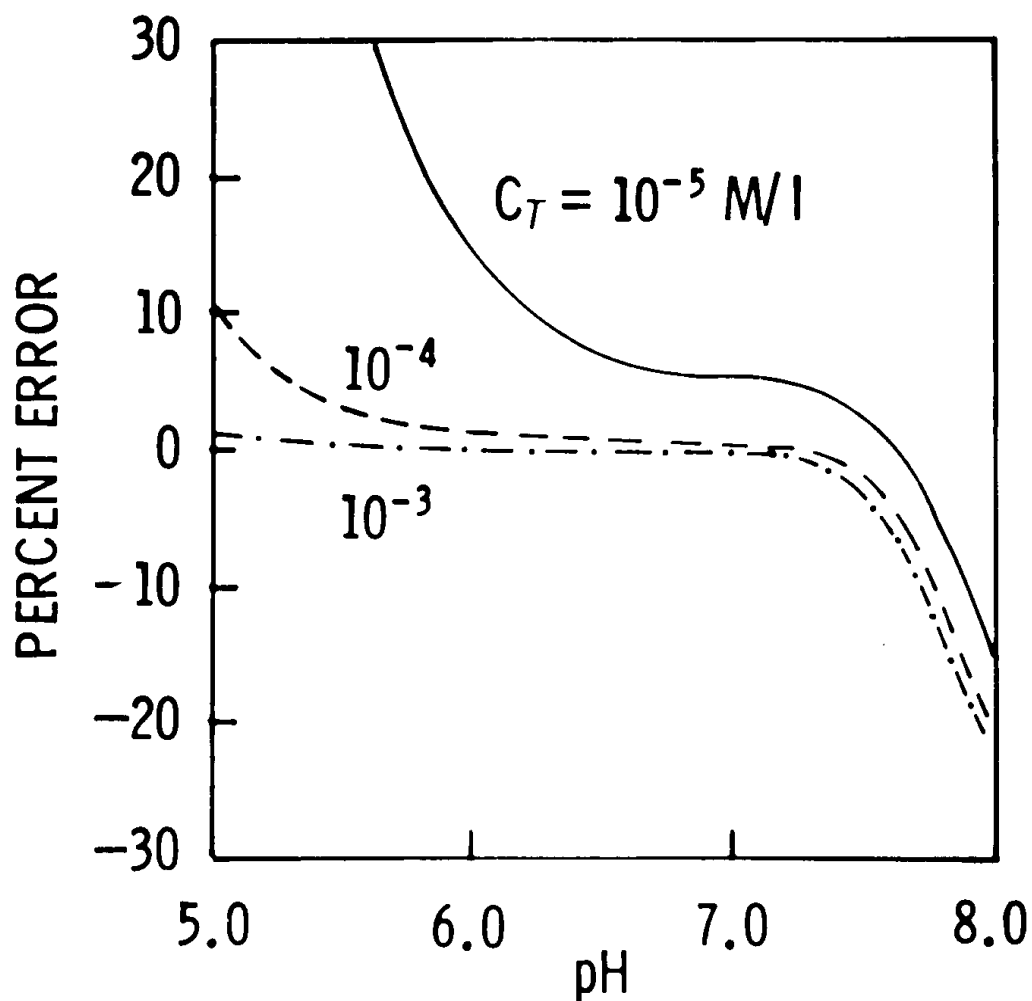
24

Figure 7. Percent error in assuming $[CO_2 - Acy] \simeq [CO_2]$.

and further that the free energy change is related to the change in enthalpy, $\Delta G_r^°$ and entropy, $\Delta S_r^°$ as follows:

$$\Delta G_r^° = \Delta H_r^° - T \Delta S_r^° \qquad (39)$$

Hence, the equilibrium constant is given by:

$$\ln K = -\frac{\Delta H_r^°}{RT} + \frac{\Delta S_r^°}{R} \qquad (40)$$

This equation is strictly true at any temperature; the difficulty is that $\Delta H_r^°$ and $\Delta S_r^°$ are also functions of temperature. The conventional temperature at which they are available is 298.15°K or 25°C. Table 5 presents the relevant thermodynamic properties for the carbonate system and Table 6 gives the properties for the reactions of interest.

Table 5. Thermodynamic Properties at 25°C

Compound	$\Delta HG_f^°$ (kcal/-mole)	$\Delta HG_f^°$ (kcal/-mole)	$\Delta HG_f^°$ (kcal/-mole)
$CO_2(g)$	-94.051	-94.254	51.06
$H_2CO_3(aq)^*$	-167.22	-148.94	44.8
HCO_3	-165.39	-140.26	21.8
$CO_3^=$	-161.84	-126.17	-13.6
H^+	0	0	0
H_2O	-68.315	-56.687	16.71
OH^-	-54.970	-37.594	-2.57

Source: Wagman *et al.* (1968).
*$H_2CO_3(aq) = H_2CO_3 + CO_2(aq)$;
[$H_2CO_3(aq)$] = [$CO_2/(aq)$].

Table 6. Thermodynamic Properties at 25°C

Reaction	$\Delta H_r^°$ (kcal/-mole)	$\Delta S_r^°$ (kcal/-mole)
1. $H_2O = H^+ + OH^-$	13.345	-19.28
2. $CO_2(g) + H_2O = H_2CO_3$	-4.854	-22.97
3. $H_2CO_3 = H^+ + HCO_3^-$	1.830	-23.0
4. $HCO_3 = H^+ + CO_3^=$	3.55	-35.4

Two approximations are investigated:

1. Assume that $\Delta H_r^°$ and $\Delta S_r^°$ are constants over the temperature range of interest (Stumm and Morgan, 1970).

2. Apply a correction which attempts to evaluate the change in the specific heat as a function of temperature (Helgeson, 1967).

The equation for the second approximation is:

$$\ln K = \frac{1}{RT}[-\Delta H_r^° + \tau(T)\Delta S_r^°] \qquad (41)$$

where

$$\tau(T) = T_r - \frac{\Theta}{w}[1 - e^{(T-T_r)/\Theta}] \qquad (42)$$

and T_r = 298.15 °K
Θ = 219.
w = 1.00322

These approximations are compared to the experimental equilibrium constants in Table 7. As can be seen the approximations are quite good with the nonlinear relationship giving somewhat better results at the lower temperatures. Thus, to within a few percent, these approximations are quite adequate.

Table 7. Temperature Dependence Comparison

Reaction = $HCO_3^- = H^+ + CO_3^=$
Enthalpy of Reaction = 3550.0000 cal/mole
Entropy of Reaction = 55.4000 cal/deg-mole

Temp °C	Experimental Pk	Method 1 Pk*	Percent Error	Method 2 Pk**	Percent Error
0.0	10.6250	10.5770	-.45	10.6181	-.07
5.0	10.5570	10.5260	-.29	10.5523	-.04
10.0	10.4900	10.4767	-.13	10.4917	.02
15.0	10.4300	10.4292	-.01	10.4360	.06
20.0	10.3770	10.3832	.06	10.3852	.08
25.0	10.3290	10.3389	.10	10.3389	.10
30.0	10.2900	10.2959	.06	10.2970	.07
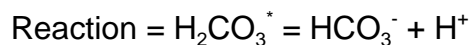
Reaction = $H_2CO_3^* = HCO_3^- + H^+$
Enthalpy of Reaction = 1830.0000 cal/mole
Entropy of Reaction = -23.0000 cal/deg-mole

Temp °C	Experimental Pk	Method 1 Pk*	Percent Error	Method 2 Pk**	Percent Error
0.0	6.5790	6.4908	-1.34	6.5175	-.93
5.0	6.5170	6.4645	-.81	6.4816	-.54
10.0	6.4640	6.4391	-.38	6.4489	-.25
15.0	6.4190	6.4146	-.07	6.4191	.00
20.0	6.3810	6.3909	.16	6.3922	.18
25.0	6.3520	6.3681	.25	6.3681	.25
30.0	6.3270	6.3459	.30	6.3466	.31
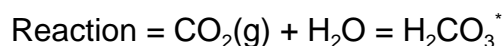
Reaction = $CO_2(g) + H_2O = H_2CO_3^*$
Enthalpy of Reaction = 4854.0000 cal/mole
Entropy of Reaction = 22.9700 cal/deg-mole

Temp °C	Experimental Pk	Method 1 Pk*	Percent Error	Method 2 Pk**	Percent Error
0.0	1.1100	1.1364	2.37	1.1630	4.78
5.0	1.1900	1.2062	1.36	1.2233	2.80
10.0	1.2700	1.2735	.28	1.2832	1.04
15.0	1.3200	1.3385	1.40	1.3430	1.74
20.0	1.4100	1.4013	-.62	1.4026	-.53
25.0	1.4700	1.4620	-.54	1.4620	-.54
30.0	1.5300	1.5207	-.61	1.5214	-.56

Table 7. Temperature Dependence Comparison (Continued)

Reaction = $H_2O = H^+ + OH^-$
Enthalpy of Reaction = 13345.0000 cal/mole
Entropy of Reaction = -19.2800 cal/deg-mole

Temp °C	Experimental Pk	Method 1 Pk*	Percent Error	Method 2 Pk**	Percent Error
0.0	14.9435	14.8911	-.35	14.9134	-.20
0.5	14.7338	14.6991	-.24	14.7135	-.14
10.0	14.5346	14.6140	-.14	14.5221	-.09
15.0	14.3463	14.3352	-.08	14.3390	-.05
20.0	14.1669	14.1626	-.03	14.1636	-.02
25.0	13.9965	13.9958	-.01	13.9958	-.01
30.0	13.8330	13.8344	.01	13.8350	.01

*Stumm and Morgan, 1970
**Helgeson, 1967

5.5.4 Equilibrium Models - Exploratory Calculations

In order to explore the computational feasibility of including chemical reactions in water quality models, a series of computations have been performed utilizing the Rand Chemical Composition Program (Shapley and Cutler, 1970). It is expected that this computer program will form the basis for the chemical submodel calculations to be included in Great Lakes water quality models.

The computations are for the system CO_2 - H_2O for which the partial pressure of CO_2(g) is fixed and varying amounts of acidity and alkalinity are added.   The results are computed for the temperature range 0° to 30°C using the linear approximation for the temperature dependence of ΔG_r° for the three reactions of interest. Figure 8a gives the total inorganic carbon that is in equilibrium with an atmosphere for which the partial pressure of CO_2(g) is 10-3.5 atmospheres. As alkalinity is added, the C_T increases and it is approximately true that $[C_T]$ = [Alk] with the pH in the range 7.5 to 8.5. The temperature effects change the pH of the

resulting solutions by approximately 0.25 pH units as shown in Figure 8b.

For varying partial pressures of CO_2(g) and Alk = 0, the results are shown in Figure 8c and 8d. A substantial temperature effect occurs with the C_T in solution varying by a factor of two over the range of interest, whereas the pH variation is smaller, due to its logarithmic units.

Computation time for the numerical solution of one set of conditions is on the order of 0.1 sec of CPU time on a CDC 6600. Thus, for daily evaluations of the chemistry for a year simulation for ten layers would consume on the order of 300 seconds, which is not excessive so that the computation is feasible.

5.5.5 Theoretical Considerations

A formal derivation of Equations (32) and (33) requires that ionization reactions be considered explicitly as sources and sinks of the components. Assume that the following three reactions are the mechanisms by which hydration and ionization take place:
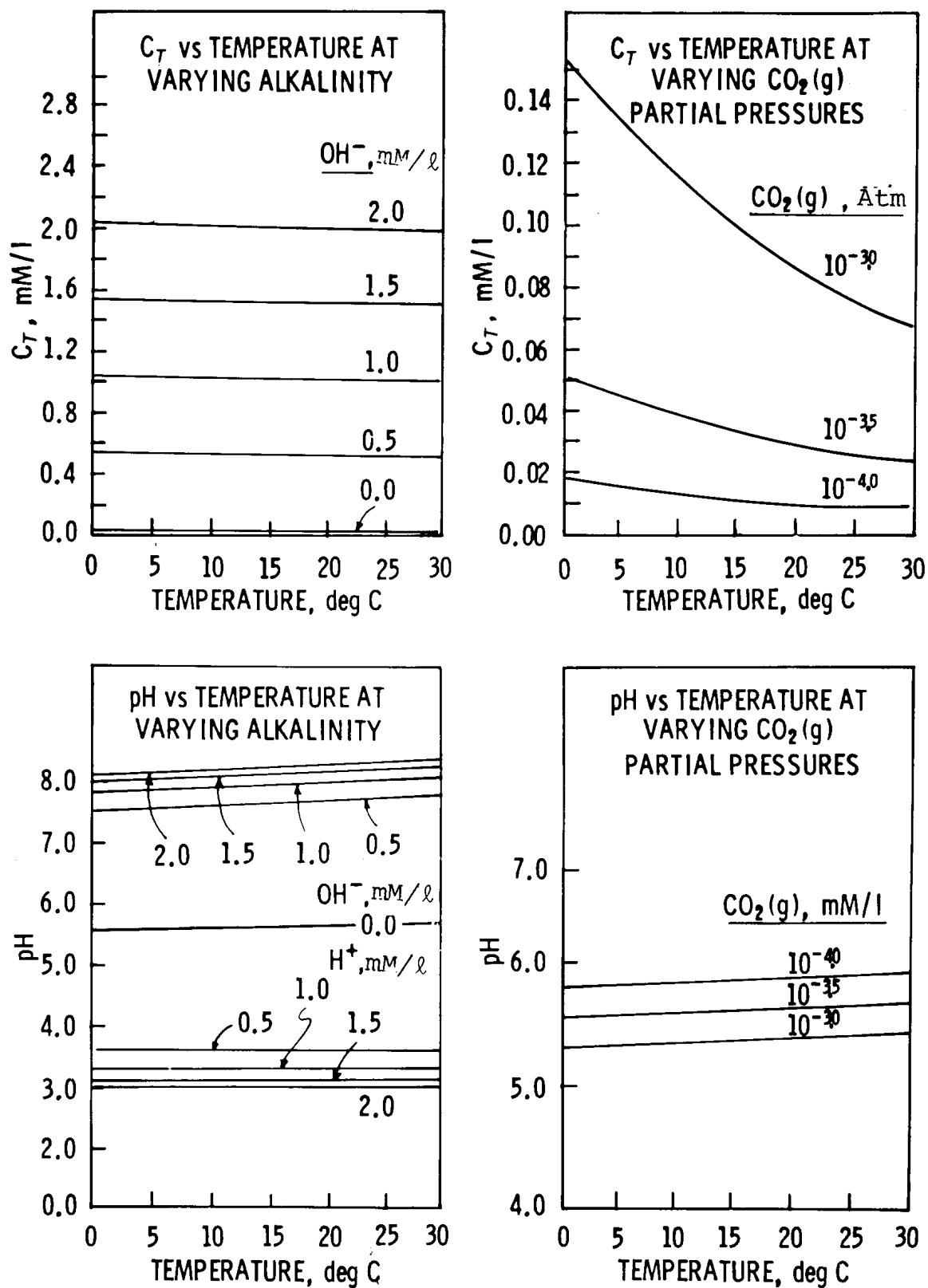
28

Figure 8. Computations for CO_2 - H_2O system.

$$CO_2 + H_2O = H^+ + HCO_3^- \; ;$$
$$r_1 = k_{v1}(K_1[CO_2] - [H^+][HCO_3^-])$$
$$HCO_3^- = H^+ + CO_3^= \; ; \tag{43}$$
$$r_2 = k_{v2}(K_2[HCO_3^-] - [H^+][CO_3^=])$$
$$H_2O = H^+ + OH^- \; ;$$
$$r_3 + k_{v3}(K_W - [H^+][OH^-])$$

and that the law of mass action correctly describes the rates of reaction as indicated. For notational convenience, let D denote the mass transport differential operator, i.e., the lefthand sides of Equations (32) and (33) are denoted by D[Alk] and D[C_T]. The conservation of mass equations for each species is obtained by equating mass transport to sources and sinks:

$$D[CO_2] = -r_1 + S_{CO_2} \tag{44}$$

$$D[H^+] = r_1 + r_2 + r_3 + S_H \tag{45}$$

$$D[HCO_3^-] = r_1 - r_2 + S_{HCO_3} \tag{46}$$

$$D[CO_3^=] = r_2 + S_{CO_3} \tag{47}$$

$$D[OH^-] = r_3 + S_{OH} \tag{48}$$

The S's are whatever direct sources of the species exist, and the r's are the rates associated with the assumed reactions. It is, of course, possible in principle to solve these simultaneous nonlinear differential equations numerically. The values chosen for the k_v's would be large enough so that the solution is unaffected by their magnitude. This procedure has been tried and found to be quite unstable numerically, the cause being the "stiffness" of the equations due to the large reaction rates which makes convergence difficult to achieve. Also the k_v's are, in a sense, artifacts of the

formulation since they are present only to introduce the ionizations correctly in a formulation that requires such reactions to be included as kinetic expressions. Therefore, it would be convenient to obtain equations which are devoid of the reaction rates entirely. This can be done by defining new variables which are appropriate sums of the species in such a way that the reaction terms cancel out. Thus if C_T = [CO_2] + [HCO_3^-] + [$CO_3^=$] then by adding Equations (44), (46), and (47) the result is:

$$DC_T = S_{CO_2} + S_{HCO_3} + S_{CO_3} \tag{49}$$

The other variable is, of course,

$$Alk = [HCO_3^-] + 2[CO_3^=]$$
$$+ [OH^-] - [H^+] \tag{50}$$

and since D is a linear operator,

$$D[Alk] = D[HCO_3^-] + 2D[CO_3^=]$$
$$+ D[OH] - D[H^+] \tag{51}$$

and using Equations (45), (46), (47), and (48) the result is Equation (32) as before, with the r's cancelling out in a satisfying way.

So far no approximations have been made; the equations for Alk and C_T are exact, regardless of the magnitude of the k_v's. They are the invariant of the reactions (Shapiro, 1962) in the sense that their values are unchanged by the kinetics. The approximation, and it is an excellent one for this application, is to compute the concentrations of the species from the equilibrium expressions, Equation (27), rather than the differential Equations (44-48).

There is a slight theoretical flaw in the above derivation since the explicit forms are assumed for the reactions considered and a reaction of the form.

$$CO_2 + OH^- = HCO_3^-$$
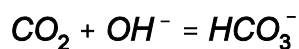
was not explicitly considered. It is a simple matter to verify that the inclusion of this reaction does not affect the validity of the resulting equations for Alk and C_T but no guarantee has been presented that such a reaction does not exist. This can be done (Shapiro, 1962) although it requires some results from linear vector space theory. The crux of the demonstration lies in showing that the subspace spanned by the reactions implied by the equilibrium equations is orthogonal to the subspace spanned by the invariant quantities, Alk and C_T, and that the dimension of the orthogonal subspace is two which implies that no other independent invariant quantities exist, and that the dimension of the reaction subspace is three, indicating that all the possible reactions have been taken into account for the five quantities of interest.

The theoretical framework and a theorem which indicates that the invariant quantities are always easy to find has been structured (Di Toro, 1974b). The results are essentially a generalization of the previous derivations.

CHAPTER 6

LAKE 1 MODEL

6.1 BASIC STRUCTURE AND EQUATIONS

Because of the complexity of the overall modeling structure, a simplified version of the lake has been developed to explore the kinetic behavior in greater detail. This is indicated in the modeling strategy of Figure 4. The simplified model, designated Lake 1, assumes that Lake Ontario is well mixed horizontally and gradients are allowed to develop only in the vertical dimension. Such a simplification obviously does not permit nearshore versus open-lake comparisons or the effect of the Rochester or Toronto discharges on the local lake environment. However, an inspection of the data on nutrients and chlorophyll does not appear to indicate substantial horizontal gradients, although variations do exist in certain areas. (Lake Ontario can be contrasted in this regard to Lake Huron which marked horizontal gradients from Saginaw Bay or Lake Erie with important horizontal gradients from the western basin to the eastern basin.)

Because of the complexity of the interactive systems, and most importantly, the computational time involved in obtaining solutions, the horizontally well-mixed assumption appears to offer a reasonable starting point for understanding the dynamic behavior of Lake Ontario. Figure 9 is a schematic of the Lake 1 model and shows the three vertical segments that comprise the basis geometry. The principal physical features included are: (a) horizontal transport, (b) vertical dispersion between the epilimnion and hypolimnion, and (c) vertical settling of the phytoplankton. The lake shown in Figure 9 has a defined epilimnion depth of 17 meters and a hypolimnetic depth of 73.3 meters. The Lake 1 model is well-mixed in the winter and spring, stratifies during the summer and then goes through a fall overturn. The effects are simulated by control of the vertical mixing. Table 8 presents the physical data of the Lake 1 model.

With the vertical segmentation as given in Figure 9 and Table 8 and using the general Equation (3), the equations for Lake 1 are:

Segment Number 1 - Epilimnion:

$$V_1 \frac{ds_{1k}}{dt} = (Qs_k)_{B1} - Q_{1E} s_{1k} \qquad (52)$$

$$+ [\frac{EA}{\Delta z}]_{12} (s_2 - s_1)_k \pm V_1 S_{1k}$$

Segment Number 2 - Hypolimnion:

$$V_2 \frac{ds_{2K}}{dt} = (Qs_k)_{B2} - Q_{2H} s_{zk} \qquad (53)$$

$$+ [\frac{EA}{\Delta z}]_{12} (s_1 - s_2)_k \pm V_2 S_{2k}$$

Segment Number 3 - Sediment:

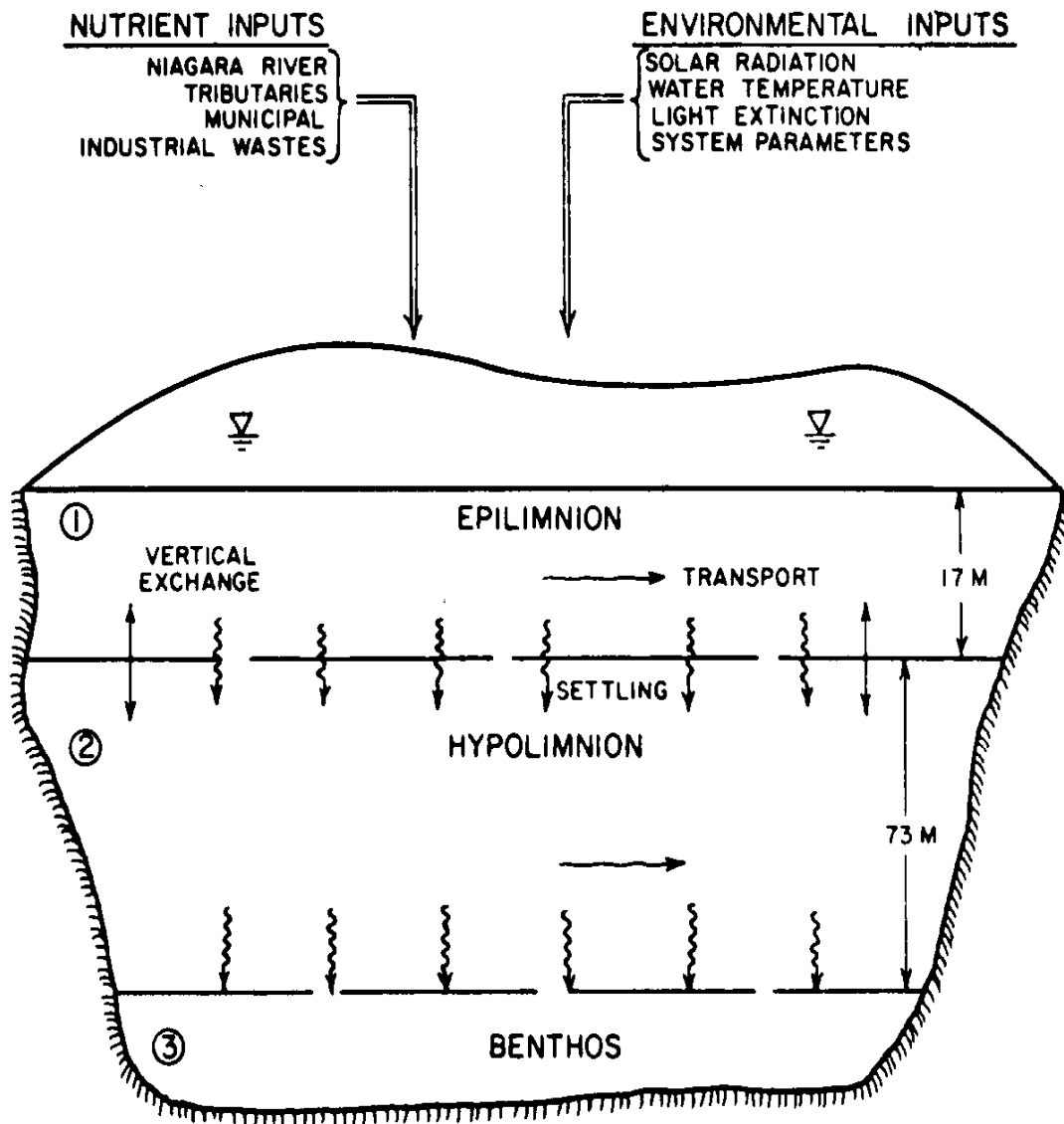$$V_3 \frac{ds_{3k}}{dt} = \pm V_3 S_{3k} \qquad (54)$$

Figure 9, Major physical features included in Lake 1 model.

Table 8. Basic Physical Data of the Lake 1 Model

Segment Number	Segment Interface	Volume (m³ x 10⁶)	%	Depth (m)	Surface Area (m²)	Flow cfs	m³/sec	%
1	1-2	297,000	19	17	1.6×10^{10}	43,500	1232	19
2	2-3	1,373,000	81	73.3	0.89×10^{10}	188,500	5323	81
3 (sediment)		-		0.15*				

Note: Vertical dispersion coefficient between segments number 1 and 2 varied from 0-90 cm²/sec (0-778 m²/day).

*Segment number 3 depth is arbitrary.

where $s_{k,B1}$ and $s_{k,B2}$ are the concentrations of the kth system inputted into the epilimnion and hypolimnion, respectively, Q_{B1} and Q_{B2} are the flows into segments 1 and 2, V_1 is the volume of segment i, E_{12} is the vertical turbulent exchange, A_{12} is the cross-sectional area between the epilimnion and hypolimnion and Δz is the average depth of the two segments. As shown in Figure 5, the Lake 1 model consists of ten systems (k = 1...10). The kinetics are as given previously in Chapter 5. A review of the Lake 1 computer program is given in Appendix A together with a listing of all system parameters, inputs and sample outputs.

6.2 MODEL CALIBRATION AND VERIFICATION

Several ways have been used to test the validity of the basic model structure as given in Lake 1. First, a series of runs were made to test the general behavior and sensitivity of the model. This is followed by inspection of the model output to determine the general order of magnitude of the response of each of the variables. The comparisons are made between the observed data and the computed output for data collected during years prior to the IFYGL. These comparisons are qualitative in the sense that an assessment of the degree to which the computed output agrees with observed data is left to the analyst. It should also be noted that

other checks can be used in the model verification; specifically, variables that can be constructed from the model output and compared subsequently to field measurements. The total verification then includes both the primary variables as given in the system diagram (Figure 5) and secondary variables constructed for the behavior of the model. The variables examined, therefore, for calibration and verification are:

1. Phytoplankton chlorophyll "a" - μg/l
2. Primary productivity - mg carbon/m²-day
3. Total zooplankton carbon - mg C/l
4. Bottom deposition rate - mg C/m²-year
5. Total phosphorus - mg/l
6. Available phosphorus (orthophosphate) - mg/l
7. Total Kjeldahl nitrogen - mg/l
8. Ammonia nitrogen - mg/l
9. Nitrate nitrogen - mg/l

The approach was to examine past data (principally from the years 1967-1971), run the Lake 1 model under different parameter settings consistent with reported values and compare to the observed data. The results of this sensitivity and calibration analysis are given below. It should be noted, however, that even with variable parameter settings (such as zooplankton grazing rates) the results are generally always consistent with the observed data. The results of the comparison to observed

data are presented after the results of the preliminary sensitivity and calibration runs.

6.2.1 Preliminary Runs and Sensitivity Analysis

A finite difference scheme is used to solve the equations using explicit time-space differencing. For the Lake 1 model, a time step of 0.5 days is used. For a one-year simulation, the central processing unit (CPU) time required for execution is about seven seconds on a CDC 6600 computer. Total CPU time required, however, is 30 seconds with additional overhead converted to equivalent CPU time being 115 seconds. The CPU time excluding overhead is equal to about 1.4 milliseconds per compartment step. A number of preliminary runs were made using the Lake 1 model structure to: (1) test program elements, (2) study the behavior of the system and its sensitivity to various system parameters and inputs, and (3) prepare a preliminary verification of the Lake 1 model using data collected prior to IFYGL. These early runs, therefore, represent a type of "tuning" of the model using past data as a basis for additional verification of the IFYGL data. The Lake 1 model has been used to examine several areas including, for example, variable levels of spring and fall vertical mixing, and settling velocities for phytoplankton in addition to zooplankton grazing rates, and effect of half-saturation constant for phosphorus. Some of the output from these areas is discussed below.

6.2.2 Variable Vertical Mixing

Vertical mixing plays an important role in the dynamics of phytoplankton population in lakes. Several paths were followed in order to obtain an estimate of the vertical dispersion in Lake Ontario. A survey of the literature on vertical mixing indicated that generally the vertical dispersion coefficient is several orders of magnitude lower than the horizontal coefficient. Oceanic vertical dispersion coefficients are in the range of 10-100 cm^2/sec and generally decrease with depth. Recently, during IFYGL, Murthy *et al.* (1974) estimated values from 0.1 cm^2/sec to

22 cm^2/sec depending on effects such as wind conditions and density stratification. In the Lake 1 model, the vertical dispersion was, therefore, treated as a parameter and sensitivity analyses made under an expected range from complete stratification (no mixing) throughout the year to variable mixing up to 90 cm^2/sec. More extensive analysis of vertical mixing was carried out in the Lake 2 and 3 models using temperature as a tracer variable. The details of these analyses are given in this chapter.

Figure 10 shows the effect of vertical dispersion on chlorophyll *a*. The runs include a sinking velocity of 0.05 m/day. A bimodel distribution of phytoplankton occurs in all cases due to the interaction of the two higher zooplankton levels used in these runs. As populations build up in the spring, the herbivorous zooplankton increase. This, together with nutrient depletion, decreases the phytoplankton population and at about the same time the carnivorous zooplankton prey on the next lowest trophic level. The phytoplankton can then increase again in the late summer.

As shown in Figure 10, the main effect of vertical mixing is in the spring, where populations increase more rapidly when no mixing is allowed and reaches a peak earlier. With mixing, the first peak is delayed and reduced in magnitude. The results in the summer and early fall are generally comparable under the different dispersion regimes, although the timing of maximum and minimum is changed.

6.2.3 Variable Phytoplankton Settling Velocity

A number of analyses using the Lake 1 model have been made to examine the behavior of the phytoplankton population under different settling velocities. The reported values for phytoplankton sinking in quiescent waters (see Chapter 3) are apparently too high to support adequate growth in the Lake 1 model. This is due in part to the crude vertical definition and the interaction between the sinking of phytoplankton and their physiological state. The settling
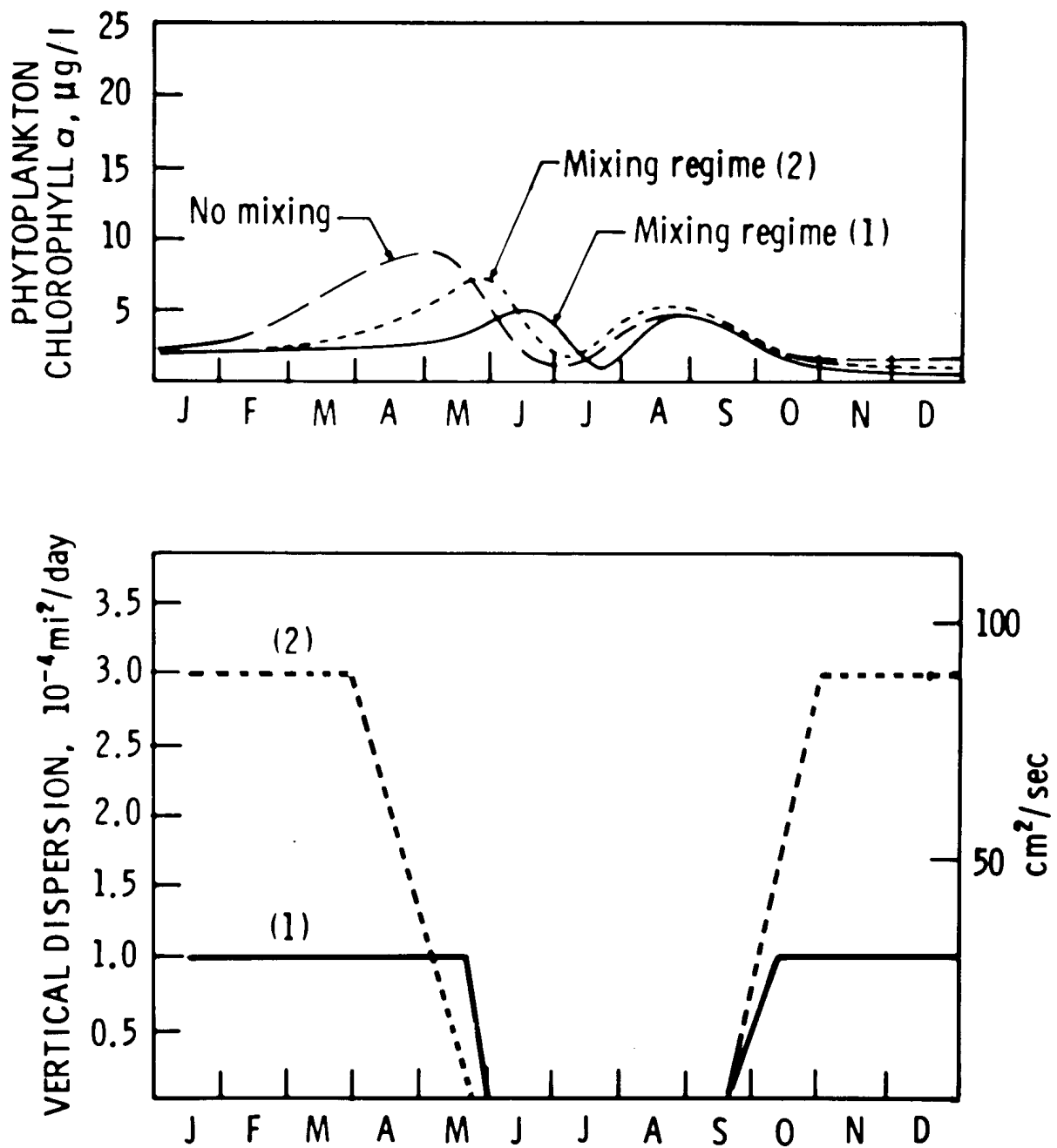
Figure 10. Effect of vertical mixing.

velocity has been treated as a parameter ranging from 0 to 0.5 meters/day.

Figure 11 summarizes the results from several analyses using different sinking velocities. For these runs, zooplankton grazing was set at 0.06 1/mg C day °C, no vertical mixing was used and the Michaelis constants were 25 µg/l and 10 µg/l for nitrogen and phosphorus, respectively. At a velocity of 0.5 m/day phytoplankton populations never exceed about 3 µg chlor/l and total zooplankton carbon (Figure 8) never exceeds about 0.08 mg C/l. Both values are less than observed. The reason for the low levels is that under a settling velocity of 0.5 m/day (which for the 17 meter depth of the epilimnion represents a "decay" coefficient of .03/day), the phytoplankton are not retained In the upper layer long enough to undergo net growth. As a consequence, zooplankton levels are also low and the nutrient concentrations remain high and are not reflective of observed nutrient depletion. Using a velocity of 0.05 m/day, the behavior of the phytoplankton biomass is quite different as shown in Figure 11. Now, the lower trophic level has a chance to grow and a reasonable predator-prey relationship begins to develop.

The half-saturation constant for phosphorus, K_{mp}, has an important effect, however. An order of magnitude reduction in this coefficient to 1 µg/l does permit growth of the phytoplankton at the higher settling velocity of 0.5 m/day. Figure 11 and 12 show this effect and indicate the trade-off between a population adapted to low phosphorus concentration and settling velocity. These results also tend to indicate the possible interaction of settling velocity and the active growth phase of the population.

The sinking velocity of phytoplankton also has an important effect on the nutrient uptake as shown in Figure 13, which is a plot of nitrate and available phosphorus concentrations calculated under the conditions of K_{mp} = 10 µg/l. In addition, Figure 13 shows the nitrogen and phosphorus limitation terms, i.e., the ratio of total inorganic nitrogen to total inorganic nitrogen plus the Michaelis for nitrogen and similarly for available phosphorus (see Equation 8). It can be seen that nutrient uptake and growth limitation is minimal for the case of sinking velocity = 0.5 m/day. This is a result of the minimal phytoplankton growth. At the lower sinking rate, however, nitrate uptake is increased but as indicated in the upper curves of Figure 13, nitrogen does not significantly limit growth for the case of K_{mp} = 10 µg/l.

The lower curves representing the phosphorus dynamics, however, do exhibit a limiting effect. If attention is directed to the phosphorus limitation term, it is seen that for both settling velocity cases, levels of phosphorus are such that a limitation of 0.50 - 0.60 prevails during the early and later parts of the year. However, substantial differences occur in the spring and late summer. At day 135, a minimum value of about 0.2 is calculated indicating that phosphorus is acting as a significant limiting factor in the phytoplankton growth. This helps explain the decrease in phytoplankton biomass beginning at day 120 (see Figure 11). Two effects are occurring: (1) herbivorous zooplankton are growing rapidly and (2) phosphorus levels are being depleted to below the half-saturation constant thereby acting to reduce the growth rate. It is interesting to note then that a bimodel distribution in phytoplankton can be obtained without a species differentiation. The latter is often offered as the explanation for the observed two peaks in the phytoplankton. In order to accomplish this, however, at least two trophic levels must be included above the phytoplankton. This permits a higher order predation, e.g., carnivorous zooplankton which reduces the lower zooplankton level. The reduction permits phytoplankton to grow again in late summer. This is explored in greater detail below.

6.2.4 Effect of Michaelis Constant

As indicated in Equation (5), the growth of the phytoplankton is considered to be limited by a Michaelis-Menten product term of total inorganic nitrogen and available phosphorus given by Equation (8). The dynamics of growth, therefore,

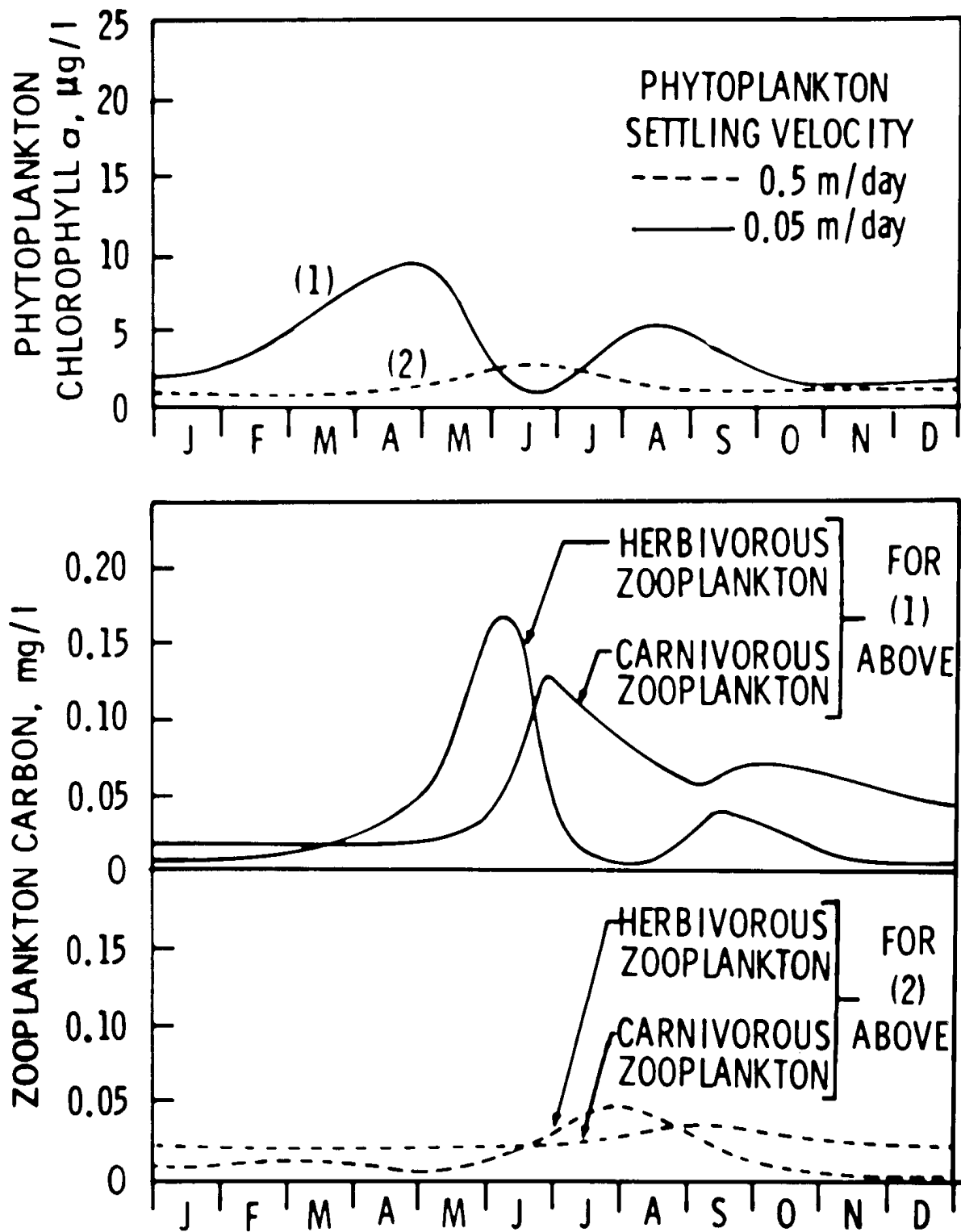Figure 11. Effect of phytoplankton settling velocity, K_{mp} = 10 μg/l.
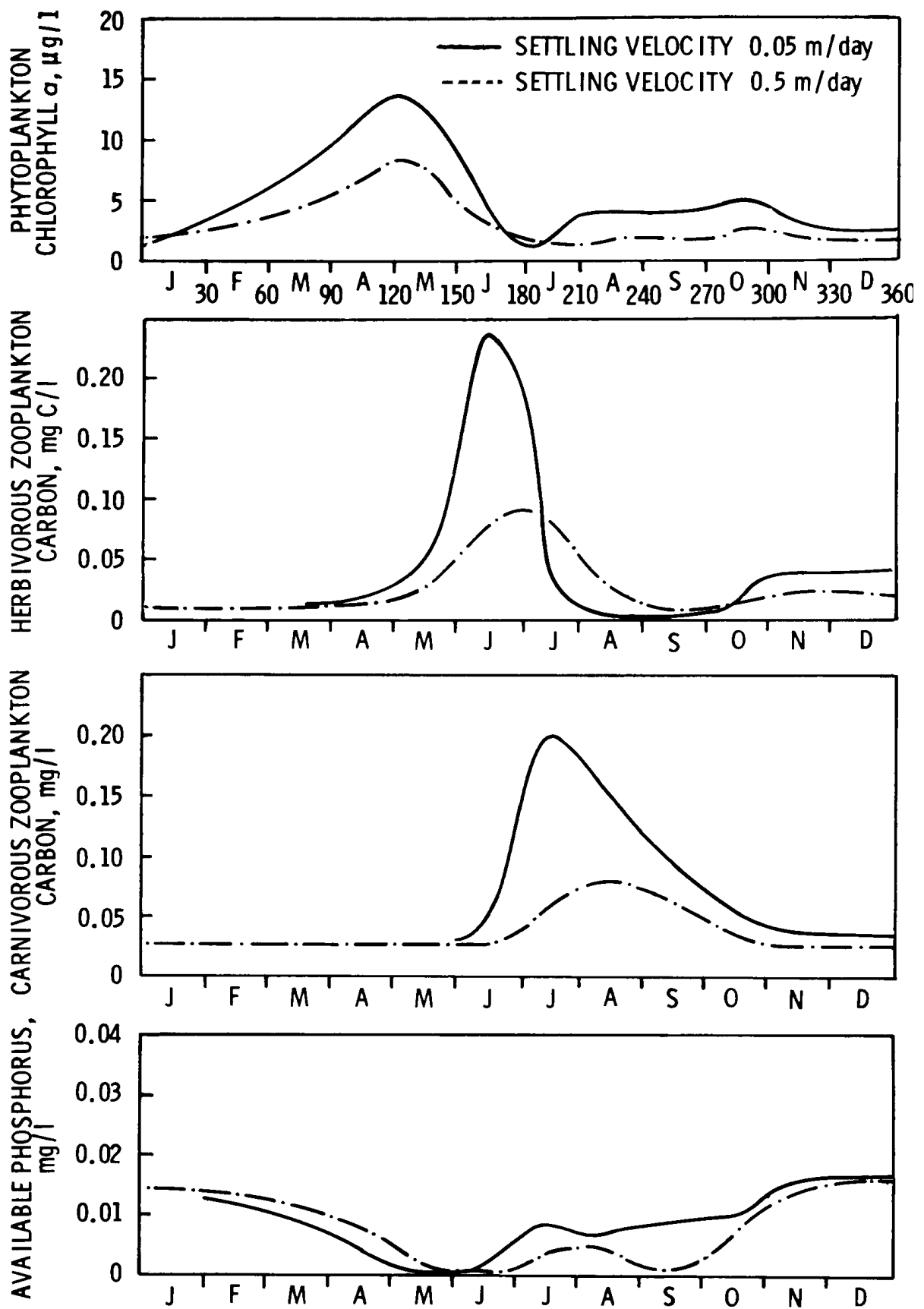
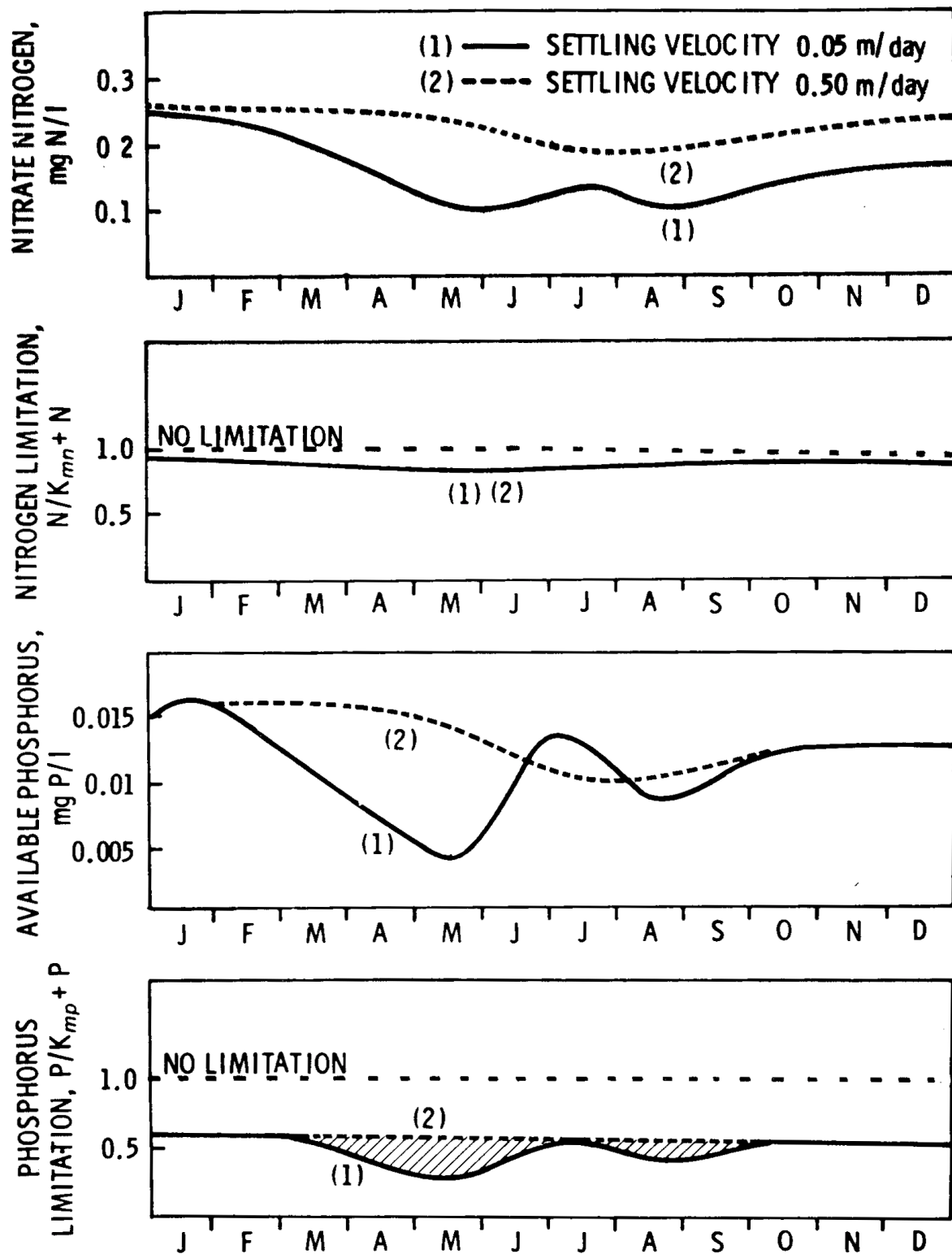Figure 12. Effect of phytoplankton settling velocity, K_{mp} = 1 µg/l.

Figure 13. Effect of phytoplankton settling velocity on nutrients and nutrient limitation, K_{mp} = 10 µg/l.

are affected by the levels of K_{mn} and K_{mp}, the half-saturation constants for nitrogen and phosphorus, respectively. Several sensitivity runs have been made, therefore, specifically examining two levels of K_{mp}, 1 and 10 µg/l both of which encompassed the range of published values. Phosphorus is emphasized because of the waste removal programs presently underway in the Great Lakes basin.

Figures 14 and 15 show the results of two computations at an order of magnitude difference in K_{mp}. For both runs, settling velocity was 0.05 m/day, K_{mn} (nitrogen half-saturation constant) is 25 µg/l and zooplankton are included as before. As seen in Figure 14 at the 1 µg/l level, phytoplankton biomass grows earlier more rapidly and reaches a peak value of 14 µg/l chlorophyll/l at the end of April. At the 10 µg/l value, growth is later, slower and reaches a maximum value of about 9 µg/l almost a month later at the end of May. Values in the late summer are comparable. The nutrient plots shown in Figure 14 indicate that in May, phosphorus is limiting under the 1 µg/l case while in August-September, nitrogen appears to be limiting. This is shown more clearly in Figure 15 - which is a plot of the nitrogen and phosphorus limitation terms under both conditions. It can be noted that at 1 µg/l, the growth is limited by phosphorus for only a short period in May and the system tends to be nitrogen limited throughout the rest of the growing season. On the other hand, at a phosphorus Michaelis constant of 10 µg/l, the system is more phosphorus limited throughout the year although nitrogen is still an important limiting interest in late summer.

The results indicate the importance of reasonably accurate estimates of the half-saturation constant. This will be particularly important during any simulation of nutrient reduction programs. The results also indicate that reliance on a single nutrient as "the limiting nutrient" does not recognize the interaction between nutrients and may be quite misleading in estimating the effects of a control program.

6.2.5 Effect of Alternate Growth Formulation

As discussed in Chapter 3, Equations (5) and (9) represent different expressions for the growth term in the phytoplankton equation. In order to examine the behavior of the response to each form, the Lake 1 growth kinetics were modified to incorporate Equation (9). The results for three output variables are shown in Figure 16. Both runs displayed therein are for identical conditions, except for the alternate growth formulation as indicated in the figure.

Equation (9) results in immediate and rapid growth of the phytoplankton with subsequent total depletion of the phosphorus. The dynamic behavior of the results using the formulation of Equation (9) do not even approximately agree with observed data. This is especially true for the high levels of phytoplankton in the early and late months of the year and the zero concentration of phosphorus throughout the better part of the year. The dynamic shape is also not consistent with the observed data (see Figure 3). From this one comparison, then, Equation (5) the original product formulation is still to be preferred.

6.2.6 Time to Dynamic Equilibrium

With the relatively long detention time of about eight years for Lake Ontario, the time to reach a dynamic steady-state (i.e., where the solution becomes periodic) is an important management consideration. For a single non-conservative variable in a completely mixed lake, the solution for a mass input of W is

$$s = \frac{W}{Q + KV}[1 - e^{-(k + 1/t_o)t}]$$
$$+ s_o\,e^{-(k + 1/t_o)t}$$

(55)

where s_o is the initial condition of s and t_o is the detention time given by V/Q. For K = 0, the conservative case, the time to reach 95% of a new steady value is about three detention times, which for the whole of Lake Ontario is about 24
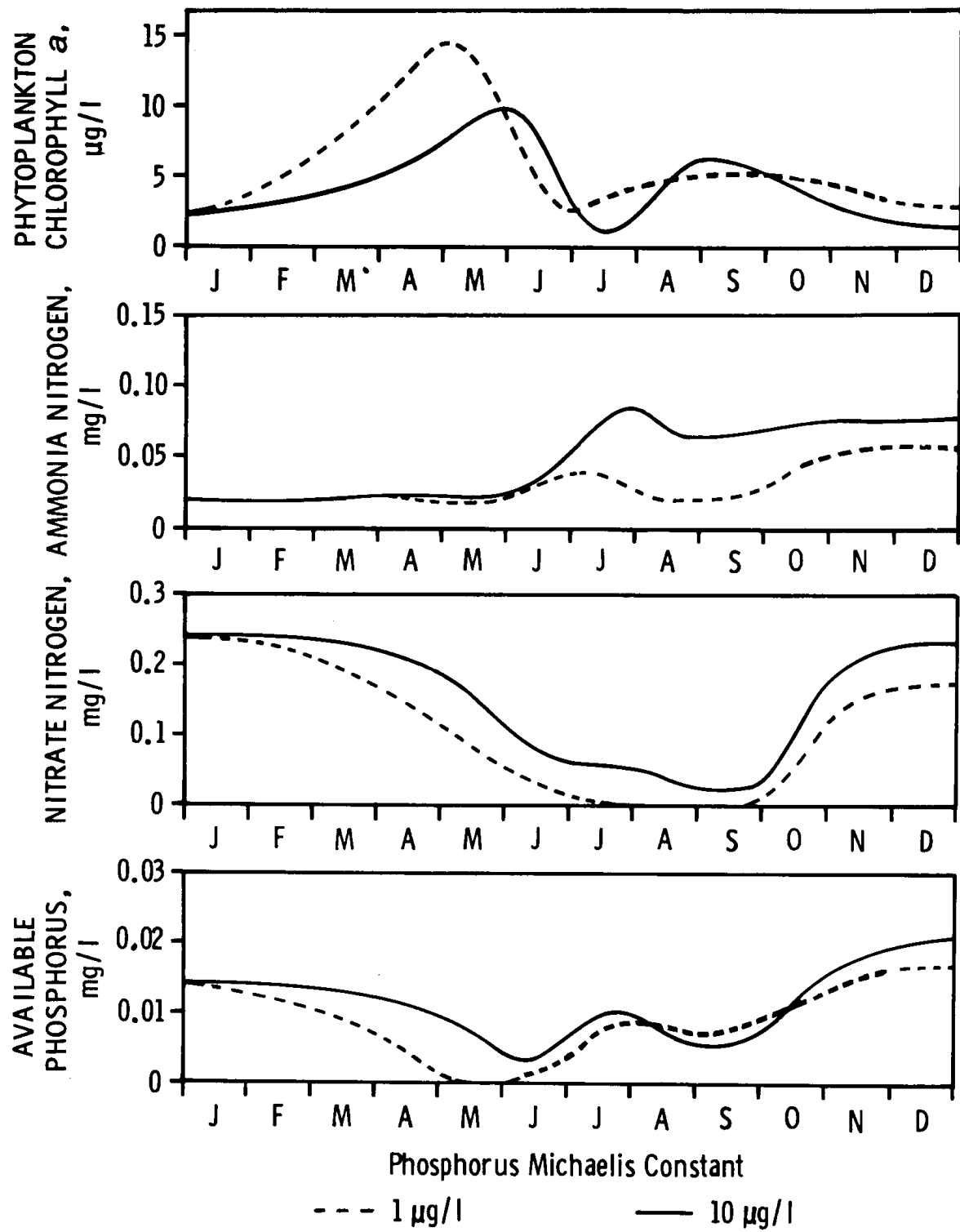
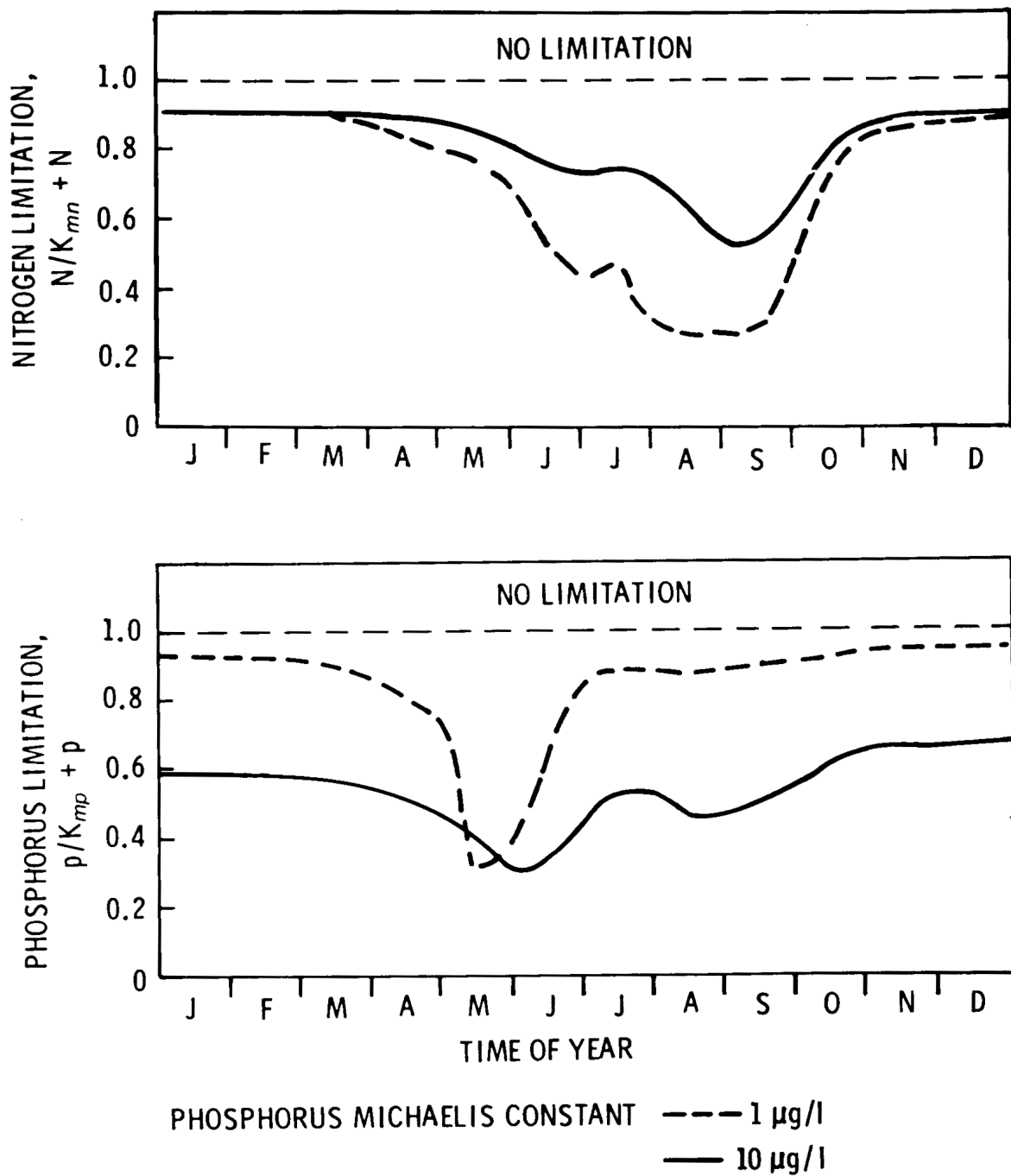Figure 14. Effect of Michaelis constant for phosphorus on primary variables.

Figure 15. Effect of Michaelis constant for phosphorus on nutrient limitation of nitrogen and phosphorus.
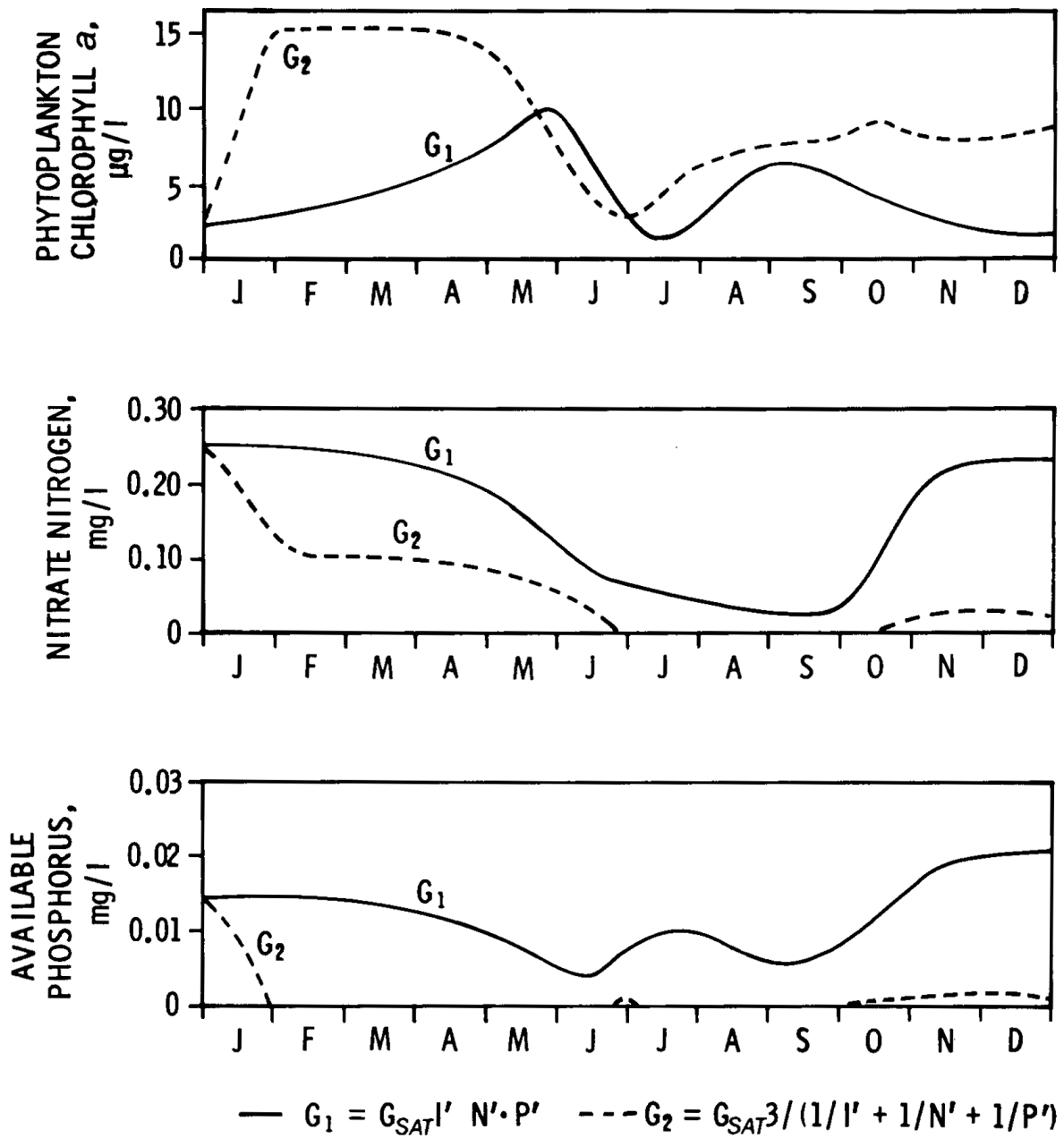
Figure 16. Responses due to two phytoplankton growth formulations.

years. Furthermore, the initial conditions will also take approximately that long to "die down" and not influence the solution. Any solution, therefore, that is calculated for only one year (as per the previous figures) is dominated by the initial conditions and the effect of the mass input is negligible. For verification purposes, however, a single year run is sufficient to explore the general behavior of the system. For any projections of the effects of reduced inputs, longer runs are needed. Therefore, the solutions must be run for a period of time until the initial conditions for all variables are repeated year-by-year. With the complex interactions of the Lake 1 model, this time to reach a dynamic equilibrium is not immediately obvious. Accordingly, several long-term runs were prepared to illustrate this effect.

Figure 17 shows a time history plot of 16 years of solution equivalent to two detention times. The conditions are comparable to previous runs but use a Michaelis phosphorus constant of 10 µg/l. As shown, peak phytoplankton levels in the spring gradually decrease from greater than 9 µg/l in the first year to about 7 µg/l by the eighth year after which time a dynamic equilibrium has been reached. Thus, a time of about one detention time for Lake Ontario was required for the phytoplankton to reach a steady-state. However, due to internal cycling between the various nutrient sub-systems, shorter or longer times may be required for some of the nutrient forms. This is shown in Figure 18 which indicates system response under two phosphorus Michaelis constants. The upper figure indicates a parallel decrease in the phytoplankton maximum under the two conditions and, although the two runs began with a peak difference of almost 3 µg/l, the difference is about half of that at equilibrium.

The lower two plots of Figure 18 are quite interesting and illustrate further the difference in the dynamic behavior under the two phosphorus Michaelis levels. Under the lower level of 1 µg/l, equilibrium is reached almost immediately in both phosphorus and total inorganic nitrogen. Under an order of magnitude increase in the

level to 10 µg/l, dynamic steady-state is not reached for the inorganic nitrogen until almost two detention times or 16 years. With the lower level of 1 µg P/l, phytoplankton growth is increased due to the increased ability to utilize low phosphorus concentrations. As a consequence, however, nitrogen utilization is increased and as shown in the middle plot of Figure 18, the system becomes nitrogen limited. The times of the year of the nitrogen and phosphorus limitation are different, however, as shown in Figure 15.

In essence then, these runs illustrate the need to carry out any simulations of a proposed nutrient reduction program about 8-16 years to determine the expected phytoplankton levels under a different waste load input. If, however, the loads are changing from year-to-year, as for example, in a linear increasing or decreasing fashion, then even longer times may be required. Indeed, under changing loads, a dynamic equilibrium may never be theoretically possible. For many practiced purposes, the system will probably reach steady-state in a 10-20 year time horizon after significant changes have been made.

6.2.7 Preliminary Comparison

Figures 19 and 20 show one of the early comparisons of observed data and model output. The Michaelis constant for phosphorus was 10 µg/l and settling velocity was 0.05 m/day. In the preliminary comparisons, a variety of similar plots was generated. Figures 19 and 20, therefore, represent a type of a first level of calibration. In general, the overall comparison is quite good and indicates that even with first, approximate analysis, results are obtained from the model that are in general agreement with the observed data. This tends to support the contention that the basic model structure does represent the principal features of the phytoplankton biomass.

Several details of Figures 19 and 20, however, remained to be exploited in greater depth before a "final" verification could be obtained. For
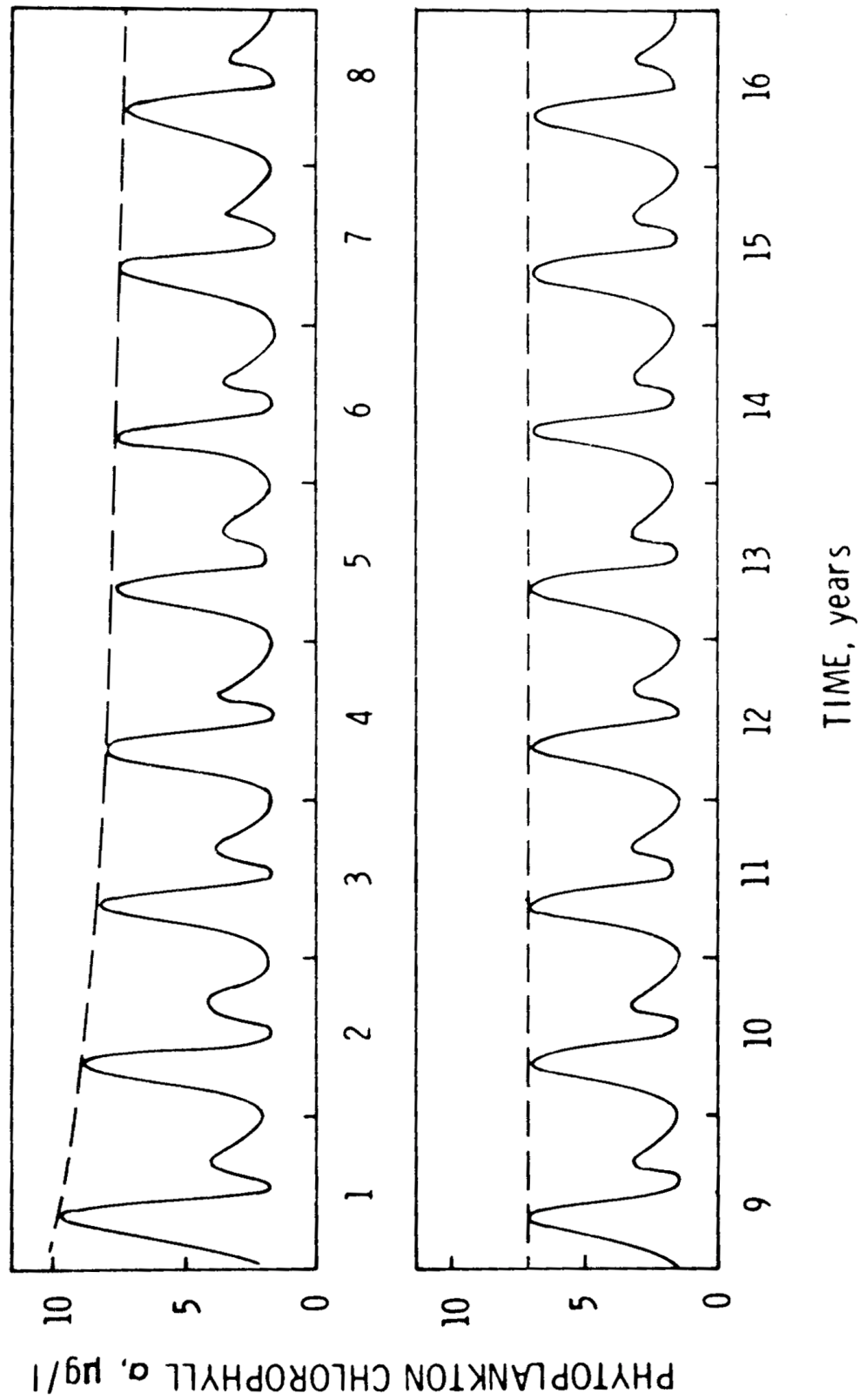
Figure 17. Sixteen-year computed output of phytoplankton chlorophyll.
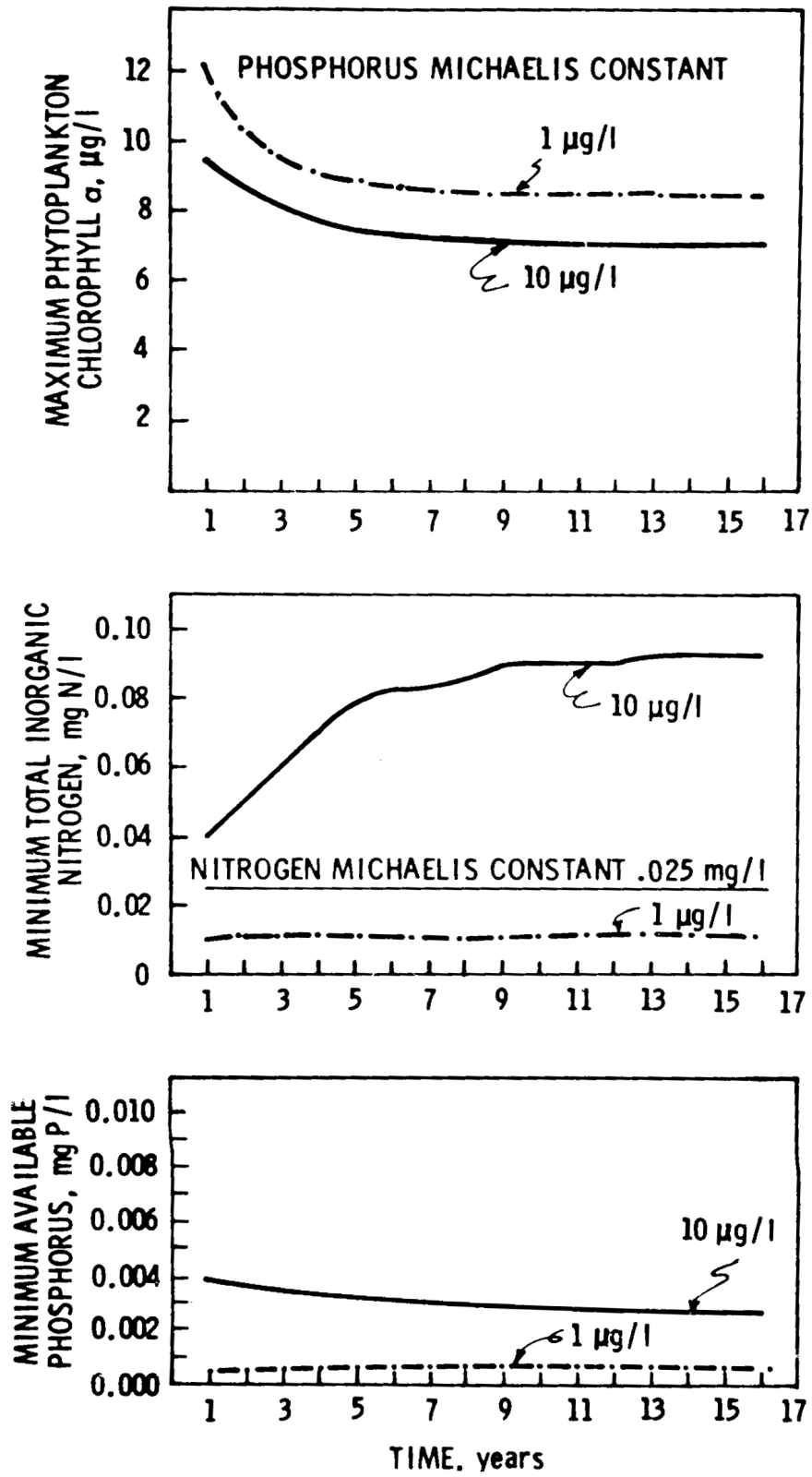
46

Figure 18. Long-term behavior of model components under two phosphorus Michaelis constants.
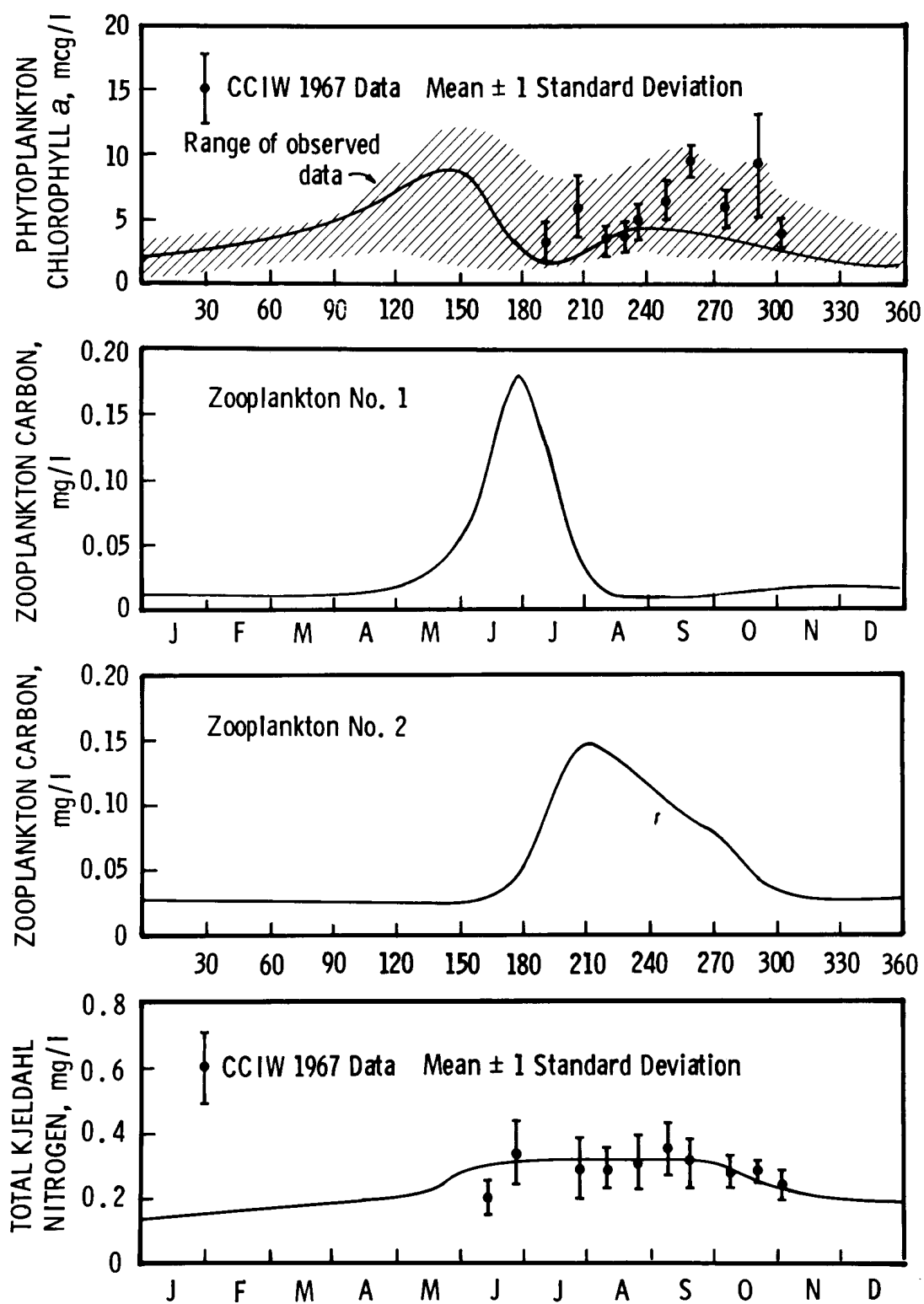
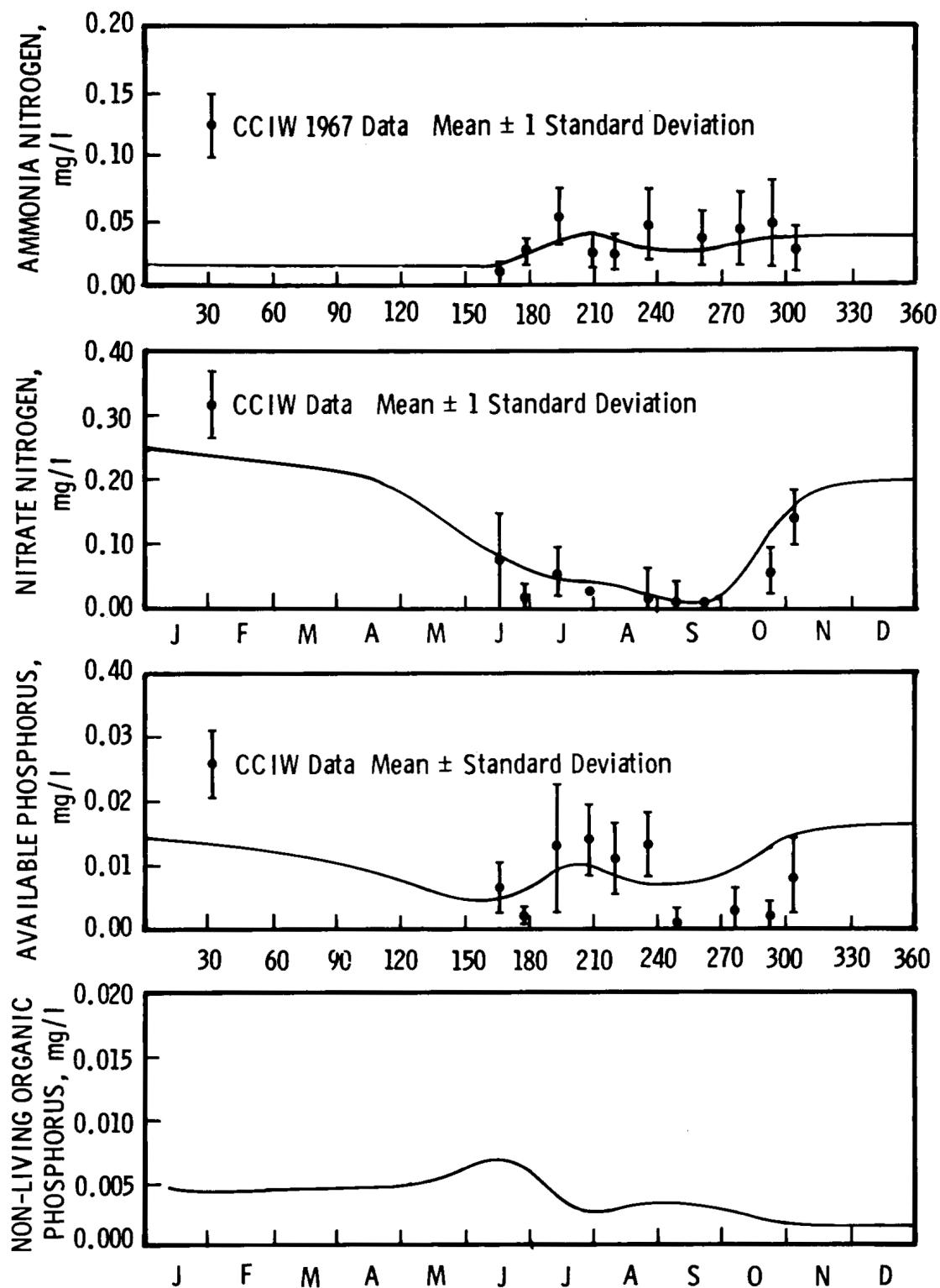Figure 19. Preliminary comparison of model output and observed data.

Figure 20. Preliminary comparison of model output and observed data (continued).

example, in the preliminary runs, the fall peak in phytoplankton is only approximately reproduced and, in addition, the total zooplankton carbon is generally too high. Finally, the dynamic behavior of the nutrients such as phosphorus and ammonia, while generally satisfactory, could be improved. Using, therefore, the sensitivity runs discussed previously and the results of the preliminary comparisons, further verification analyses were conducted to construct a coherent picture of the dynamics of the lake. The goal then in this final verification phase of Lake 1 model was to produce a set of parameters and accompanying hypotheses that represents as good a comparison as possible to available data.

6.3 RESULTS OF "FINAL" VERIFICATION ANALYSIS

Data were available for the years 1967-70 collected by the Canada Centre for Inland Waters (CCIW) for this final verification phase. These data were supplemented by other observations in the literature. Values for the various coefficients, parameters and exogenous variables were obtained from published sources as discussed previously and all values used are within reported ranges in the literature. More than 80 runs have been made of Lake 1 to examine the effects of various phenomena such as settling velocity, vertical mixing, zooplankton predation and half-saturation constants for nitrogen and phosphorus. Out of these runs, a consistent set of parameter values which satisfactorily explains the observed data on a variety of different variables has emerged. A plausible explanation for the dynamic behavior of the phytoplankton is, therefore, possible and is discussed below.

Figures 21 and 22 show the verification of the Lake 1 model upper layer (0-17 meters) while Figure 23 shows the verification for the hypolimnion (data in range, 50-150 meters). Table 9 shows the principal coefficients used for the runs. As shown, the verification for plankton in the epilimnion is quite good and satisfactorily duplicates the spring peak, subsequent mid-summer die-off and fall bloom. Five other

variables in addition to the phytoplankton chlorophyll are satisfactorily verified in the comparison. It should be noted here that it is generally not possible to obtain the verification shown in Figures 21-23 by arbitrary specification of the coefficients, so that the results shown do not simply represent a "curve fitting" exercise. Rather, the results, which are based on the theory discussed earlier, are representative of the observed data in a much more meaningful way than just through arbitrary statistical coefficients. Since the model permits computation of the components of the dynamic behavior, considerable insight can be gained by examining the influence of various phenomena on the growth and death rates of the phytoplankton.

Figure 24 shows the dynamics of the kinetic growth rate of the phytoplankton (G_p in Equation (4)). As shown, maximum growth rate reaches a peak in mid-September in the Lake 1 model at about 1.8/day and then decreases rapidly due to the fall overturn. The reduction in the maximum growth rate due to light is substantial and shifts peak growth to early August. A further reduction in growth rate is due to the nutrient limitation so that the resultant growth rate, G_p is lowest at the end of May and peaks at about 0.25/day in August. The peak value represents an overall reduction of 90% from saturated growth conditions. Primary productivity values calculated from the growth rate and phytoplankton biomass, Equation (11), give peak values of about 600 mg C/m^2-day at the end of August and values of about 500 mg C/m^2-day at the height of the spring bloom. The former value is in general agreement with Glooschenko *et al.* (1974) while the latter is somewhat lower than the Glooschenko's estimated spring values of 500-1100 mg C/m^2-day.

Figure 25 shows the dynamics of the kinetic death rate of the phytoplankton (D_p in Equation (4)). Three effects are to be noted: (1) phytoplankton settling, (2) water temperature effect on endogenous respiration, and (3) effect of zooplankton grazing. Peak resultant death rate is 0.25/day at the beginning of August and
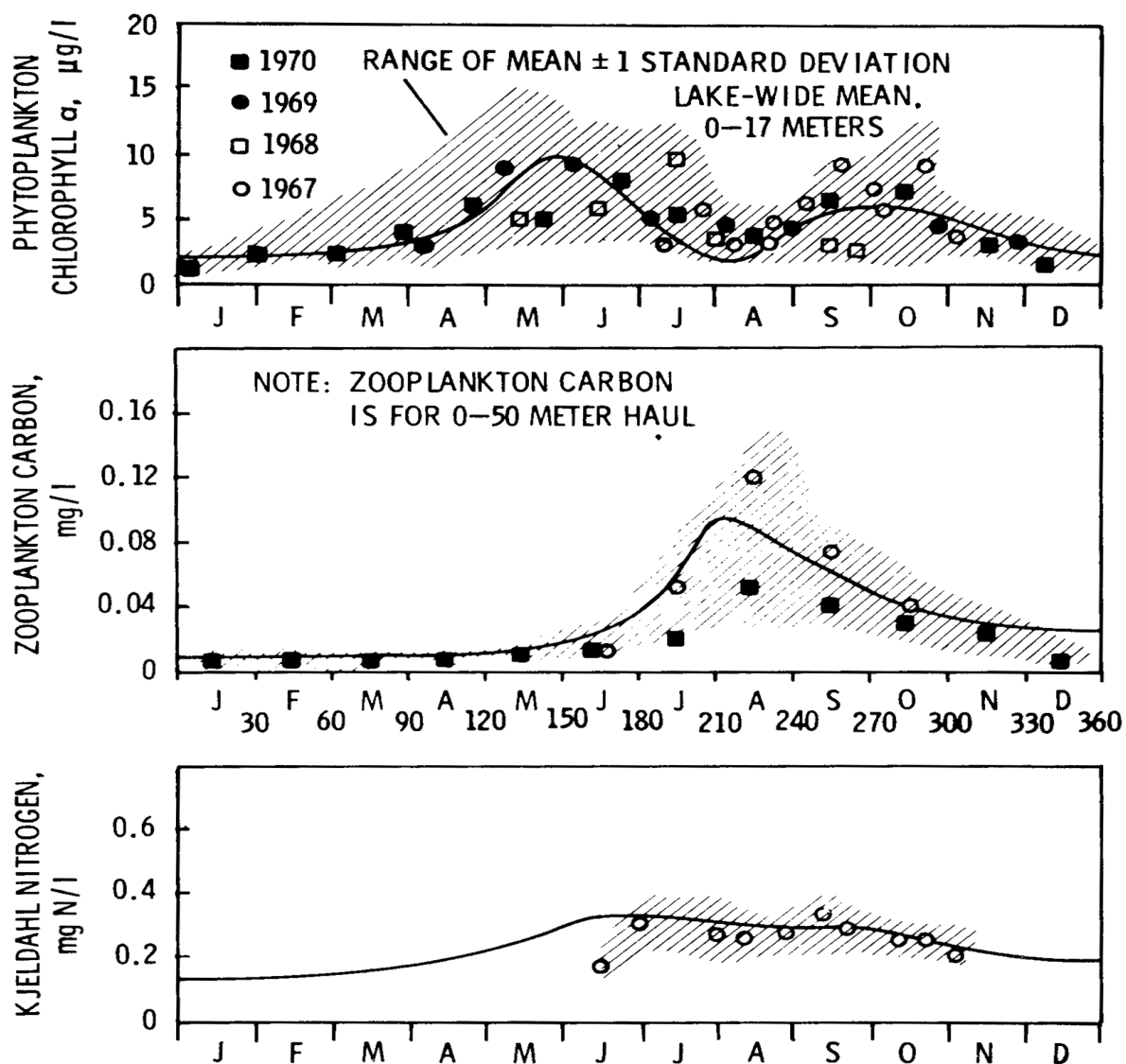
Figure 21. Lake 1 model verification, 0-17 meters.

51
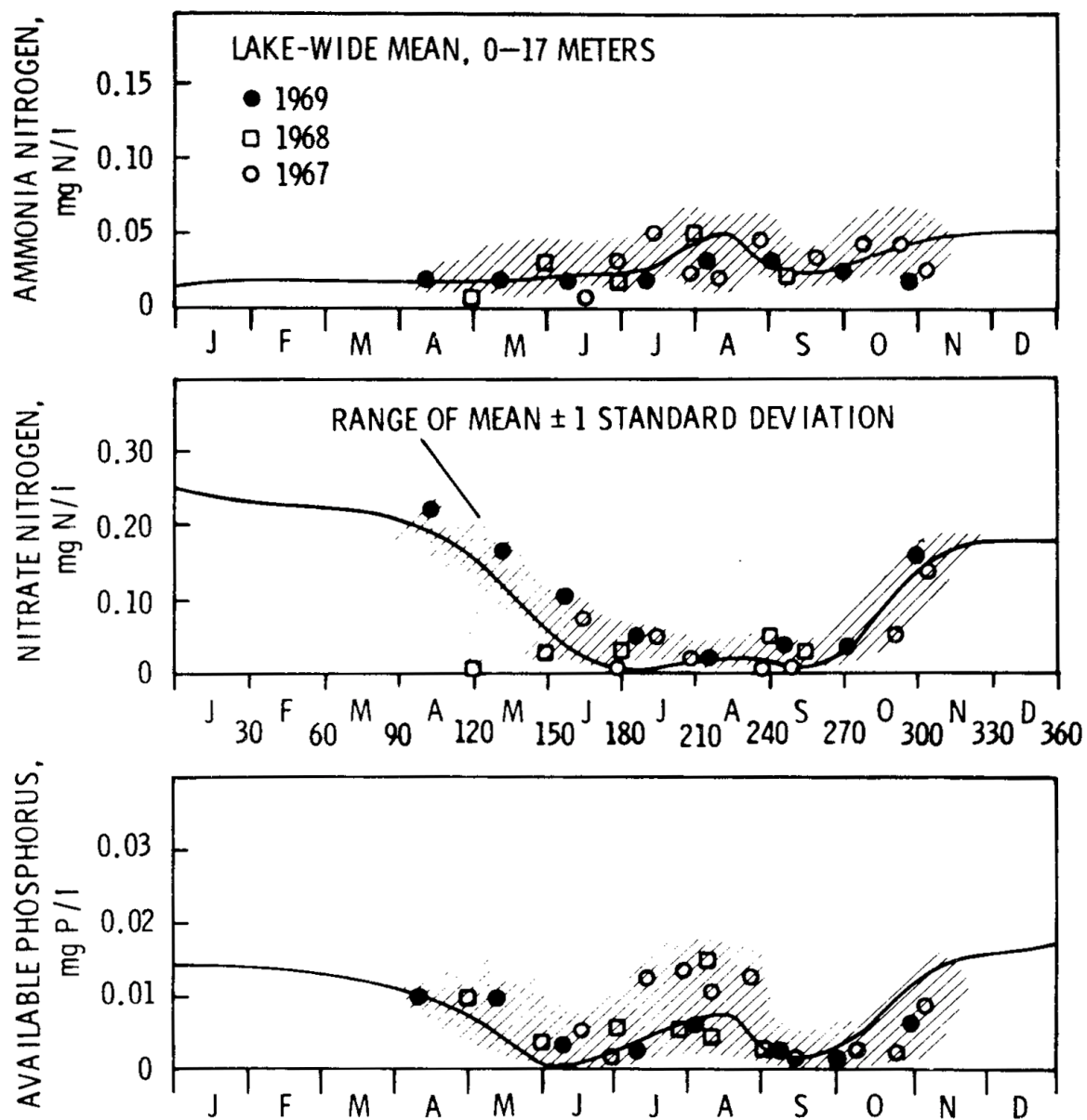
Figure 22. Lake 1 model verification, 0-17 meters (continued).
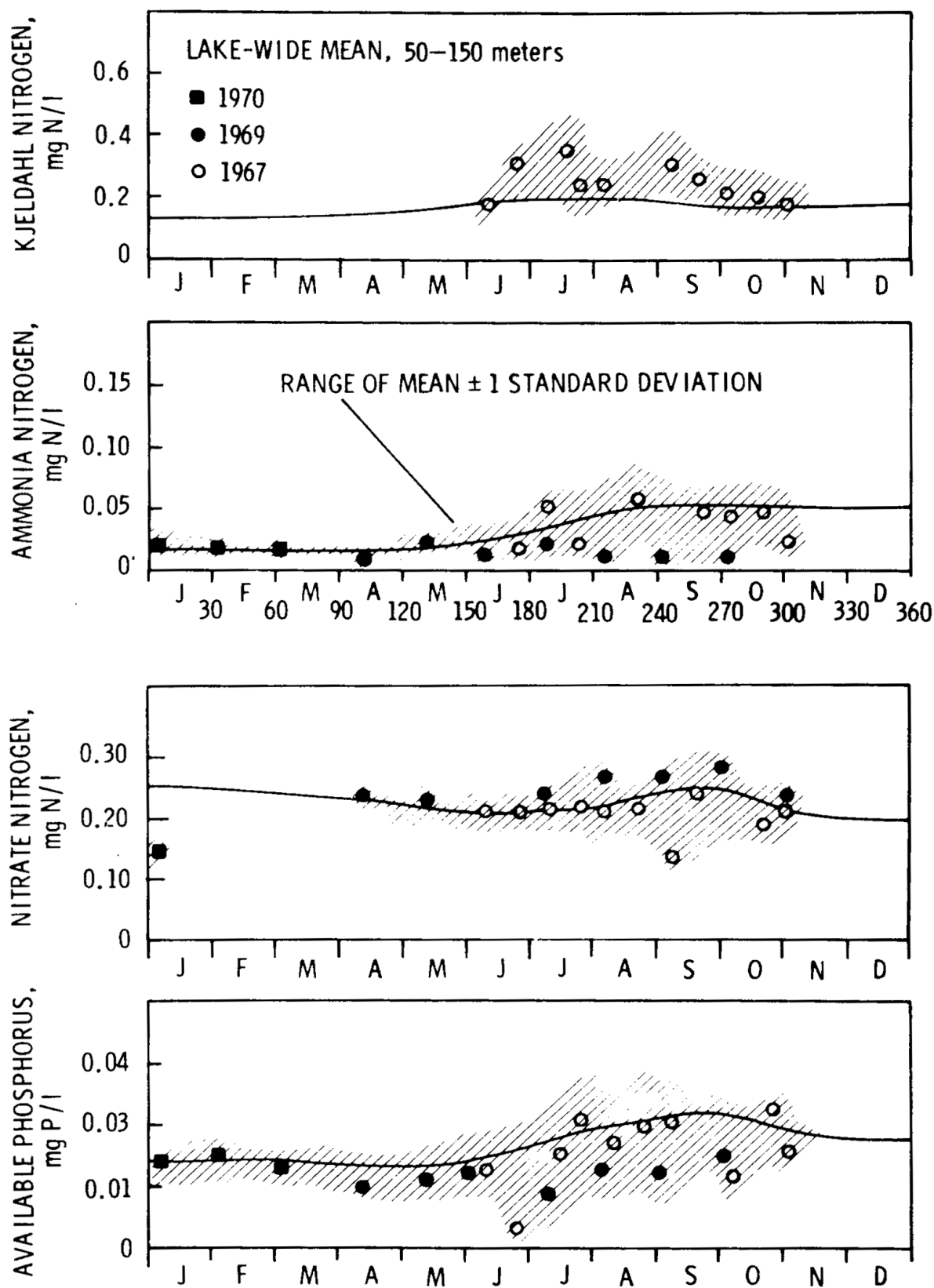
Figure 23. Lake 1 model verification, 50-150 meters.

Table 9. Principal Parameter Values Used in Lake 1 Model Output (Shown in Figures 21-23)

Notation	Name	Value	Unit
K_{mn}	Half-saturation constant-nitrogen	25	µg N/l
K_{mp}	Half-saturation constant-phosphorus	2	µG P/l
C_g	Grazing rate for zooplankton	.06	1/mg C-day-°C
K_g	Half-saturation constant-phytoplankton	10	µG Chlor/1
K_2	Endogenous respiration rate-phytoplankton	0.1	$Days^{-1}$ (at 20°C)
a_{zp}	Zooplankton conversion efficiency	0.6	-
K_z	Zooplankton endogenous respiration rate	.001	$(Days-°C)^{-1}$
K_1	Decomposition rate of organic nitrogen	.00175	$(Days-°C)^{-1}$
K_{22}	Ammonia to nitrate nitrification rate	.002	$(Days-°C)^{-1}$
K_{op}	Decomposition rate of organic phosphorus	.007	$(Days-°C)^{-1}$
a_1	Nitrogen-chlorophyll ratio	10	µG N/µg Chlor
a_p	Phosphorus-chlorophyll ratio	1	µG P/µg Chlor
a_c	Carbon-chlorophyll ratio	50	µG C/µg Chlor
w	Settling velocity of phytoplankton	0.1	m/day

Dynamics of Phytoplankton Growth Rate
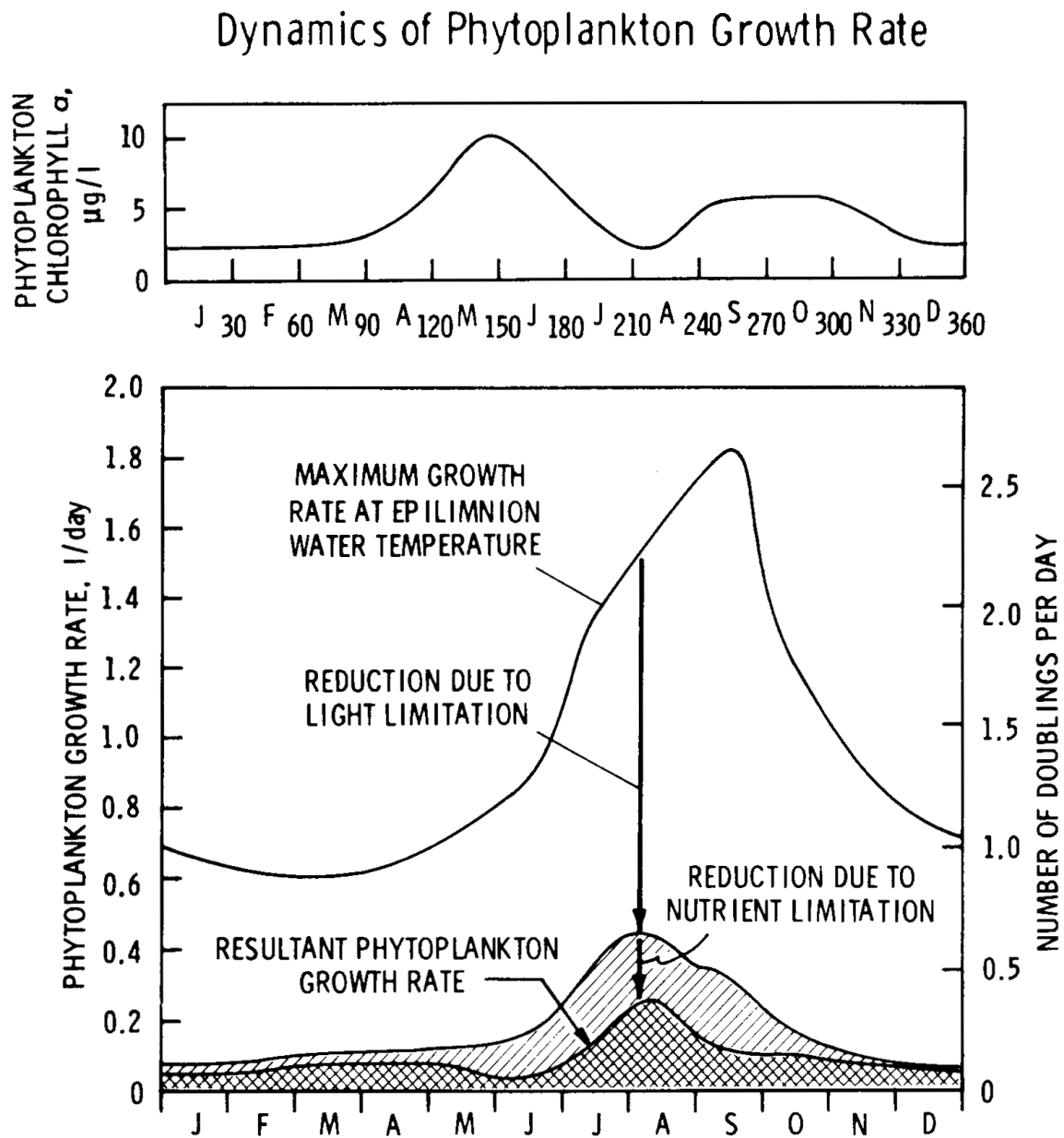
Figure 24. Dynamics of the phytoplankton growth rate.
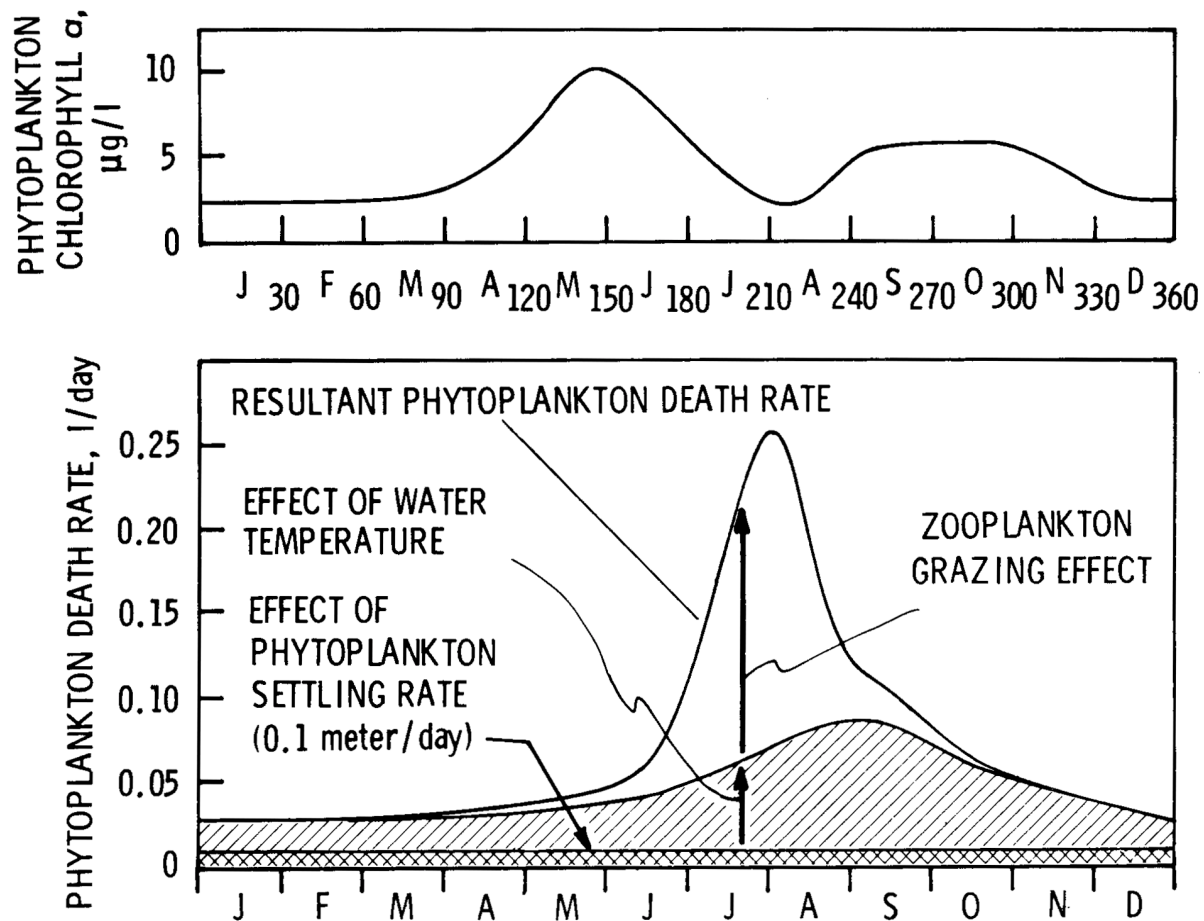
Figure 25. Dynamics of the phytoplankton death rate.

is primarily due to zooplankton predation and quantitatively explains the mid-summer decline in phytoplankton biomass.

The dynamics of phytoplankton net production, i.e., chlorophyll/liter-day, d_P/dt, are shown in Figure 26. Net production here includes the kinetic interactions of growth in Figure 21, death and predation in Figure 25, and the effect of vertical mixing and lake outflow. The results shown in Figure 23 summarize the basic hypotheses of phytoplankton dynamics in Lake Ontario.

The spring growth phase to approximately mid-May is due primarily to increasing light and temperature. There are little zooplankton as yet, so growth continues until nutrient limitation becomes significant in early June. (This is principally phosphorus limitation as discussed below.) The spring growth and spring peak are, therefore, simply described by a nutrient interaction effect with light and temperature dominating the growth and death terms. Following the spring peak, however, the situation becomes considerably more complex and indeed a significant effort was devoted to unraveling the complex interactions which lead to a mid-summer decline and subsequent broad fall peak.

It is hypothesized, as computed in Figure 26, that during mid-summer, and following the nutrient limitation effect, zooplankton grazing becomes important and accounts for the minimum values of biomass in July. However, at increased zooplankton grazing, biological recycling of nutrients becomes more significant. Nutrients are released back to the epilimnion through excretion as well as phytoplankton endogenous respiration. In late July then, growth exceeds death due to nutrient regeneration and an active growth phase begins again. Nutrients, however, are already at low levels so growth is not pronounced and proceeds slowly (as shown by the net production approaching zero in September but not yet entering a negative growth phase). The fall overturn of the lake then reduces the growth of phytoplankton biomass primarily because of mixing with the colder hypolimnion waters.

Figures 27 and 28 explore these dynamic effects at another level of detail. The model permits calculations of nutrient limitation effects as well as the flux of nutrients due to zooplankton excretion and release of nutrients due to endogenous respiration by the plankton. Figure 27 shows the nutrient effects. As seen, the spring bloom is halted essentially by a reduction in phosphorus that is quite pronounced and growth is reduced by a factor of about 0.35 due to the low phosphorus levels. At the same time, nitrogen is not limiting and is at a level twice that of the phosphorus. Nitrogen, however, does become limiting during July and again in September at which time phosphorus also exerts a limiting effect on growth. Figure 27 shows, therefore, that the spring peak is primarily phosphorus controlled. The dynamics after the spring peak are, however, controlled by both nitrogen and phosphorus (as well as zooplankton predation).

Figure 28 shows the estimated sources of phosphorus recycled to the epilimnion by both biological effects and vertical mixing effects from the hypolimnion. As shown, during early spring, the hypolimnion contributes almost twice as much nutrients to the epilimnion as from external inputs and by early summer in June-July, biological recycling reaches almost five times the mass rate of external phosphorus sources due to waste residuals, Niagara River, and other contributors. Zooplankton excretion recycles almost twice the input rate and in late summer-early fall, biological recycling reaches another peak but then drops rapidly due to fall overturn. The flux of nutrients from the more nutrient-rich hypolimnion during October is not sufficient to offset the drop in water temperature in the epilimnion. Biological recycling, therefore, drops rapidly in October and the phytoplankton biomass declines (see Figure 21). The results shown in Figure 28 indicate quantitatively the significance of biological recycling and vertical mixing relative to the level of external nutrient inputs. A reduction in input phosphorus load,
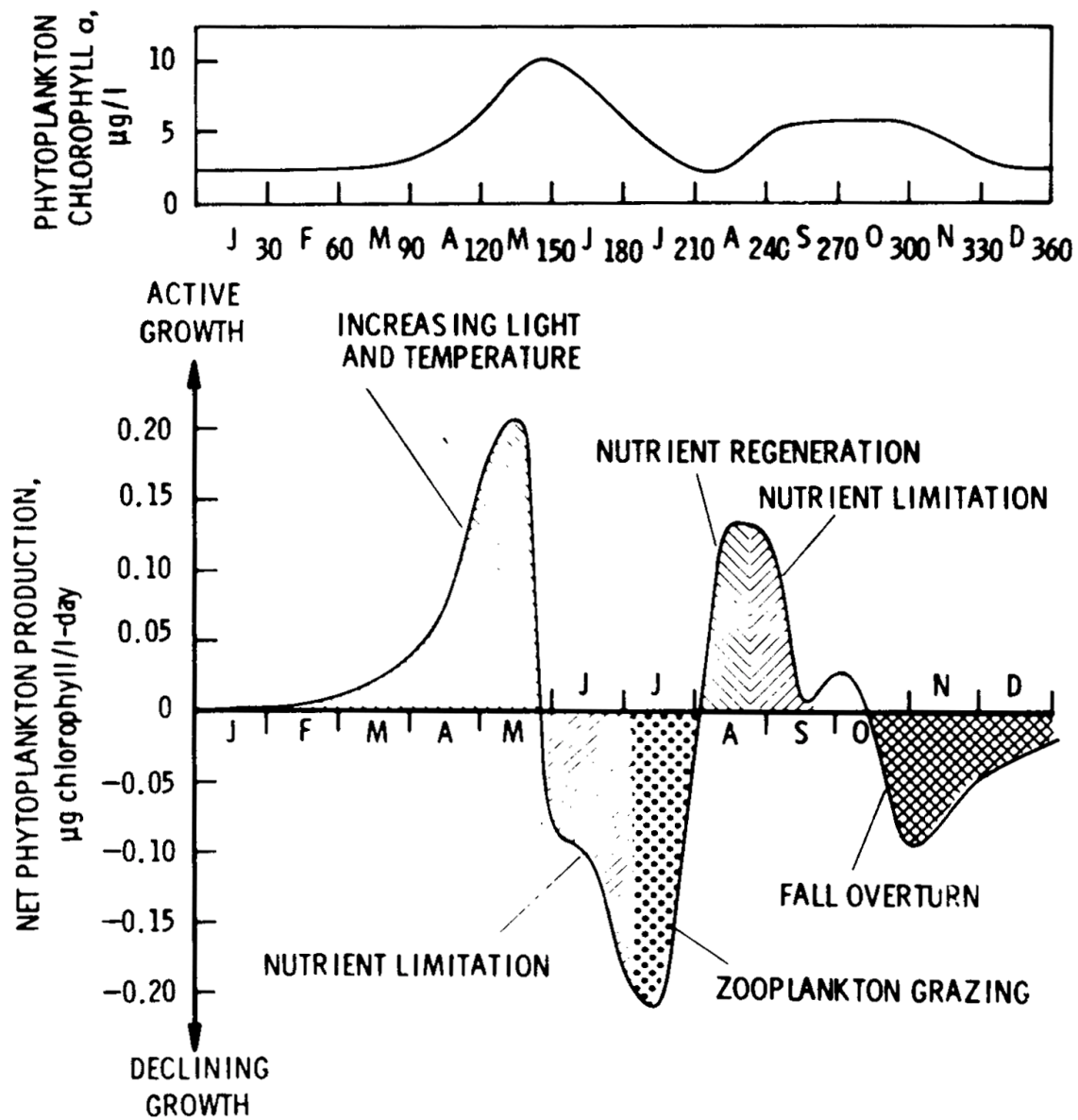
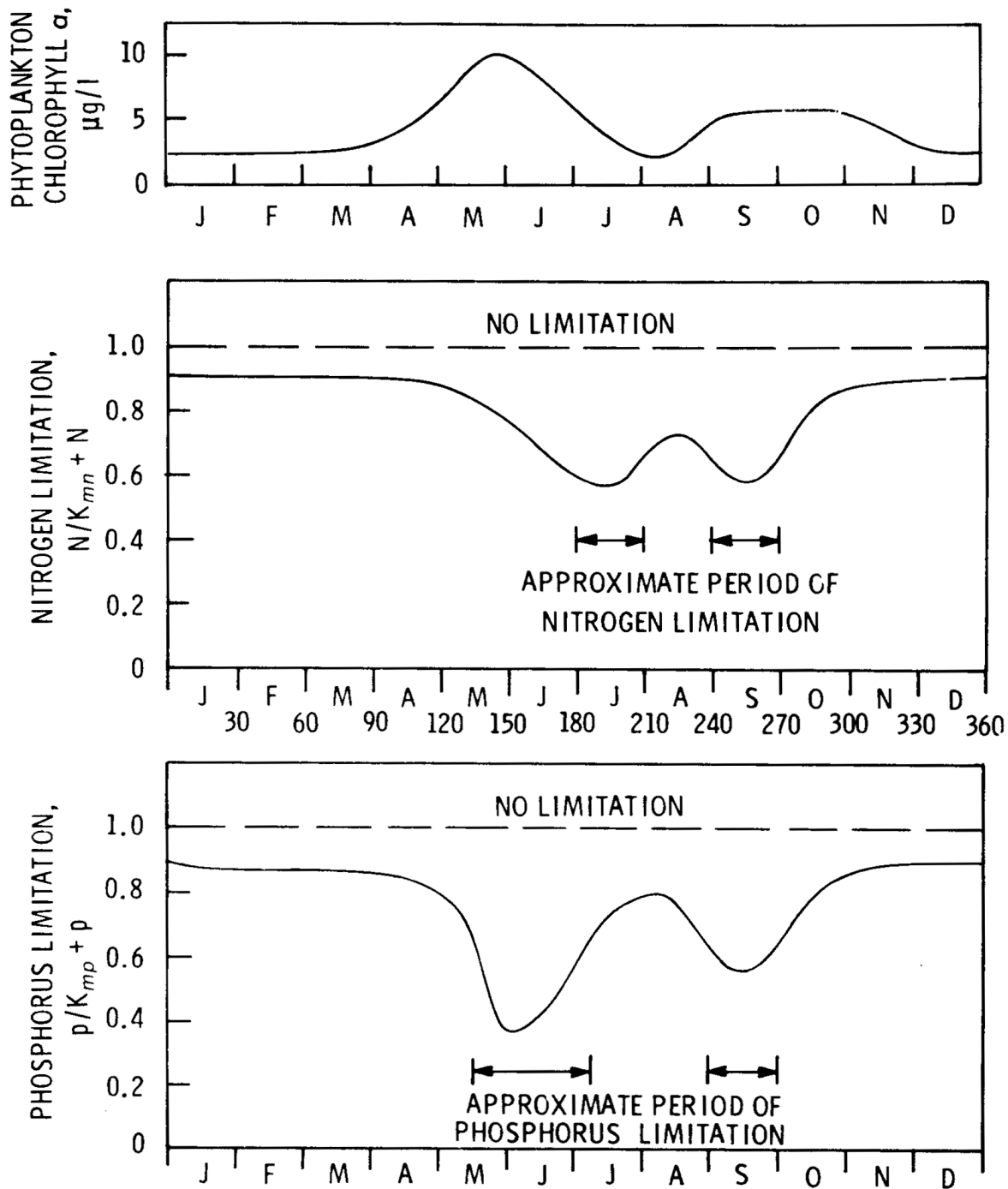Figure 26. Dynamics of the phytoplankton net production.

Figure 27. Dynamics of nitrogen and phosphorus limitation.

59

Biological Recycling
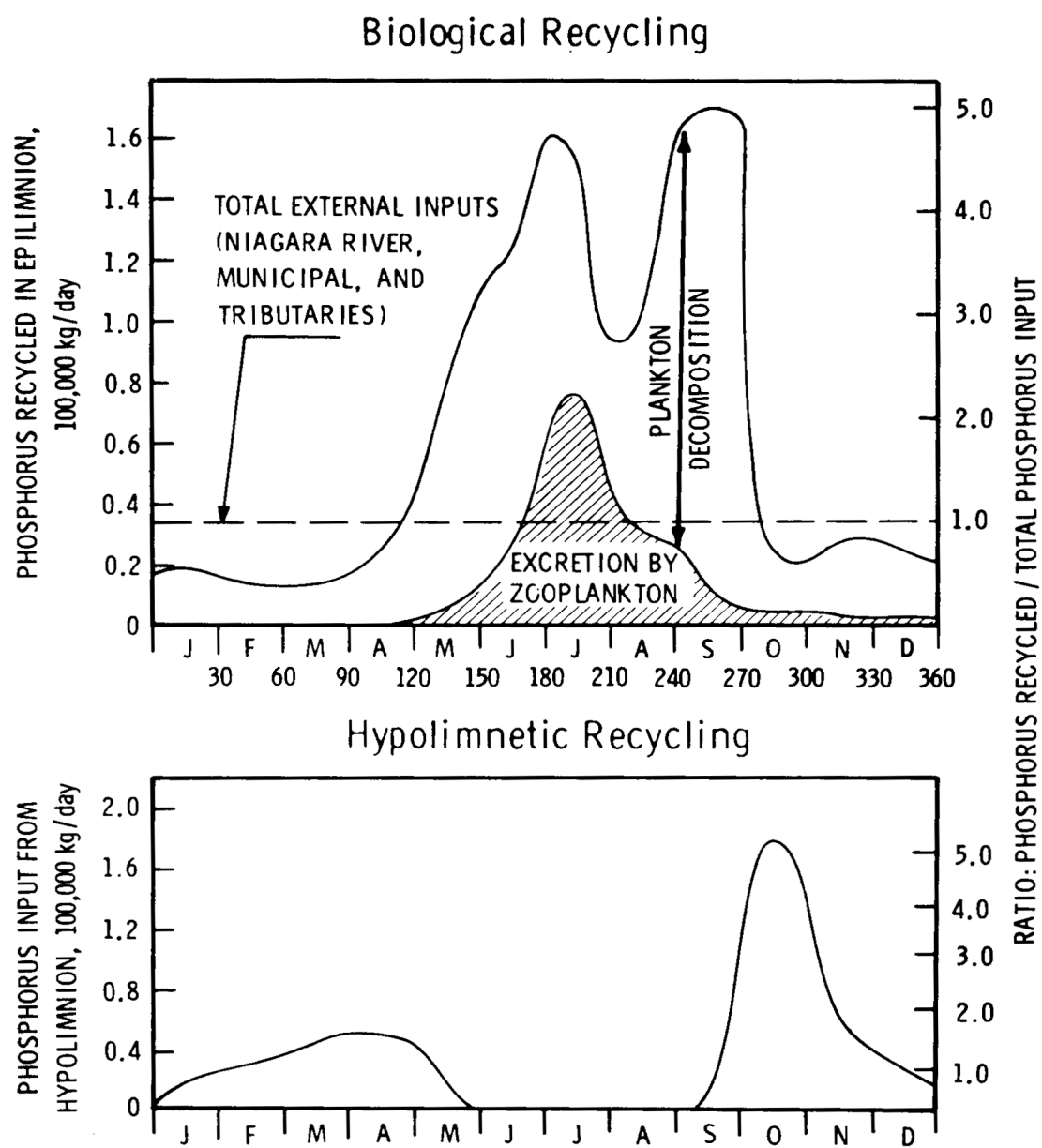

Hypolimnetic Recycling

Figure 28. Biological and hypolimnetic recycling of phosphorus.

therefore, may not necessarily result in a concomitant reduction in biomass. Further, the time to reach a new equilibrium biomass level will extend beyond a single year due, in part, to the recycling effects discussed previously, and long detention times in Lake Ontario.

In summary, the Lake 1 modeling effort, to date, has indicated that a considerable degree of quantitative insight into the behavior of phytoplankton biomass can be obtained with a spatially simplified model that consists of an epilimnion, hypolimnion and sediment but is horizontally well-mixed. The model, using acceptable ranges for plankton growth parameters, verifies observed data on phytoplankton, zooplankton and nutrient levels and as such can form a first basis for estimating the lake-wide effects of a nutrient reduction program.

The results indicate that the spring growth phase and peak phytoplankton biomass are primarily controlled by increasing light and temperature and phosphorus limitation. The mid-summer minimum in phytoplankton is estimated to be due principally to zooplankton grazing and nitrogen limitation. The broad fall peak in phytoplankton is a complex interaction of nutrient regeneration (up to five times the external nutrient inputs), subsequent nutrient limitation and then fall overturn. Both nitrogen and phosphorus are important nutrients in this dynamic succession.

From a water quality viewpoint, peak values of biomass in the spring are important, and are generally limited by phosphorus concentrations which reduce the nutrient growth rate by 35%. Nitrogen also has an additional effect of about a further 10% drop in growth rate. In the late summer months, it appears that the system is nitrogen-limited as well as phosphorus-limited. There may be important implications of this hypothesis; to wit, nutrient removal programs

aimed solely at phosphorus may not achieve a sought-after objective especially in the late summer recreation months. This is especially relevant when one recognizes that generally this period of the year is dominated by the green and blue-green algae, which have greater potential for water use interference than do the diatoms.

A period of 10-20 years may be necessary for Lake Ontario to reach a new level of dynamic equilibrium in phytoplankton biomass after a nutrient program is instituted. The long detention times, recycling effects and large store of nutrients in the hypolimnion are the principal reason for this long response. Therefore, the Lake Ontario presently being observed represents conditions of about 10-20 years ago and since loads into the upper basin (e.g., Lake Erie) have been increasing steadily over the years, Lake Ontario is obviously in a "slowly" varying state from year-to-year. Thus, the effects of a waste removal program may not be apparent for approximately one-two decades and if some residual loads are allowed to continue to grow, significant changes in Lake Ontario quality may "never" be apparent. This also implies that a detailed program of sampling of effluents and tributaries and concurrent lake-wide sampling are correlated only through an approximate ten-year lag. The results also indicate that surveillance of large lake systems such as Lake Ontario may best be accomplished in a time scale of perhaps once every five years rather than year-to-year.

All of these observations on response times apply to the lake as a whole. The more detailed Lake 3 model which includes horizontal detail will obviously reflect more localized situations which may (or may not) reach dynamic equilibrium in shorter times.

CHAPTER 7

LAKE 2 ANALYTICAL INVESTIGATIONS

7.1 INTRODUCTION

As illustrated in Figure 4, a strategy of essentially parallel investigations has been pursued in the development of Lake Ontario phytoplankton models. The Lake 2 investigation has results in a theoretical analysis, as opposed to numerical investigations of the vertical interactions in phytoplankton populations. Two specific areas are addressed: the behavior of the asymptotic population growth rate and the effect of vertical settling velocity.

The form of the equations for a quantitative theory of the distribution of phytoplankton biomass have been known for some time (Riley *et al.*, 1949) and their applications to various Great Lakes problem settings is ongoing (Di Toro *et al.*, 1973; Canale *et al.*, 1973; Thomann *et al.*, 1973). An analyses of the conditions required for temporal steady-state accompanied their introduction; however, no time varying analysis of their general properties has been made.

The condition under which a population can maintain itself against transport loss (Kierstead and Slobodkin, 1953) are related to the analysis to be presented insofar as an eigenvalue problem results, which gives the bounds on the parameter groups that result either in population increase or decrease. What has not been recognized is that if the population does increase, it asymptotically approaches a condition which is a substantial simplification of the general solution of the biomass conservation equation. In particular, it can be shown that there exists an asymptotic population growth rate, μ, which is independent of position, and an asymptotic population distribution, which completely characterize the solution to the biomass equation. The asymptotic solution depends on the kinetic and transport parameters and to find these dependencies it is necessary to make some simplifying assumptions. However, the general existence of the asymptotic solution follows directly from the assumption that, in fact, this prediction is born out by observed phytoplankton biomass distributions.

The specific spatial setting for the analysis presented subsequently is in the vertical dimension. The motivation for the investigation is a desire to calculate the effects of vertical settling velocity on phytoplankton population development; in particular, what are the important dimensionless parameter groups. Depending on the question to be addressed, a series of dimensionless plots are presented which give quantitative answers to the importance of the various parameters. In this way an economy is realized so that the complexity of even these idealized situations is kept to a manageable level.

A final product of this analysis is a demonstration that mathematical theory and biological fact can be brought into accord if the complexities of the latter are aggregated in such a way that the larger scale relationships are susceptible to a necessarily simplified mathematical treatment. The use of biomass as a the primary dependent variable is a biological example; the use of a dispersion coefficient is a physical example. The

result is a tractable mathematical problem which yields an array of information that can then be checked against observation. In this case, the prediction is the existence of an asymptotic population growth rate which is independent of position.

7.2 THEORETICAL CONSIDERATIONS

The conservation of phytoplankton biomass in the presence of vertical transport processes requires that the rate of change of the biomass with respect to time is the result of the balance between the kinetic source and sink of biomass and the vertical transport, the effect of which is to remove biomass from the euphotic zone. The equation is quite well known:

$$\frac{\partial P}{\partial t} - \frac{\partial}{\partial z}\left(E\frac{\partial P}{\partial z}\right)$$
$$+ \frac{\partial}{\partial z}(wP) = (G - D)P \tag{56}$$

where E = vertical dispersion coefficient
 w = settling velocity, positive downward
 G = growth rate
 D = death rate
 P(z,t) = phytoplankton biomass

In the absence of vertical transport, the population of each depth would either grow exponentially if $G(z) > D(z)$ or decay exponentially if $G(z) < D(z)$. In fact, for E = w = 0, it is clear that the solution is of the form:

$$P(z,t) \sim exp\,[G(z) - D(z)]t \tag{57}$$

so that G-D is the net growth or decay rate of the population in a kinetic reactor with conditions comparable to those at depth z. The magnitude of G is quite well known (Di Toro et al., 1971; Eppley, 1972) from numerous short-term growth experiments. For the case of excess nutrients and constant optimal light intensity, G is in the range of 1.5-2.5 day^{-1} at 20°C. The decay rate, D, for a population isolated from a light source is

on the order of 0.05 to 0.2 day^{-1} at 20°C (Riley et al., 1949). Thus, in the absence of vertical transport and with excess nutrients present, there should exist a depth at which the population is growing at a rate on the order of 1.0 day^{-1} so that in ten days the population at this depth increases by approximately 22,000 times. At large depths, however, the population should, in ten days, decrease to approximately 37% of its initial concentration. Such explosive growth does occasionally occur (patch blooms) but the more normal course of events is a much slower growth of the entire population until either nutrient exhaustion, zooplankton predation, or self-shading reduce G-D to a point at which population growth ceases. The question of interest is how does the population growth rate depend on the kinetic parameters, G and D, the transport parameters, E and w, and the variation of growth rate with depth due to light extinction.

If conditions are such that the population does increase with time, and for a period the transport and kinetic parameters are constant in time, then there are mathematical reasons, given subsequently, to expect that after a relatively short time the population distribution will be of the form:

$$P(z,t) \simeq P(z)\,e^{\mu t} \tag{58}$$

that is, the entire population will be growing at an asymptotic population log growth rate, μ, independent of depth. The asymptotic population growth rate and the asymptotic population distribution as a function of depth, P(z), aside from a constant multiple, are independent of the initial biomass distribution P(z,0) at the time of the start of the population growth (arbitrarily taken as t = 0). They depend only on the kinetic and transport parameters which characterize the period of population growth. This is a substantial simplification of what, in general, are complex and difficult solutions to the biomass equation and from this simplification follows substantial insights into the behavior of phytoplankton populations during their growth phase.

63

7.3 ASYMPTOTIC POPULATION GROWTH RATES

To establish that, in fact, phytoplankton biomass behaves as predicted by the mathematical analysis, a series of plots of log P(z,t) versus time at various depths are presented in Figures 29 through 32.

During the winter and spring, the horizontally averaged phytoplankton biomass in Lake Ontario increases quite slowly but the increase is approximately exponential as shown in Figure 29. The data collected during the 1973 IFGYL cruises shows this population growth and, in particular, it is approximately the same for all depths to 50 meters. Since the population growth rate is quite small, and the time for the development of the asymptotic distribution is on the order of $1/\mu$, in this case approximately 100 days, it is not surprising that the lower layers have not yet responded in the predicted manner.

During the intensive Project Hypo study of central Lake Erie (Burns and Ross, 1972), the phytoplankton population increased approximately five-fold in 35 days. As shown in Figure 30, the asymptotic population growth rate was $\mu \simeq 0.043$ day^{-1} and again the population increased at this exponential rate at 1, 12 and 17-20 meters, with the population in the deeper layers (21-25 meters) acquiring this growth rate near the end of the sampling period. The time to achieve the asymptotic distribution in this case is on the order of 25 days.

Onondaga Lake is a small (12 km^2 surface area, 20 m maximum depth), highly eutrophic lake in New York State (O'Brien and Gere Engineers, Inc., 1971). The duration of the growth period for the phytoplankton population is 150 days during which the population increases 1,000-fold to concentrations of 105 cells/ml corresponding to a population growth rate of $\mu = 0.048$ day^{-1}. As shown in Figure 31, the population growth rate is approximately the same at the four depths sampled even though there is almost an order of magnitude less biomass in the deeper layers.

St. Margaret's Bay is a coastal inlet on the southern shore of Nova Scotia (Platt and Irwin, 1973). Similar behavior is observed during the period of exponential growth. The population growth rate is 0.16 day^{-1}, substantially larger than those of the previous examples. The deviations from the predicted constant population growth rates in the lower layers cannot be attributed to the time it takes to achieve the asymptotic distribution since at this large μ, ten days should be quite sufficient. It appears that self-shading is causing the growth rate in the lower layers to decrease as the population increases in the top layers, thus violating the assumption that the parameters are constant in time.

Taken as a whole, the data presented strongly suggests that during the exponential growth of a population, if the kinetic and transport parameters are constant, an asymptotic population growth rate occurs which characterize the growth of the entire population, independent of position.

7.4 SOLUTIONS FOR SPECIFIC CASES

The existence of an asymptotic population growth rate, independent of depth for temporally constant parameters, is a consequence of the properties of the general mass balance equation. In order to investigate the relationship between this growth rate and the parameters of the equation, it is necessary to make certain assumptions concerning the variations in depth of the kinetic and transport parameters. In particular, assume (not very realistically for some cases) that all the parameters, save the growth rate, are constant. For the growth rate, two forms lend themselves to analytical solutions:

A two-layer approximation:

$$G(z) = G \qquad 0 \prec z \prec L$$
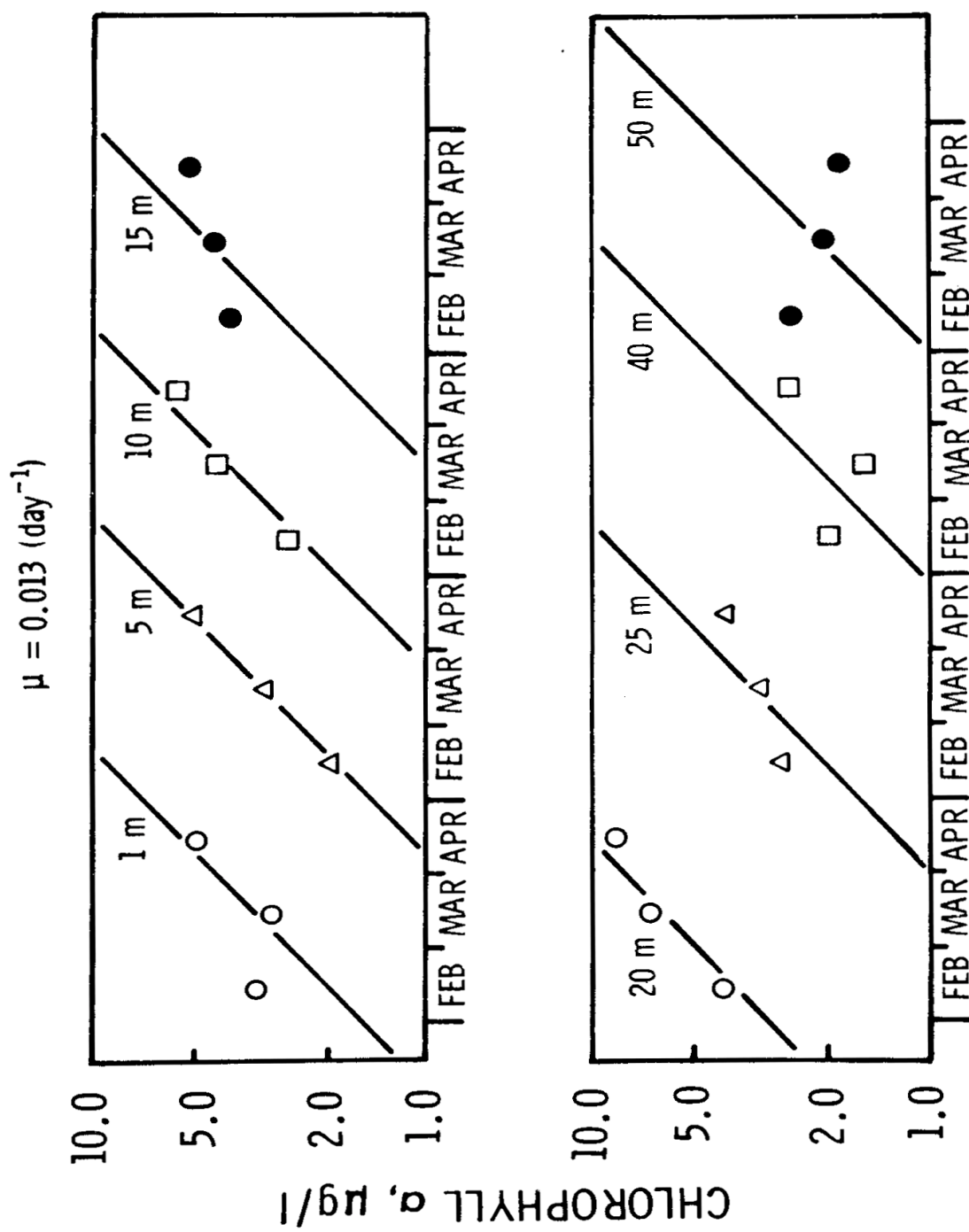$$= 0 \qquad L \prec z \tag{59}$$

64

Figure 29. Lake Ontario phytoplankton biomass, horizontal averages, IFYGL, 1973.
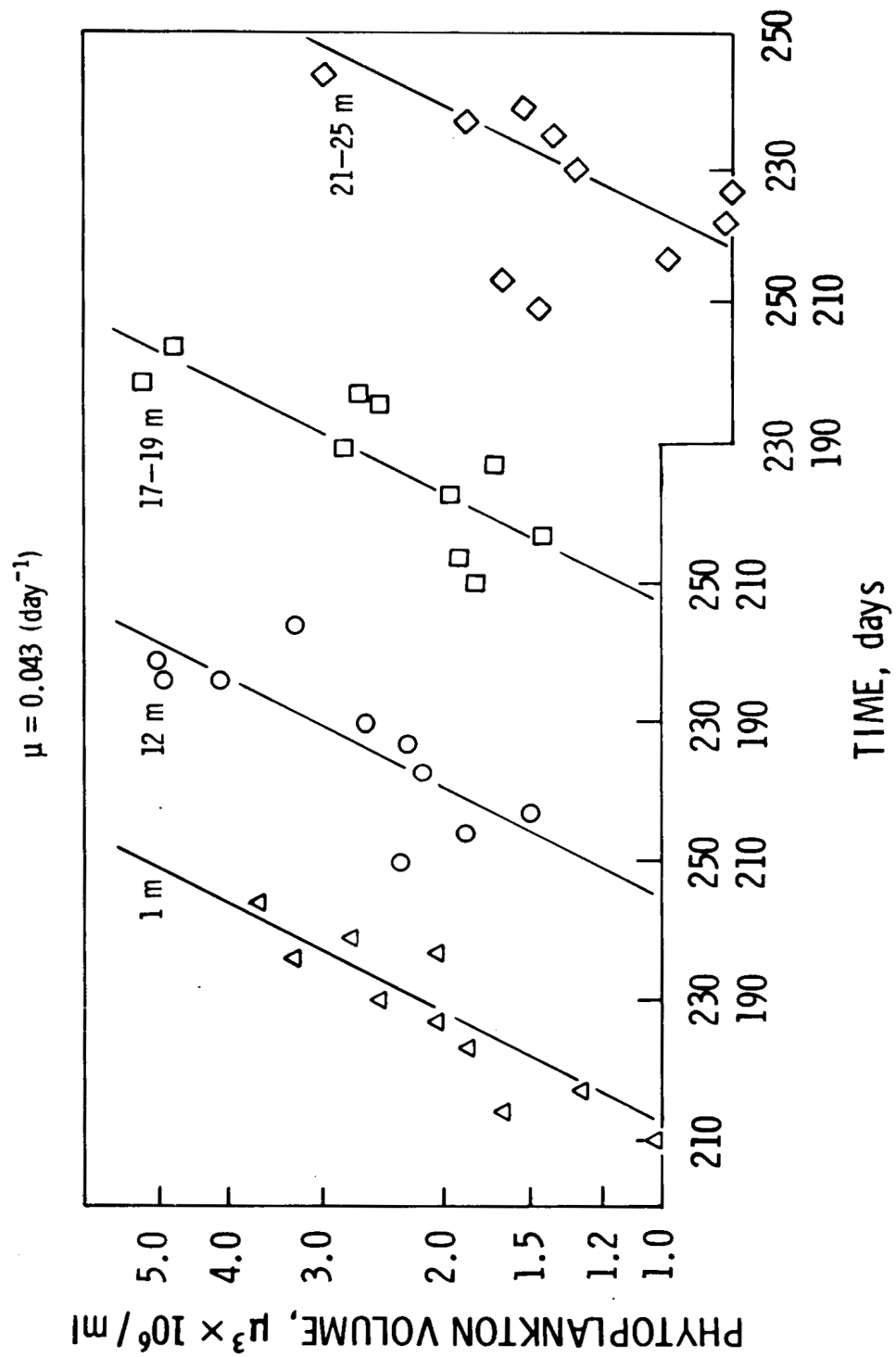
Figure 30. Central Lake Erie phytoplankton biomass, four station log averages, Project Hypo, 1970.
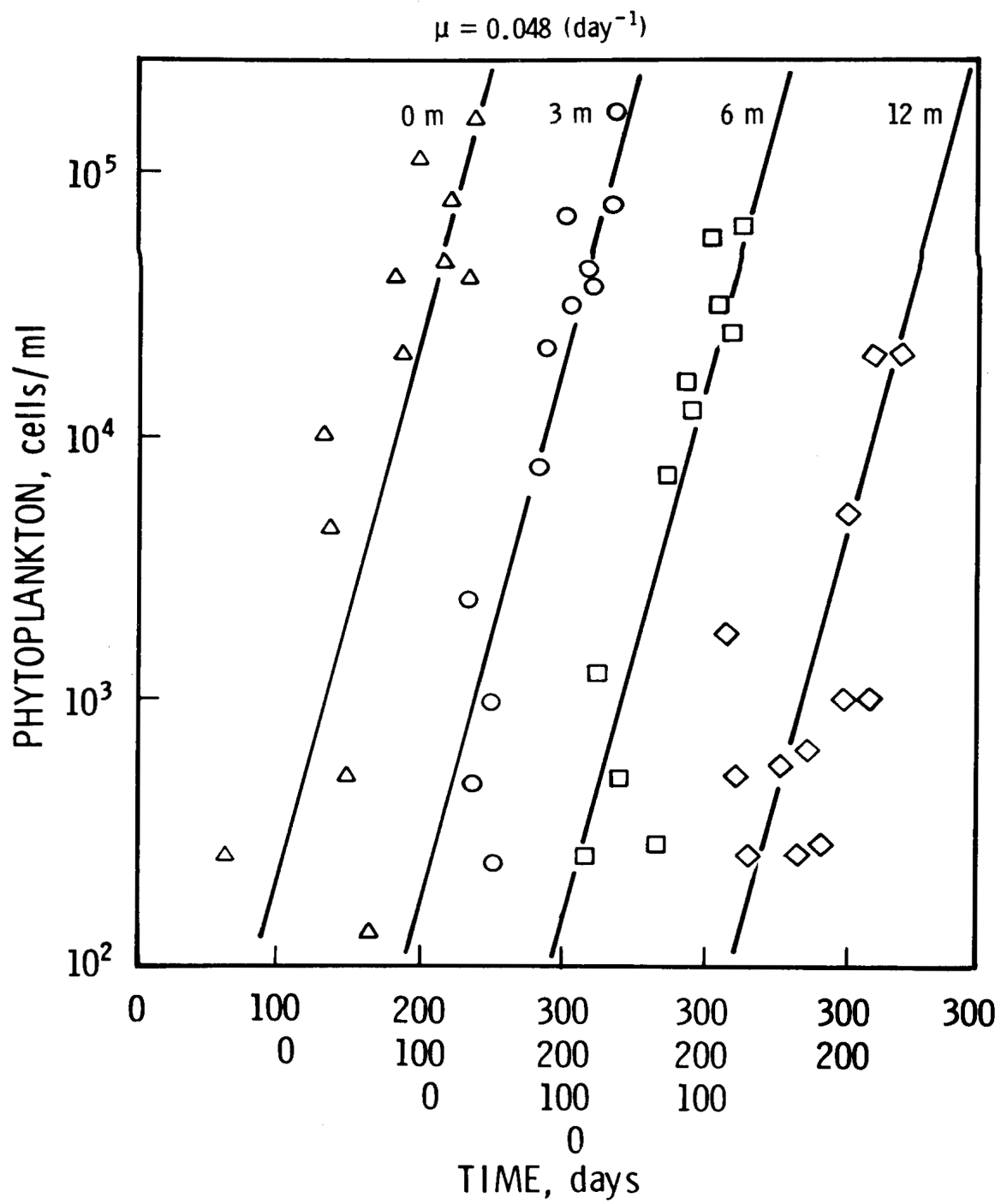
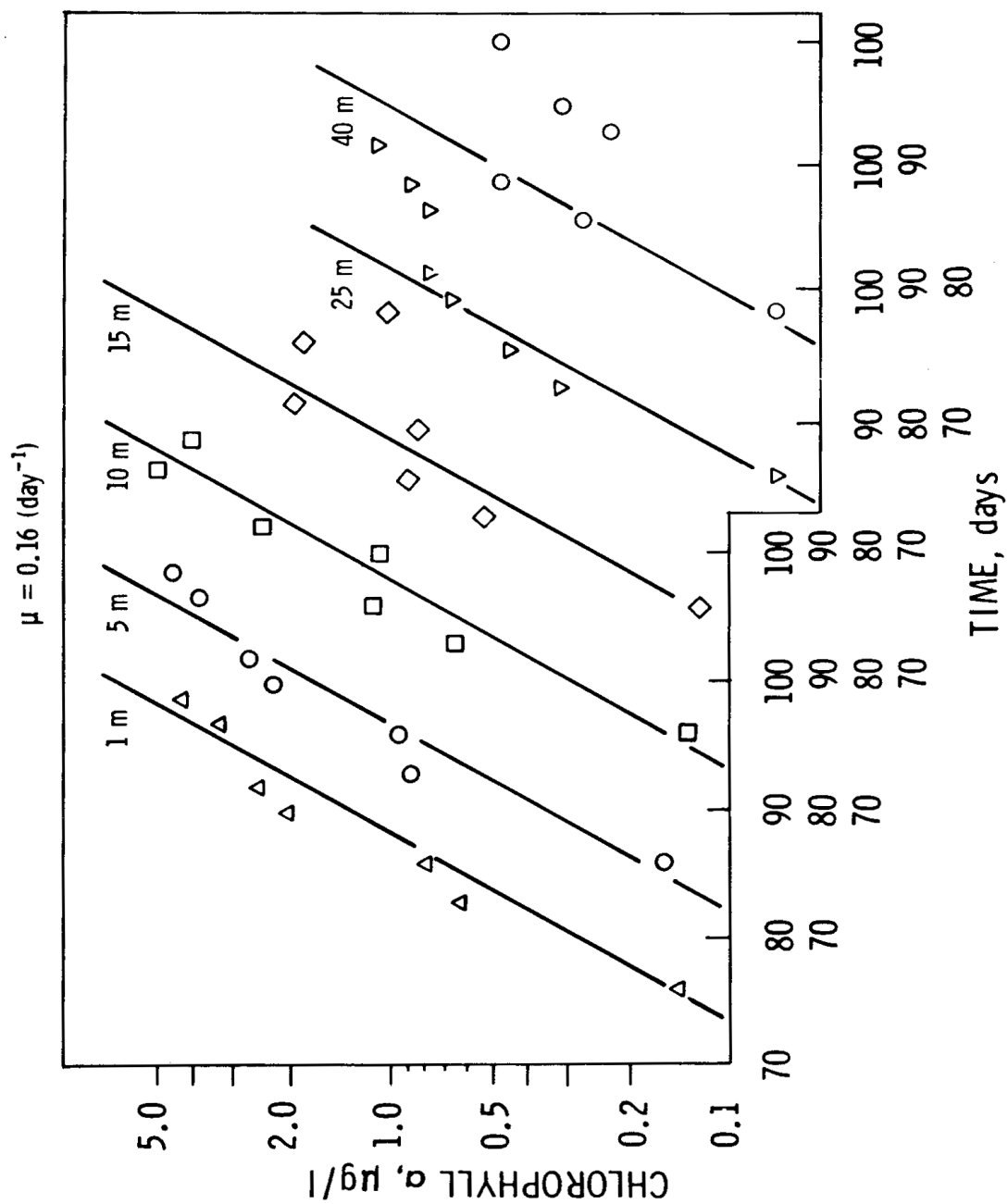Figure 31. Onondaga Lake phytoplankton biomass, two stations, 1969.

Figure 32. St. Margaret's Bay phytoplankton biomass, Station A, 1969.

and an exponential approximation:

$$G(z) = G e^{-z/L} \tag{60}$$

The solution proceeds directly using the asymptotic solution (Equation 58). Substituting it into the conservation of mass equation (56) yields:

$$-E\frac{d^2P}{dz^2} + w\frac{dP}{dz} = [G(z) - (D + \mu)]P \tag{61}$$

This equation is solved together with the boundary condition at the water surface:

$$-E\frac{dP}{dz} + wP = 0 \ \ at \ z = 0 \tag{62}$$

which requires that no biomass cross the air-water interface, and the boundary condition at infinite depths, for which we require that the biomass remain finite. The result is an eigenvalue problem to find μ and $P(z)$ for the above ordinary differential equation with the homogenous boundary conditions.

For the exponential case, the differential equation (56) becomes:

$$-E\frac{d^2P}{dz^2} + w\frac{dP}{dz} - [Ge^{-z/L} - (D + \mu)]P \tag{63}$$

which has a solution (Murphy, 1960):

$$P(z) = e^{\pi z/2L} J_v (2\lambda e^{-z/2L}) \tag{64}$$

where $\ \ v = \sqrt{\pi^2 + 4\lambda^2/\kappa}$

$$\kappa = G/(D + \mu)$$

$$\pi = wL/E$$

$$\lambda = L\sqrt{G/E}$$

and $J_v(z)$ is a Bessel function of the first kind. At large depths, the solution becomes:

$$P(z) \approx \exp{[(-\sqrt{1 + \frac{4\lambda^2}{\pi^2\kappa}}) \frac{\pi z}{2L}]} \tag{65}$$

which approaches zero exponentially. The eigenvalue equation is obtained from the boundary condition at z = 0 (Equation 62):

$$J_v(2\lambda)(1 + \frac{v}{\pi})\frac{\pi}{2\lambda} = J_{v+1}(2\lambda) \tag{66}$$

A multiplicity of μ's are solutions for the equation; the one of interest is that which is largest and, more important, positive since it is the asymptotic population log growth rate. For certain sets of π and λ no positive μ exists. For such situations, no population increase is possible.

For the two-layer case, the solution is obtained in two parts: a sinusoidal solution in the euphotic zone, 0 < z < L, and a decreasing exponential thereafter. The eigenvalue equation is:

$$\pi = \frac{tan^{-1}(\frac{1}{\beta}) + tan^{-1}(\sqrt{\frac{1 + 4n}{\beta}})}{B/2} \tag{67}$$

where: $\ \ \beta = \sqrt{4n(\kappa - 1) - 1}$

$$n = (D + \mu)E/w^2$$

and $\ \ \ \ \kappa = \overline{G}/(D + \mu)$

The solutions of these eigenvalue equations is shown in Figure 33 in terms of the dimensionless ratio of growth rate of the sum of death rate and population growth rate G/D + μ; a penetration depth $L\sqrt{G/E}$ which characterizes the size of the euphotic zone in terms of the growth rate and the dispersion coefficient; and a peclet number wL/E, which is the ratio of advective
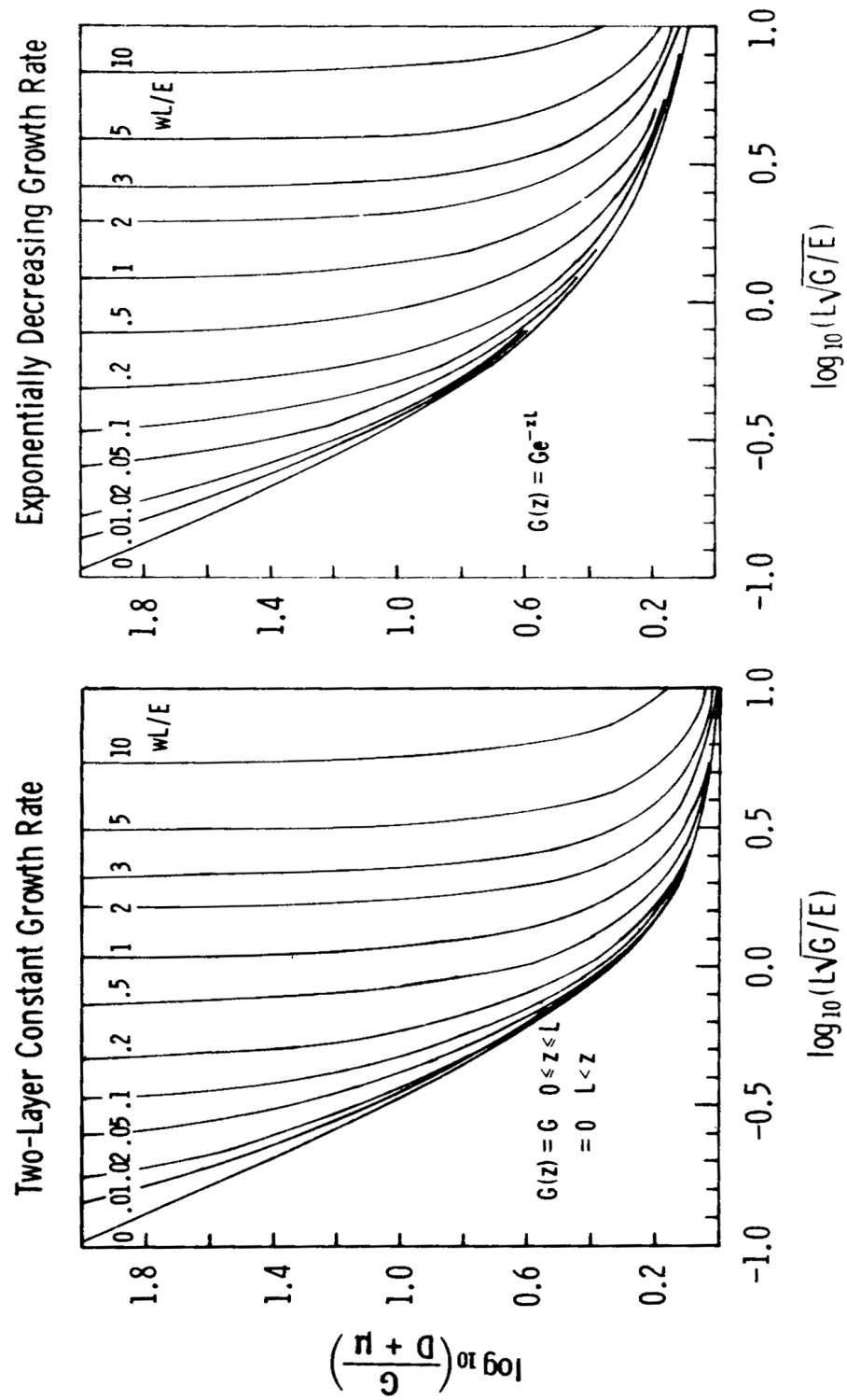
Figure 33. Eigenvalue equation solutions for constant growth layer and exponentially decreasing growth rate cases.

transport to dispersive transport. The values for the exponential case are given in Table 10. It is interesting to note that the shapes and magnitudes of the results are comparable, indicating that the details of the vertical distribution of the growth rate are not critical to the conclusions that can be drawn. As an example of their utility, consider the effect of settling velocity for the range of G/D + μ < 10m, it is clear that a peclet number, wL/E, of greater than 0.1 is required to affect the growth rate of the population.

It is this kind of order of magnitude analysis for which the analytical expressions are most suited. For more realistic investigations of detailed properties of the population, resort to direct numerical methods is usually necessary.

7.5 THE SINGLE LAYER APPROXIMATION

It is common practice in one-layer models (Steele, 1956) of the euphotic zone to approximate the effect of the settling velocity on the population by comparing w/L to the growth rate G. This approximation comes from the resulting differential equation for the euphotic zone layer:

$$\frac{dP}{dt} = (G - D - w/L)P + E'(P_1 - P) \qquad (68)$$

or E' the bulk mixing coefficient and P_1 the hypolimnion concentration. It is clear that in this approximation, changes in the w/L can be exactly compensated for by changes in G. To check the validity of this approximation against the continuous solution, consider Figure 34, a plot of w/L versus G, both normalized by D + μ. The exponentially decreasing growth rate case is used. It is clear that no positive asymptotic growth rate exists if w/L > G so to this extent the approximation conveys the correct impression. In order to interpret this figure in more detail,

Table 10. Log$_{10}$ (G/D + μ) for Exponentially Decreasing Growth Rate

$\text{Log}_{10}(\lambda)$ π	- 1.0	- 0.9	- 0.8	- 0.7	- 0.6	- 0.5	- 0.4	- 0.3	- 0.2	- 0.1
0.50										2.0281
0.20								1.7007	1.0358	0.7731
0.10							1.4158	1.0455	0.8251	0.6681
0.05					1.9903	1.4123	1.1192	0.9129	0.7536	0.6263
0.02			2.3352	1.7515	1.4364	1.2021	1.0105	0.8519	0.7172	0.6038
0.01		2.2545	1.8509	1.5721	1.3456	1.1512	0.9816	0.8337	0.7059	0.5966
0.00	2.0170	1.8226	1.6325	1.4464	1.2724	1.1068	0.9542	0.8166	0.6951	0.5897

| $\text{Log}_{10}(\lambda)$ π	0.0	0.1	0.2	0.3	0.4	0.5	0.6	0.7	0.8	0.9
5.00							1.2401	0.5484	0.3512	0.2479
3.00						0.7034	0.4394	0.3106	0.2322	0.0795
2.00				1.4192	0.6510	0.4352	0.3186	0.2440	0.1920	0.1540
1.00		1.4778	0.7376	0.5114	0.3842	0.3002	0.2401	0.1950	0.1602	0.1327
0.50	0.9140	0.6411	0.4880	0.3856	0.3113	0.2548	0.2106	0.1754	0.1469	0.1235
0.20	0.6083	0.4908	0.4020	0.3326	0.2771	0.2322	0.1953	0.1649	0.1395	0.1183
0.10	0.5486	0.4545	0.3789	0.3175	0.2670	0.2253	0.1906	0.1615	0.1372	0.1167
0.00	0.4994	0.4228	0.3580	0.3034	0.2575	0.2187	0.1860	0.1583	0.1349	0.1150
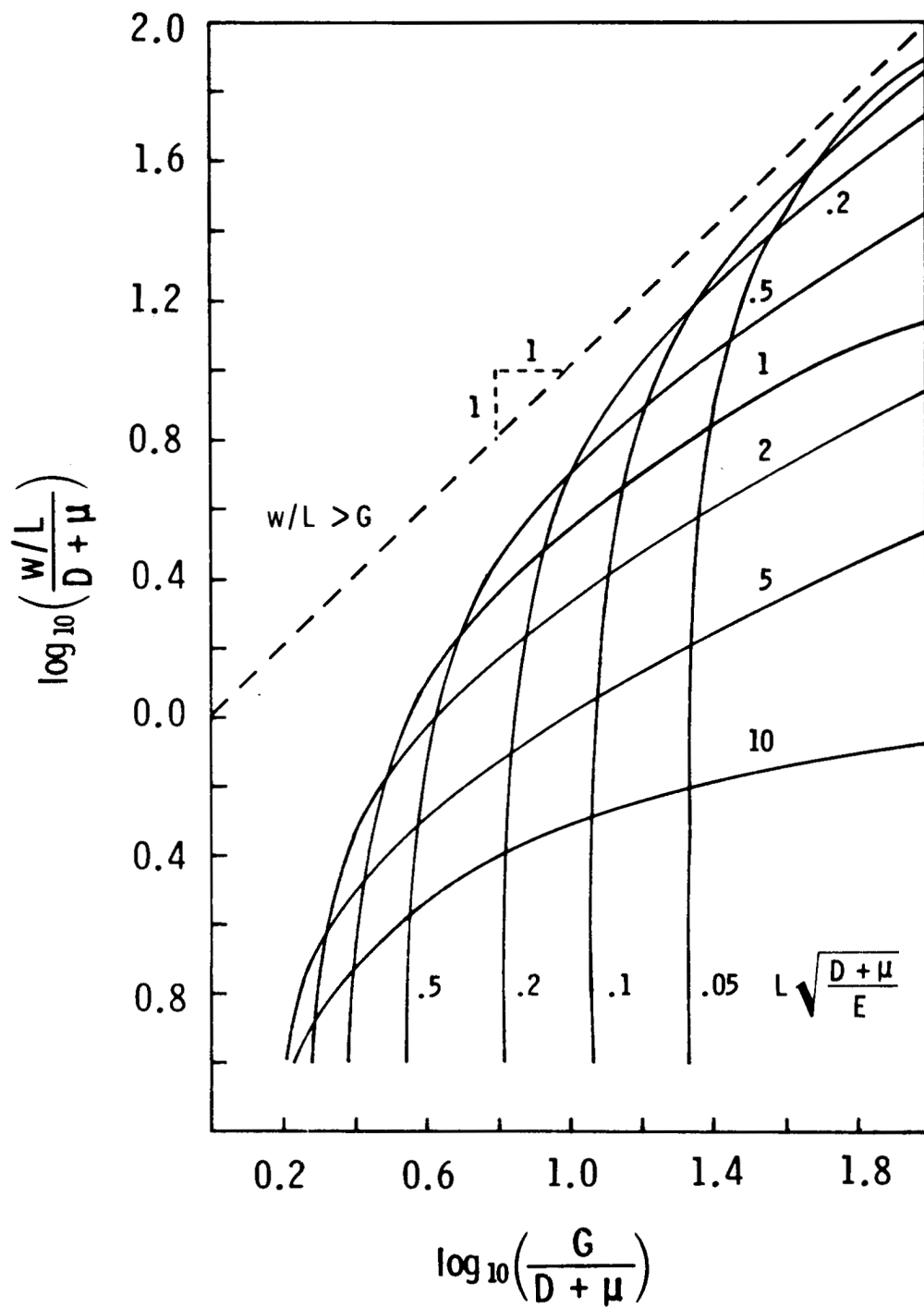
Figure 34. Settling velocity-growth rate interaction - the effect of dispersion. Exponentially decreasing growth rate case.

assume that D + μ and L are fixed, and the plot is w/L versus G for varying dispersion coefficient. For large vertical dispersion, $L\sqrt{D + \mu/E}$ is small and the solution is independent of w/L, or, put another way, w/L can change without demanding a compensating change in G to keep μ constant. What is occurring is that the settling biomass is being rapidly remixed into the euphotic zone so that the loss via this mechanism is small relative to the loss by dispersive mixing. On the other hand, for a small vertical dispersion the curves bend to such an extent that their slope is greater than one, indicating that for this situation it requires larger than proportional increases in G to compensate for increases in w/L. The meaning of this unexpected result will become clear subsequently.

7.6 THE EFFECT OF INCREASING GROWTH RATE

For various euphotic zone depths (assuming the transport parameter w and E are constant) the effect on μ of increasing G is shown in Figure 35. It is immediately clear that no solutions are possible for which μ > G - D, which is obviously true since such a situation would require that mixing and settling have no effect on the population and that the fact the G(z) decreases in depth is unimportant. Perhaps a more unexpected result is that the slopes of the curves are greater than one, indicating that a change in G causes a larger than proportional change in D + μ. As G is further increased, however, the population growth rate asymptotically approaches G - D as expected, and since there are nonzero values of G for which D + μ is zero, it is reasonable that the slopes are greater than one to enable D + μ to, in effect, catch up with G. The condition G = D + μ occurs at smaller G for deeper euphotic zone, as expected.

7.7 THE EFFECT OF INCREASING SETTLING VELOCITY

For various euphotic zone depths (assuming G and E are constant) the effect on μ of increasing w is shown in Figure 36. As w is increased, the population growth rate is not affected until a critical range is reached at which time the effect begins. Further increases cause a sharp drop off in μ until population growth is no longer possible.

7.8 THE EFFECT OF INCREASING DISPERSION

The effect on μ of increasing the dispersion coefficient, E, for various euphotic zone depths (assuming G and w are constant) is shown in Figure 37. A most surprising result is that for the range of the parameter, EG/w2 below one and LG/w < 10, increasing the dispersion increases the asymptotic growth rate. At first glance, this appears to be incorrect since the mixing causes the population in the euphotic zone to be transported out of the zone, on balance, and therefore, would tend to decrease population growth. However, biomass is also being advected out of the zone via the settling velocity. With a small dispersion coefficient, there is very little biomass at the surface since there is no way for the population, which grows as it sinks, to return to the surface layers. Hence, increasing the mixing actually benefits the population by allowing more biomass to accumulate in the surface layers where the growth rates are largest. It is this phenomena which causes the slopes greater than one in Figure 34 for small dispersion coefficients.

7.9 THE EFFECT OF BUOYANCY

It is well known that certain species of phytoplankton exhibit negative sinking velocity and an *in situ* measurement has confirmed an example (Burns and Pashley, 1974) so that instead of a liability their buoyancy is an asset which should increase population growth. Figure 38 presents the results. For negative peclet numbers with magnitude less than 0.2, not much increase in μ is calculated. However, as |w|L/E increases further, the population growth rate approaches the maximum possible, i.e., μ + G - D, independent of $L\sqrt{G/E}$ as indicated by the horizontal lines in the figure. The effect of the upward advection is to pile the biomass at the

73

Figure 35. Population growth rate versus maximum growth rate - the effect of euphotic zone. The exponentially decreasing growth rate case.
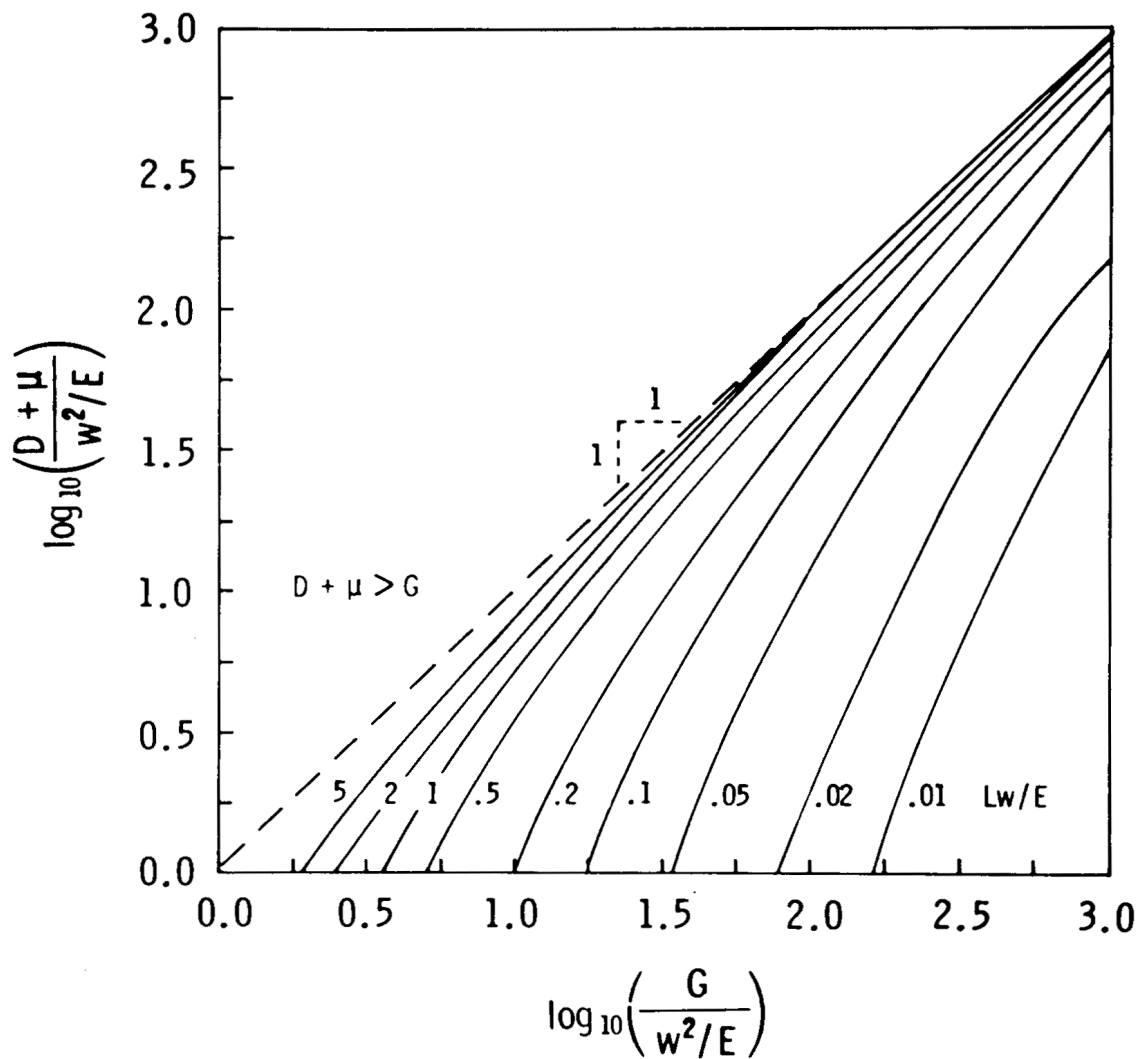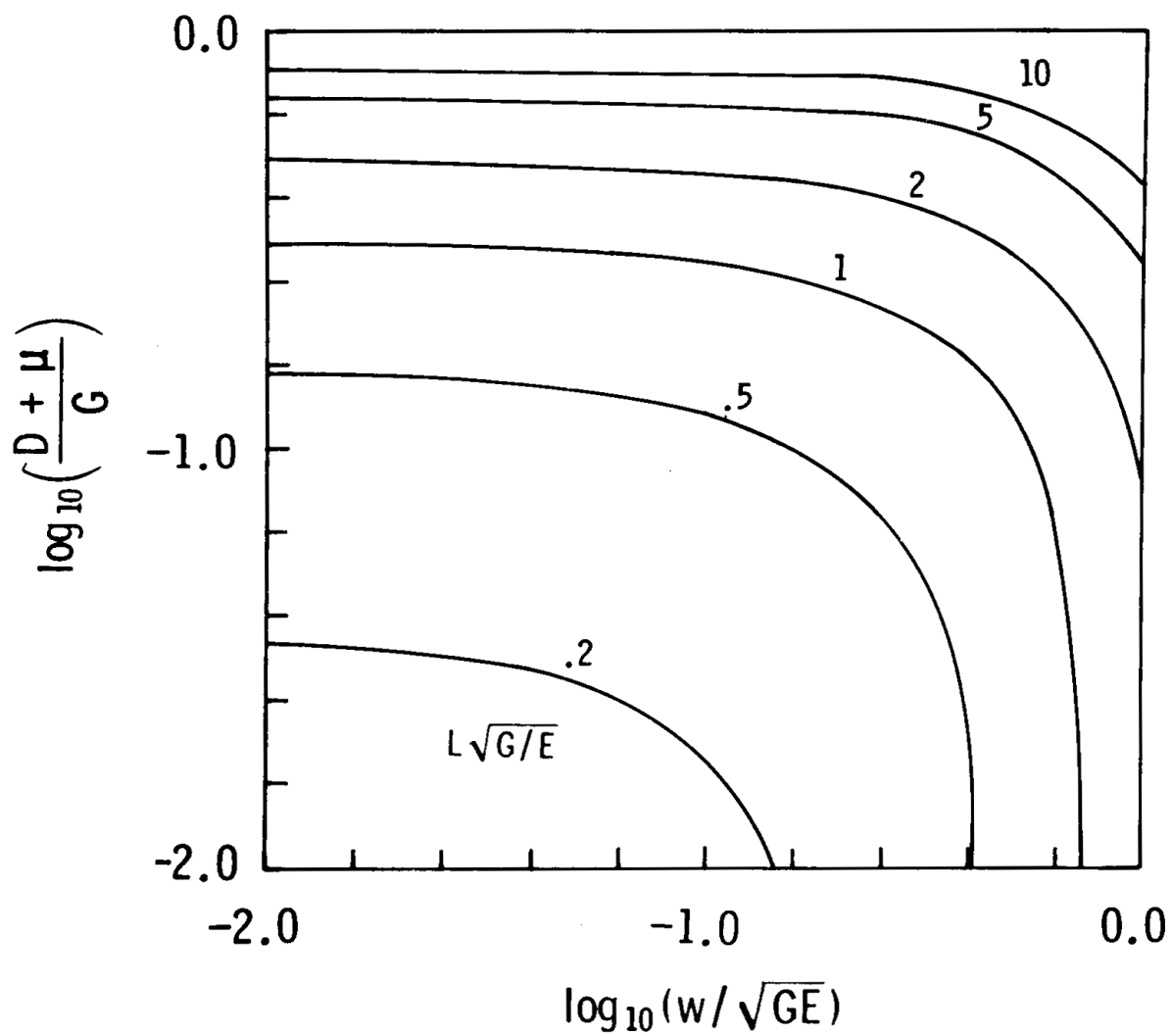
Figure 36. Population growth rate verus settling velocity - the effect of euphotic zone depth. The exponentially decreasing growth rate case.
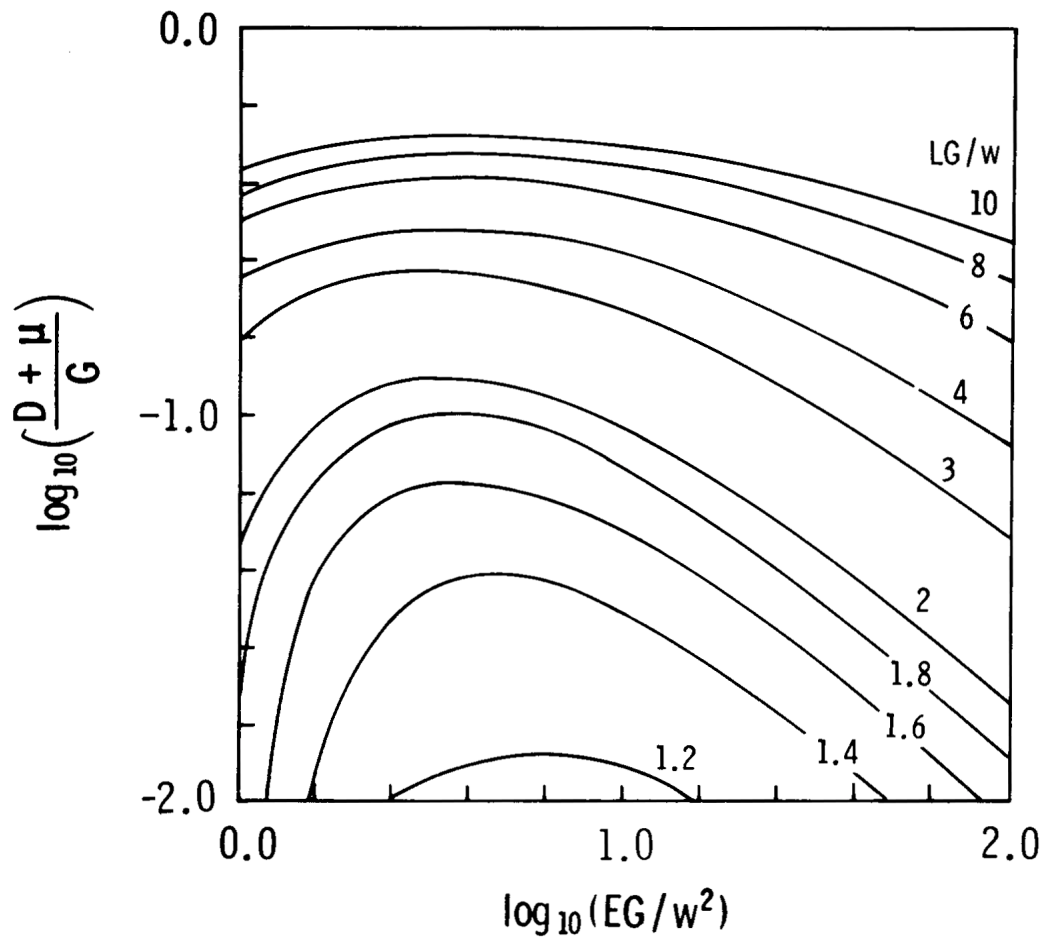
Figure 37. Population growth rate versus dispersion coefficient - effect of euphotic zone depth. The exponentially decreasing growth rate case.
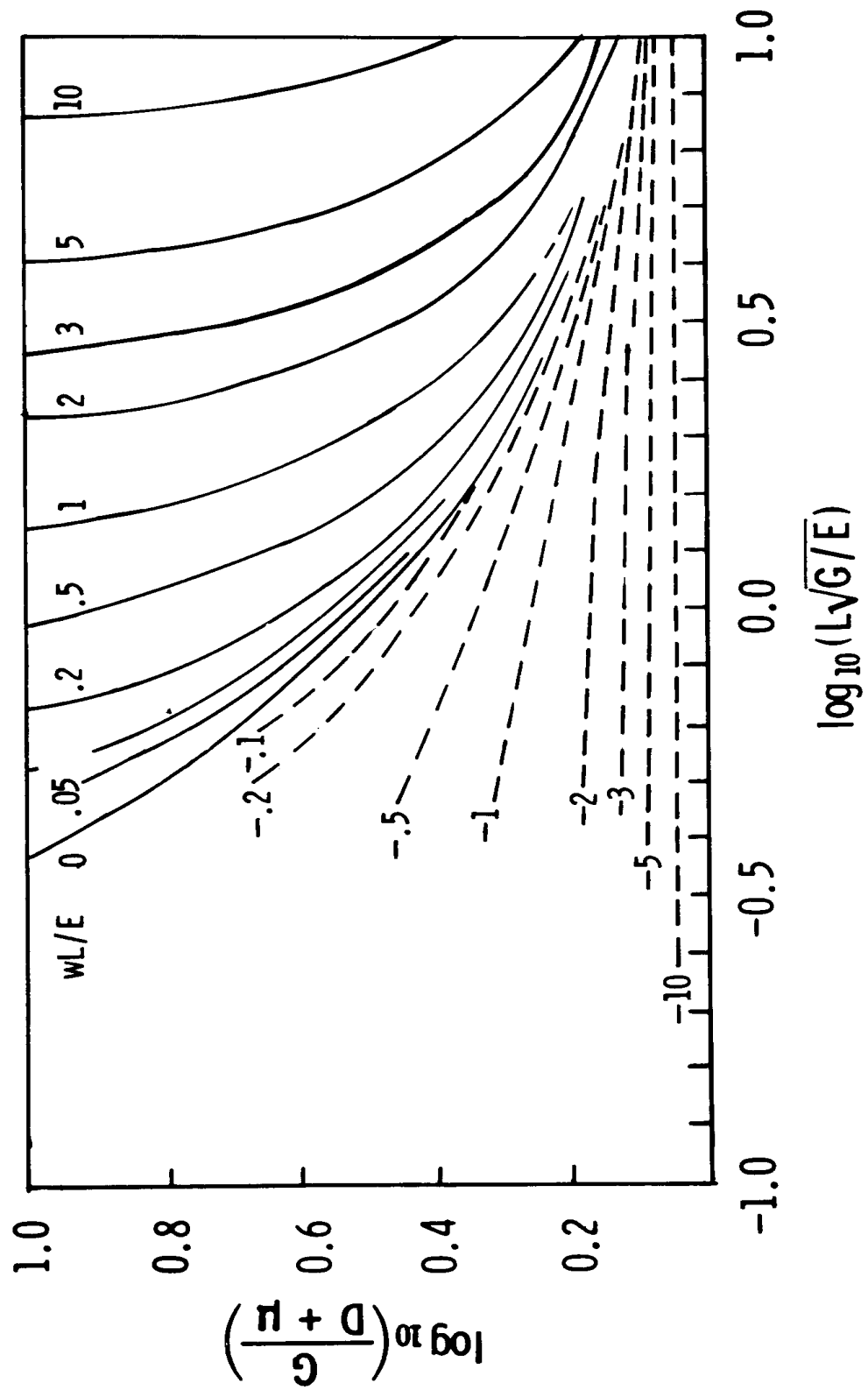
Figure 38. The effect of negative sinking velocity. The exponentially decreasing growth rate case.

surface where it can grow at the kinetic rate, G - D, independent of the dispersive forces tending to mix it downward. This effect occurs for the negative peclet numbers greater than 1.0, provided $L\sqrt{G/E}$ exceeds 0.3.

7.10 PRELIMINARY APPLICATIONS

As a first step in exploring the utility of the preceding analysis, a series of representative values for the dimensionless parameters are shown in Figure 39. The majority come from the coastal ocean (Riley *et al.*, 1949) with two lakes included. It is interesting to note that the values of G/D + μ are comparable whereas the value of $L\sqrt{G/E}$ span an order of magnitude. The major difficulty with increasing the number of points on this graph is in estimating the vertical dispersion coefficient and settling velocity. Values for G, D, and L for a given temperature, light intensity and extinction coefficient, can be approximated; μ is obtained from population observation, vertical dispersion can be obtained from vertical temperature models in which case the analysis, to within the accuracy of the assumption of constant parameters, can provide vertical settling velocities.

It is interesting to note that these data, when plotted on the figure which investigates the effect of dispersion, are in the range of the maxima for the oceanic situations and in the decreasing regions for the shallower situations. Whether this indicates some adaptive mechanisms for the characteristics of the marine phytoplankton is an interesting speculation but it is probably beyond the precision of the analysis to pursue this point.

7.11 SUMMARY OF MATHEMATICAL FACTS

The properties of Equation (56) are best illustrated by examining a spatially discretized version.

Let $P_i(t) = P[(i + ½) \Delta z, t]$ for a finite set of points starting at $\Delta z/2$ and spaced Δz apart thereafter. The spatially discrete version of the differential equation follows by using the approximations:

$$\frac{\partial^2 P}{\partial z^2} \simeq \frac{P_{i-1} - 2 P_i + P_{i+1}}{\Delta z^2} \tag{69}$$

$$\frac{\partial P}{\partial z} \simeq \frac{P_i - P_{i-1}}{\Delta z} \quad for\, w > 0$$

$$\simeq \frac{P_{i+1} - P_i}{\Delta z} \quad for\, w < 0 \tag{70}$$

There results a set of ordinary differential equation which can be written in matrix form as:

$$\frac{dP}{dt} = AP \tag{71}$$

Two properties of A are important:

1. A is essentially nonnegative, i.e.,

    $$a_{ij} > 0 \qquad I \neq j \tag{72}$$

2. A is irreducible, i.e., for any i,j there exists a finite sequence of indices k(0) = k, k(1), ..., k(r) = j, such that $a_{k(h-1),k(h)} \neq 0$ for h=1,..., r.

Property (1) follows directly from the fact that the off diagonal elements of A are made up of sums of $E/\Delta z^2$ and $w/\Delta z$ which are positive. Property (2) essentially requires that mass from any segment 1 can eventually be transported to any segment j, which is clear from the geometry of any reasonable problem.

The theorem (Birkoff and Varga, 1958) of interest is:

> The matrix A satisfying (1) and (2) has a unique (up to a multiplicative constant) strictly positive eigenvector ϕ_1, with real simple eigenvalue μ_1, i.e.,

$$A\phi_1 = \mu_1 \phi_1 \tag{73}$$

78
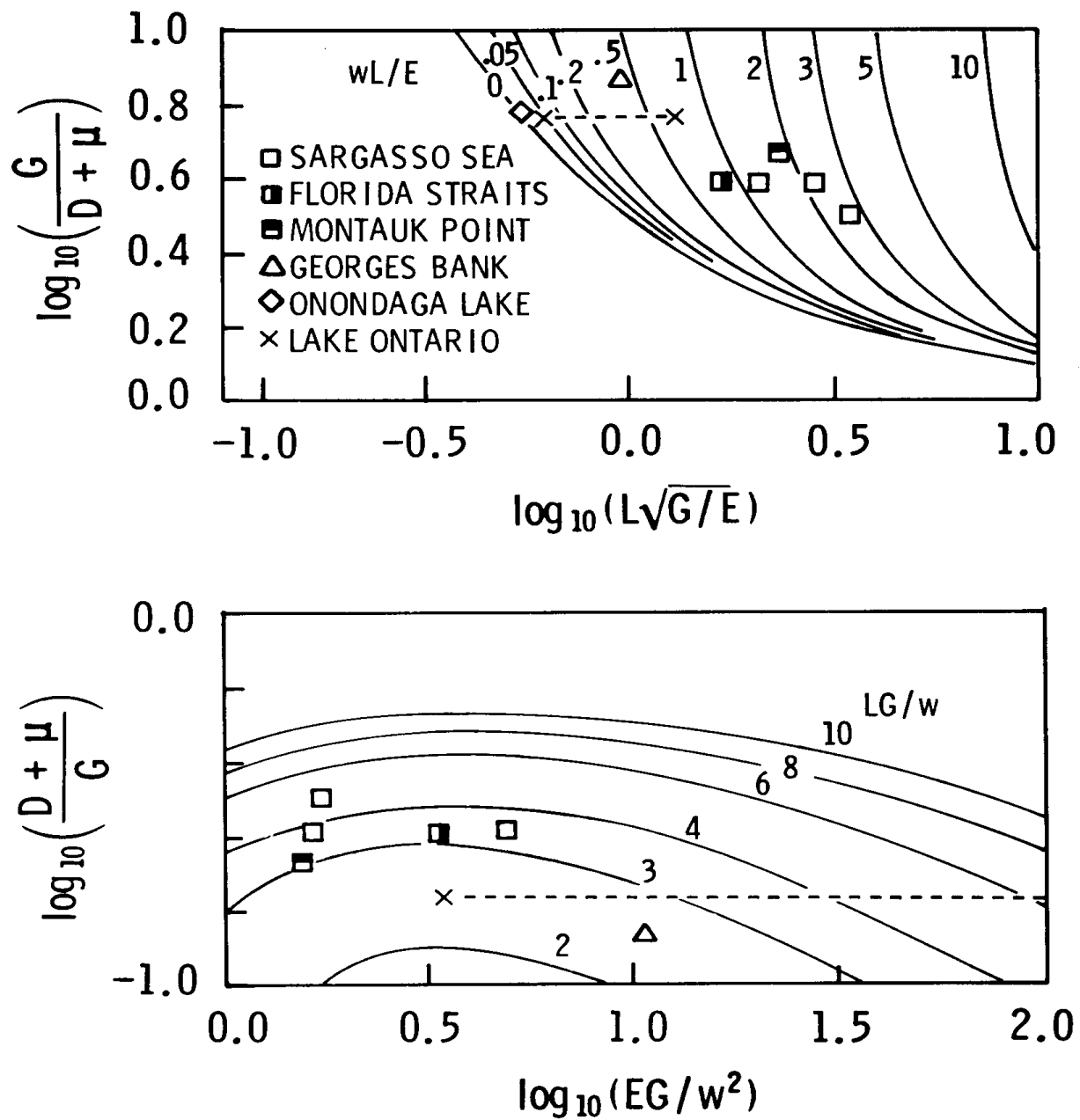
Figure 39. Application to lakes and oceans - the range of biologically relevant dimensionless numbers.

and μ_1 is the largest eigenvalue in the sense that

$$\mu_1 > Re\,[\mu_j] \tag{74}$$

for all the other eigenvalues, μ_j, of A.

It follows directly from this fact that the asymptotic solution of the differential equation (71) has the form:

$$P(t) = k\,e^{\mu_1 t}\,\phi_1 + o(e^{\mu t}) \tag{75}$$

where

$$\mu_1 > \mu > \max_{j \neq i} Re[\mu_j]$$

and k is a constant.

This fact can be proven directly (Birkoff and Varga, 1958). However, to see what is occurring assume that all eigenvalue μ_j are distinct so that n eigenvalue of the solutions exists (Bellman, 1960) of the form.

$$P(T) = \Sigma_j\,k_j\,e^{\mu_j t}\,\phi_j \tag{76}$$

where k_j are constants related to the initial condition $P(z,0)$. If μ_1 is positive and Re $[\mu_j]$ negative for all other j, then clearly the positive eigenvalue part of the solution dominates after a time on the order of $1/\mu_1$. If both μ_1 and μ_2 are positive (and μ_2 real for simplicity), the solution in segment i approaches:

$$P_i(t) = k_1\,e^{\mu_1 t}\,\phi_{1i} + k_2\,e^{\mu_2 t}\,\phi_{2i}$$

$$= k_1\,e^{\mu_1 t}\,\phi_{1i}\,(1 + \frac{k_2\,\phi_{2i}}{k_1\,\phi_{1i}}\,e^{(\mu_2 - \mu_1)t}) \tag{77}$$

but $\mu_2 < \mu_1$ so that the exponent is negative and it becomes small relative to one after a time on the order of $1/(\mu_1 - \mu_2)$ and again the maximum eigenvalue solution dominates.

CHAPTER 8

PRELIMINARY LAKE 3 MODEL

As shown in Figure 40, the Lake 3 model represents a synthesis of spatial geometry and transport structure with the biological and chemical kinetic interactions of the Lake 1 and 2 models. Lake 3 is, therefore, a three-dimensional, time-variable model which does permit some analysis of phenomena in the nearshore region as compared to the open lake region. The structure of Lake 3 represents a further step beyond the simple Lake 1 model, the extent of the step incorporating such factors as computational time for a one-year run and availability of survey data.

The work reported here is of a preliminary nature since considerably more effort is required to assure the veracity of the computed results both in terms of the numerical output and the degree to which the model verifies observed data. The full details and documentation of Lake 3 will be the subject of a future report.

The basic segmentation used for the Lake 3 model is shown in Figure 40. As shown, 67 segments are used distributed over five vertical layers. The upper two layers, 0-4 meters and 4-17 meters are considered to represent the epilimnion during periods of vertical stratification. A "ring" of segments extending 10 km out from the coast is used to represent the nearshore environment. All cross-sectional areas for interfaces in three-dimensions between the segments were planimetered and volumes were computed and summed to within 10% of total lake volume.

8.1 CIRCULATION AND DISPERSION

The emphasis in Lake 3 is on the biological and chemical kinetics rather than the hydrodynamic circulation, although the interaction between the kinetics and transport is important. The hydrodynamic circulation is, therefore, considered to be externally supplied through inferences from observations and/or hydrodynamic model output. An extensive literature exists on the circulation of Lake Ontario and relatively sophisticated mathematical models have been developed (Simons, 1971, 1972, 1973). A review of the complete development is given by Simons (1973). It is not intended, in this report, to provide a detailed review of the circulation in the lake and the various analytical and numerical model schemes that have been used to estimate the circulation. Rather, the purpose here is to simply report on the circulation that was used in some of the preliminary Lake 3 phytoplankton runs and the approximate sensitivity of phytoplankton dynamics to changes in the assumed circulation patterns.

This discussion will, therefore, outline the procedure used for establishing circulation patterns and flow exchanges in the 67-segment, five-layer, Lake 3 model. Two flow balances are presented, one corresponding to "summer circulation" and the other to "winter circulation".

It is known that Lake Ontario has two distinct net surface circulation patterns. During summer and fall the prevailing winds, the dominant factor governing water circulation, are from the west
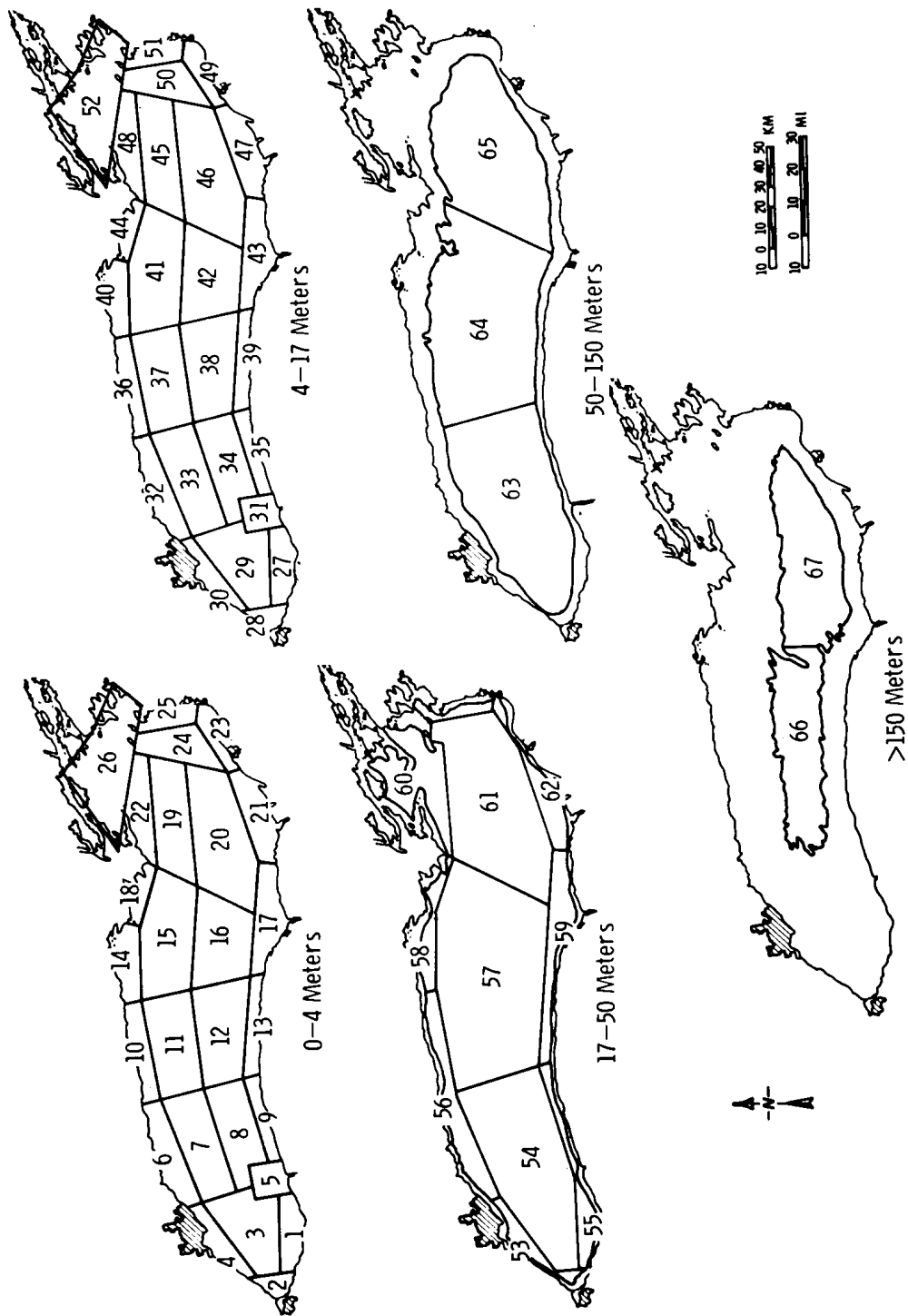
Figure 40. Lake 3 segmentation.

and southwest and one distinct circulation pattern is set up ("summer circulation"). During winter and spring, the prevailing winds are from the west and northwest and a different circulation pattern is established ("winter circulation"). The summer and winter circulations in Lake Ontario are associated with the stratified and isothermal temperature states of the water, respectively.

The IJC (1969) and the USEPA (Casey, 1965) have published summer circulation patterns for Lake Ontario. Mean monthly resultant velocity vectors that were observed and used by USEPA for establishing their circulation patterns were obtained from them for use in assigning velocity values to the general circulation vectors. Wide variance in magnitude and direction over each sampling station was encountered, however, even to the point where resultant velocity direction did not agree with the general circulation pattern. Typical stations were also chosen where values were assumed to be reflective of the average observed magnitude and direction. This procedure, however, yielded a poor flow balance and the scheme was discarded in favor of using the general values assigned to the summer circulation pattern by IJC (1969) as a guideline.

The water budget information contained in the IJC report was used for establishing tributary inflows to the various shoreline segments. It was decided to split the major inflow to Lake Ontario from the Niagara River (195,000 cfs) over the first and second vertical layers (0-4 and 4-17 meters) while restricting all other tributary inflows (Oswego River, Genesse River, Twelve Mile Creek, etc.) to the first layer (0-4 meters). The Niagara inflow was split volumetrically between segments 5 and 32 each receiving 4/17 and 10/17 of the flow, respectively.

Having established tributary inflow to the segments, segment flow balances were established and intersegment velocities were back calculated to check for agreement with the general values assigned by IJC. The final circulation pattern, as given by intersegment velocity values can be seen in Figure 41. It should be noted that since the Niagara River inflow was split between the first two layers only, there is no inflow and, hence, can be no outflow from the third layer. This is a good approximation since the average depth of the northeastern most segment (26 and 52 in the top two layers), the outflow segment, is only 20-25 meters while the third layer extends from 17 to 50 meters. In any event, the bathymetry dictates that there would not be much outflow in the third layer. No flows were assigned to segments in the fourth layer since with only three adjoining segments any inflow to one of the segments from another would have to be countered with the same back flow for a flow balance. The same applies to the fifth layer.

For the winter, the USEPA general circulation pattern corresponding to winds out of the west was used for establishing a flow balance. Bonham-Carter *et al.* (1973) wind-driven numerical model outputs a fairly similar circulation for a west wind. The model, however, indicates easterly flow along the north shore, while the USEPA circulation pattern indicates upwelling along the north shore. Since both agree the general transport is to the east, there would have to be return flow or upwelling and since the USEPA circulation pattern indicates areas of upwelling it was decided to use their general circulation pattern as a guideline for establishing a winter flow balance. Later discussion will indicate how Bonham-Carter *et al.* (1973) modeled circulation was set up to this segmentation scheme. The balanced velocity vectors are shown in Figure 42 and represent the assumed circulation for the winter condition. It should be noted that discrepancies exist in the literature in regard to Lake Ontario circulation, and that many of the numerical circulation models are awaiting IFYGL current measurements for verification. However, the Lake Ontario circulation must be calculated from the smaller (approximately 5 km) grid on to the larger grid of the phytoplankton model. As additional information becomes available, adjustments to eh circulation structure can be made.
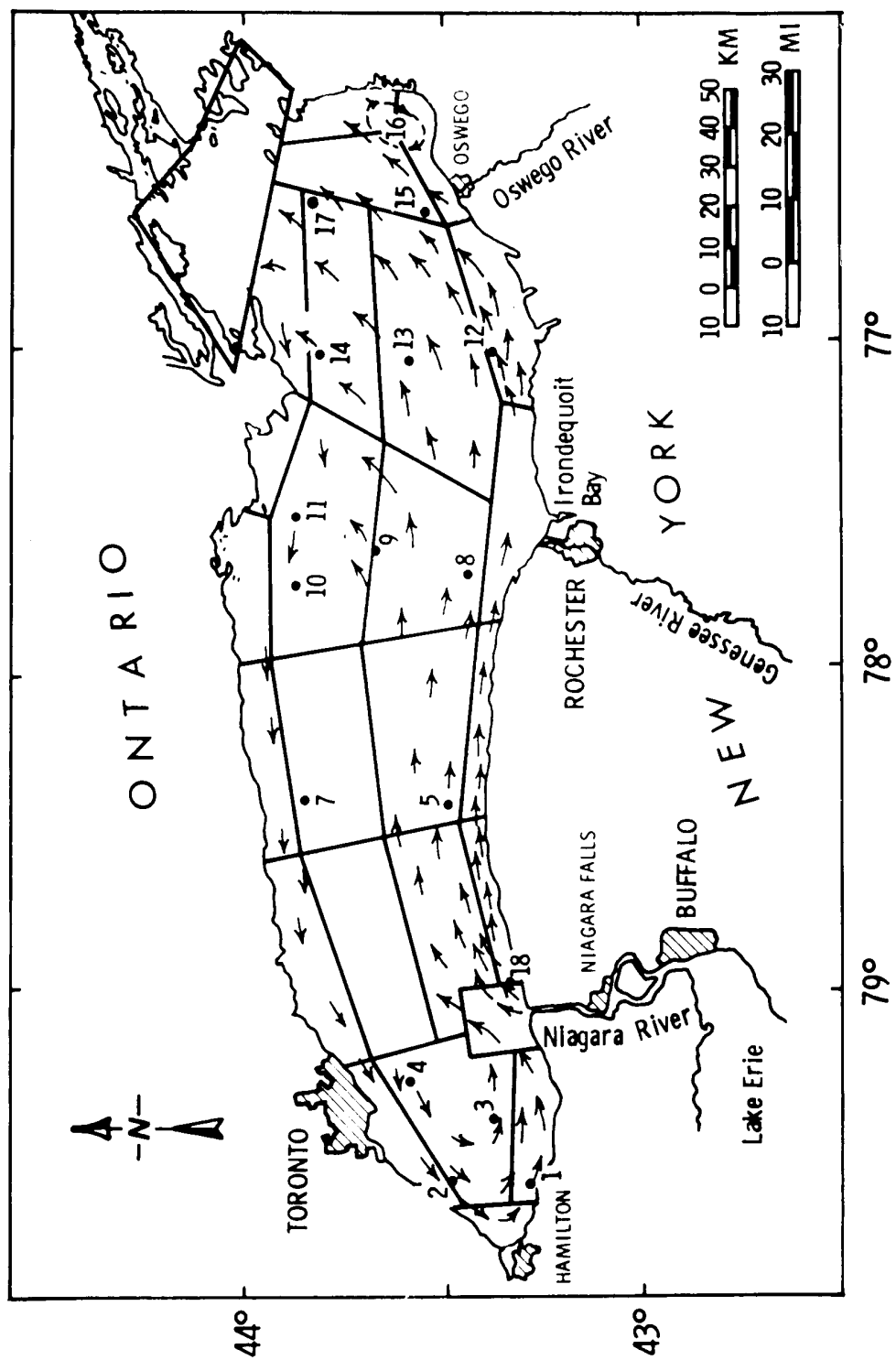
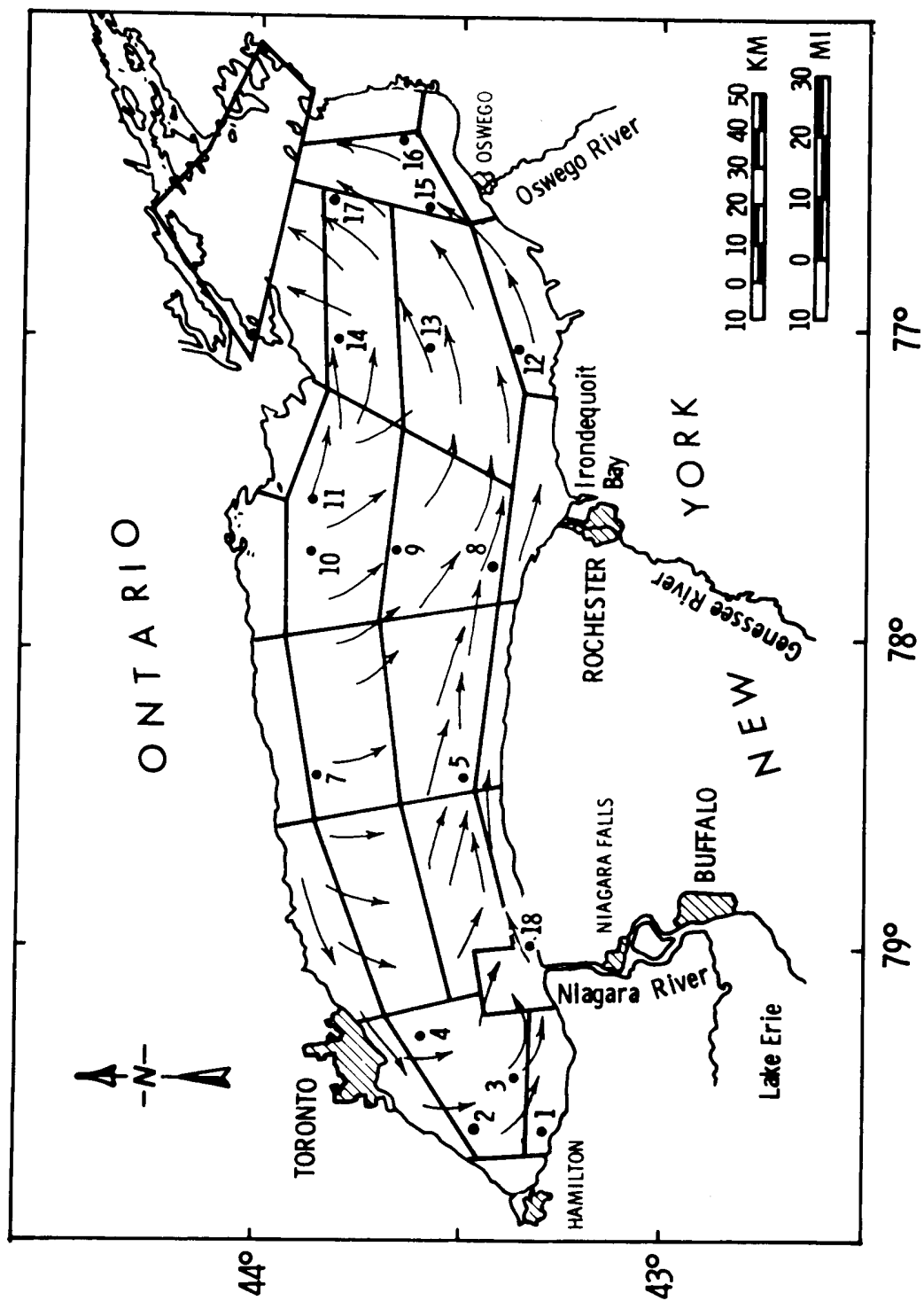Figure 41. Assumed summer circulation for Lake 3 model.

Figure 42. Assumed winter circulation for Lake 3 model.

Time and space varying horizontal and vertical dispersion coefficients are incorporated to simulate some of the more predominant features such as the thermal bar and vertical stratification. Horizontal coefficients are constant for the winter and are set to zero for the stratification period to simulate the thermal bar effect resulting in restriction of the mixing of nearshore waters with main lake waters. Vertical dispersion is also time varying in Lake 3 in a fashion similar to Lake 1 and is constant in the winter, lower and depth varying in the summer, and evaluated on the basis of a straight line function during the transition period.

Figure 43 illustrates the time varying horizontal and vertical exchange coefficients to be used in this model.

8.2 VALIDITY OF ASSUMED CIRCULATION

Since the preceding circulation represents only the crudest estimate of flow transport in Lake Ontario, analyses must be made to determine the validity (or lack thereof) of the assumed circulation structure. The strategy, therefore, at this stage of the Lake 3 model is to input a circulation pattern into the kinetic structure that is at least reasonable in its broadest outlines. Since the segments of the Lake 3 model are large (10-40 km), much of the fine scale detail of the circulation will not be reproduced. Indeed, one of the functions of this effort at this time is to determine the degree to which a detailed circulation is required for the phytoplankton dynamics.

Initial Lake 3 model runs, therefore, were aimed at verification of transport regimes using water temperature as an indicator. The analysis, while crude, served the purpose of providing some estimate of the validity of the transport regime that was assumed. An annual temperature function is inputted to the top layer of the lake as a time variable forcing function, and the hypothesized flow and dispersion regimes transports this heat throughout the entire lake, computing the time variable temperature response in each of the segments. This

response is then compared to observed regional thermal properties of Lake Ontario.

The temperature input used is based on the work of Rodgers and Sato (1971) for IFYGL, who have computed values of monthly heat flux terms for 1965 through 1968. Though discrepancies between their results and observed data are reported, the computation of a total heat storage term, Q_t, proves to be ideal for coupling to the Lake 3 model and permits inputting temperature as a lake surface forcing function.

Using Lake Ontario meteorological data and empirical relationships, then heat storage values were computed using the formula:

$$Q_t = Q_s - Q_r - Q_b - Q_h - Q_e \qquad (78)$$

Q_t is the heat storage, Q_s the incident solar radiation, Q_b the net back radiation, Q_h the heat transfer to atmosphere and Q_e is the evaporation energy where all units are cal/m^2-day. With the monthly heat flux terms, values of Q_t were calculated for the five-year period studied. These values are listed in Table 11 and the five-year average values were used in the Lake 3 runs.

Once Q_t, the total heat flux term or total heat storage in the lake, is known, then

$$T_s(t) = Q_t/H \qquad (79)$$

where $T_s(t)$ is the temperature forcing function for the surface layer (°C/day or cal/cm^3-day) and H is the depth (cm) of the first segment.

This computed temperature forcing function was inputted to the top layer segments (0-4) of the Lake 3 model, and was then advected and dispersed throughout the model by the hypothesized flow and dispersion regime. The cmputed variable temperature response in each of the segments was then compared with a
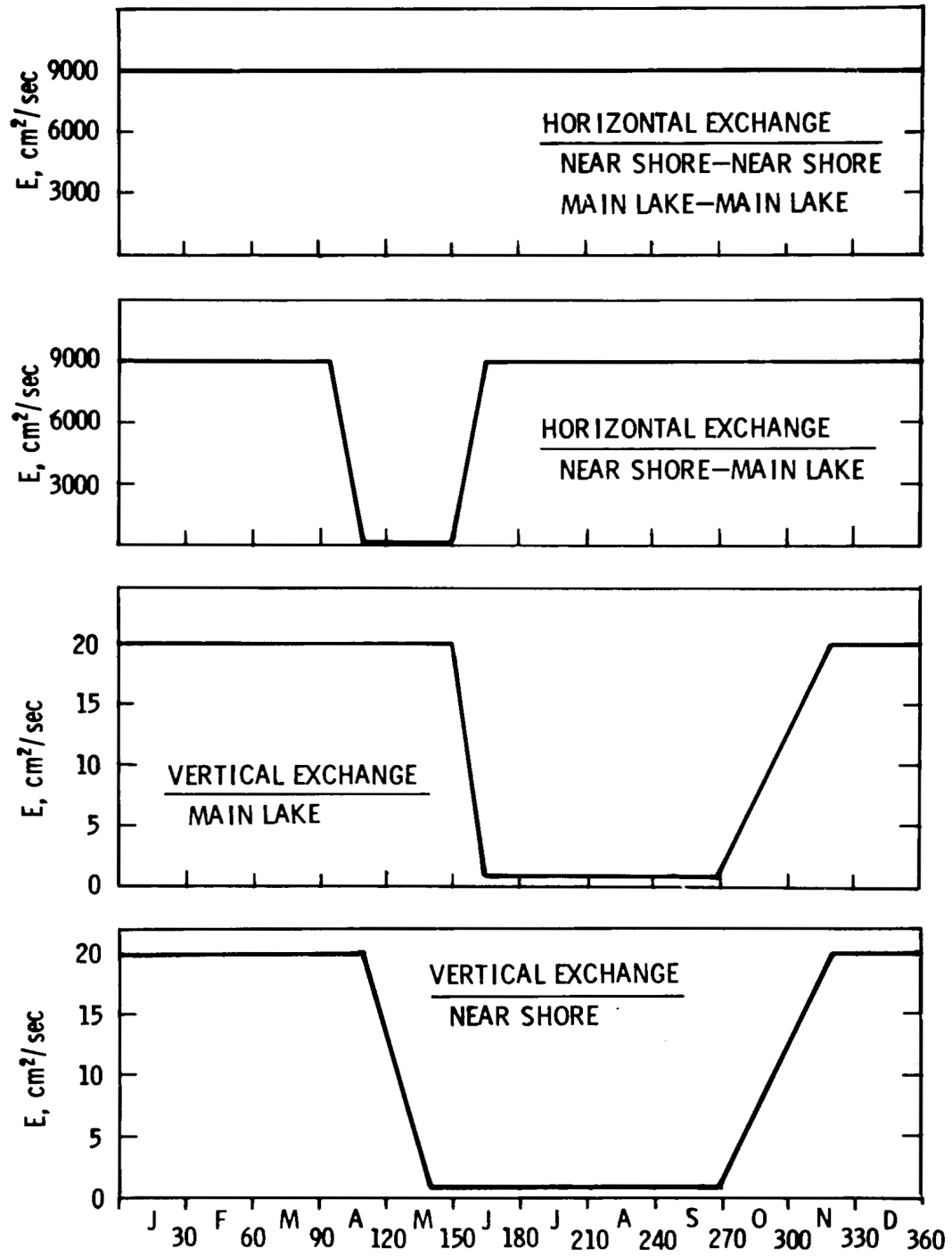
Figure 43. Assumed horizontal and vertical dispersion coefficients for Lake 3 model.

Table 11. Monthly Heat Flux Values

Month	1965 Q_t*	1966 Q_t	1967 Q_t	1968 Q_t	1969 Q_t	Five-Year Average
January	-329.1	-392.0	-214.2	-329.2	-275.5	-308.0
February	-216.6	-139.5	-278.1	-244.9	-153.6	-206.54
March	4.6	80.3	48.4	88.4	11.3	46.6
April	275.2	207.0	318.8	361.1	313.1	295.04
May	533.2	413.7	420.6	353.7	448.1	380.8
June	463.0	610.9	618.6	471.7	475.4	464.8
July	270.7	307.0	303.0	293.3	-	293.5
August	67.0	69.5	51.2	198.5	-	96.55
September	-43.7	-55.2	-92.7	102.1	-	-22.375
October	-235.8	-64.4	-108.7	-46.9	-	-113.95
November	-200.6	-162.4	-254.8	-206.7	-	-206.125
December	-226.1	-349.1	-296.8	-370.2	-	-310.55

$$*\ \frac{(cal)}{(cm^2\ day}$$

regional analysis of Lake Ontario thermal properties.

The degree of data manipulation involved to manipulate a transport regime in this 67 segment model, with its 187 dispersion interfaces and its 142 flow interfaces, is extensive so that a transport regime based on verification against generalized temperature properties rather than one verified against one-year of data with its specific meteorological conditions, was considered to be more feasible.

Based on these considerations, the verification medium chosen was the temperature characterization of Lee (1972). Composite temperature data for the years 1960-1969 were used and distinct horizontal variations of water temperature in Lake Ontario were noted. Lee distinguishes seven distinct regions of the lake where thermal properties seemed to be seasonally consistent on a year-to-year basis. This regional division of the lake, seen in Figure 44, is similar to the underlying basis of surface layer segmentation for Lake 3, namely a nearshore ring around the lake and large main

lake segments. This similarity coupled with the fact that Lee's data are based on a generalized analysis of ten years of data prompted the use of this dataset for temperature verification of transport regimes in the Lake 3 model.

Several different regimes were investigated with emphasis on the vertical and horizontal dispersion characteristics. The degree of verification of the computed output as compared with Lee's data is presented in Figures 45 and 46. Table 12 lists the equivalence between Lee's regions and the Lake 3 segments, and the values which are overplotted against Lee's data are the means of the appropriate Lake 3 segments at times corresponding to the median cruise dates reported by Lee.

Figure 45 also shows the effect of several sensitivity runs. The effects of using vertical dispersions only with no horizontal dispersion or flow, and the effect of reversing the direction of the flow field were investigated.
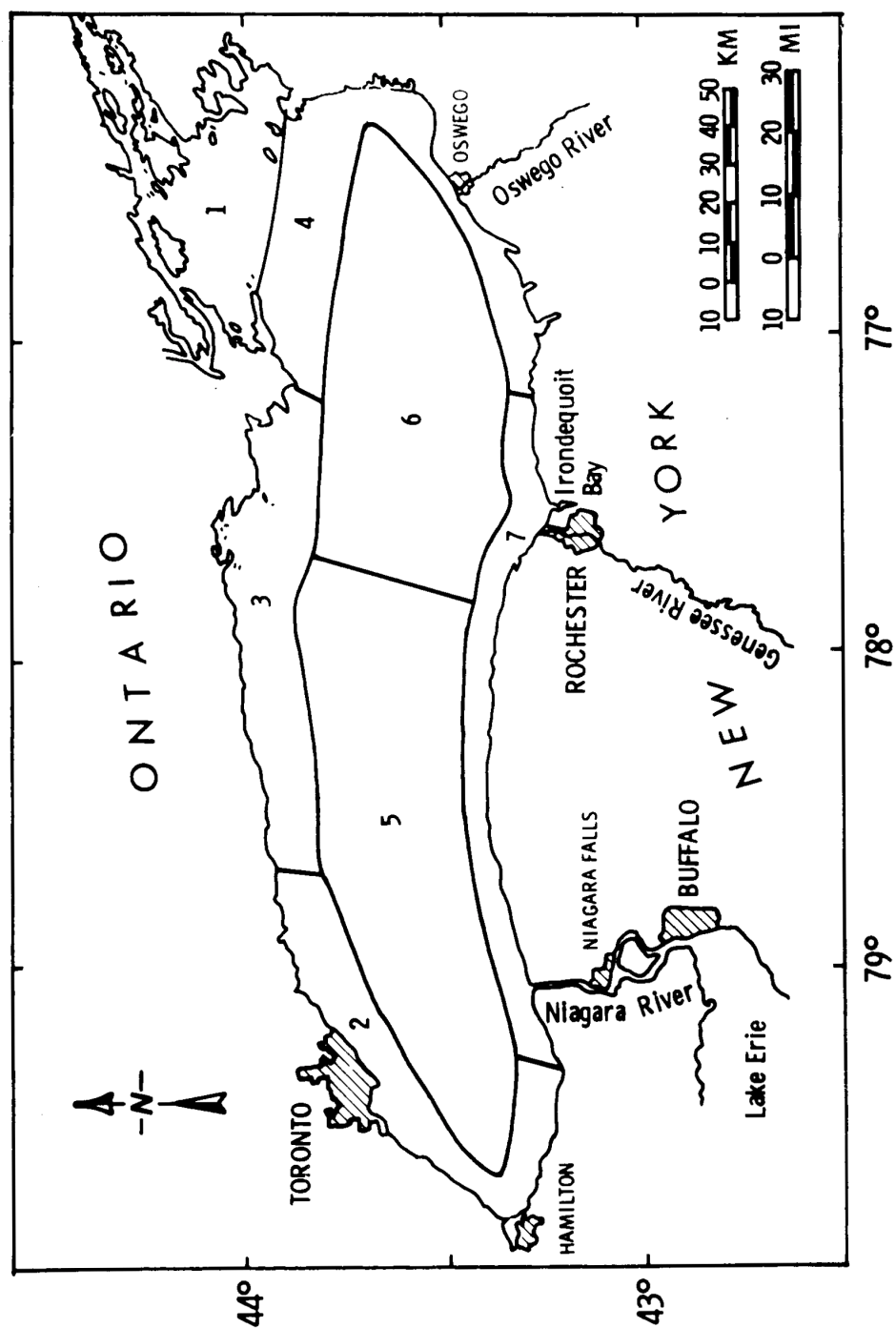
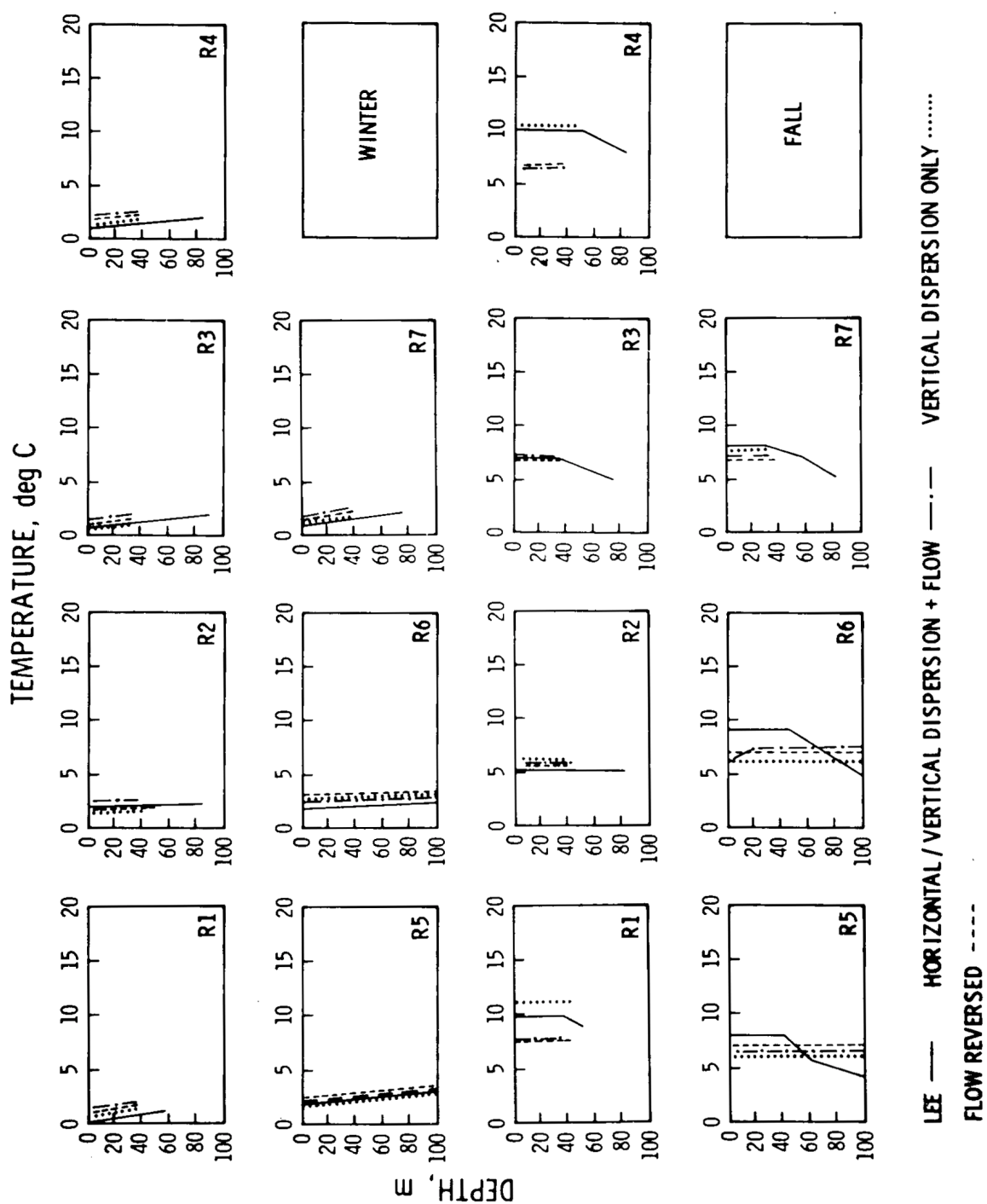Figure 44. Regional division of Lake Ontario by Lee (1972).

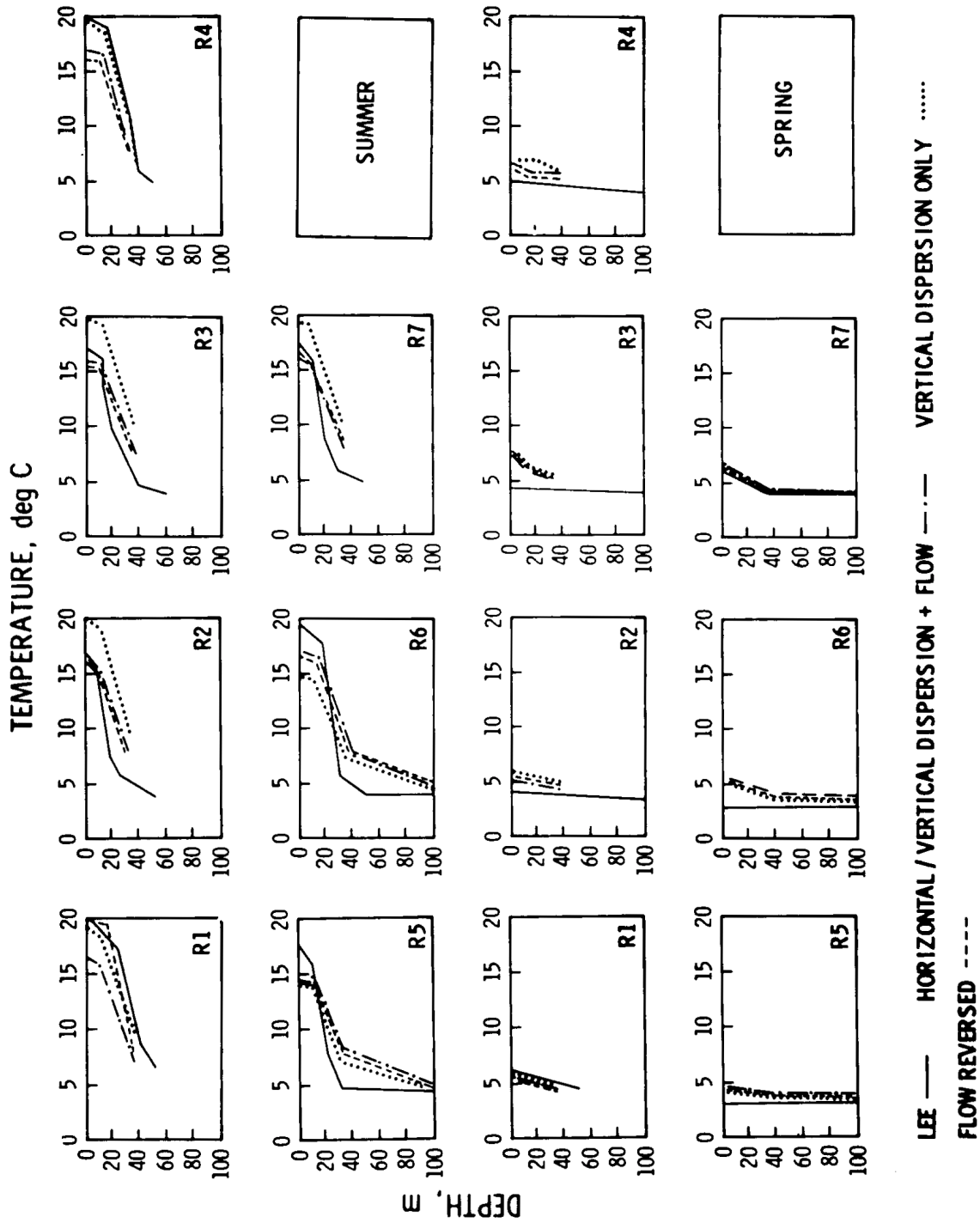Figure 45. Comparison of computed temperatures from Lake 3 model with data from Lee (1972), winter and fall.

Figure 46. Comparison of computed temperatures from Lake 3 model with data from Lee (1972), spring.

Table 12. Regional to Lake 3 Segmentation Equivalence

Lee (Region)	Segment of Lake 3				
	1	2	3	4	5
1	26	52	60	-	-
2	1,2,4,6	27,28,30,32	53,55,56	-	-
3	10,14,18	36,40,44	56,58	-	-
4	21,22,23,25	47,48,49,51	60,62	-	-
5	3,7,8,11,12	29,33,34,37,38	54,57	63,64	66
6	15,16,19,20,24	41,42,45,46,50	57,61	64,65	66,67
7	5,9,13,17	31,35,39,43	55,59	-	-

As can be seen, no marked effect on the temperature verification results when the flow transport is turned off or when flow is reversed. Though this appears to be odd, the reason is clear when one considers the size of the segments in the Lake 3 model. Though the model is large from a computational point of view and it does, because of its spatial detail, give nearshore to main lake resolution, the surface areas of the segments are so large that the interfaces for vertical transport are much greater than those for horizontal and flow transport. Hence, vertical dispersion terms dominate.

The grid is not fine enough and effects such as nearshore thermal bar flow restriction and changing wind pattern effects on horizontal transport cannot be investigated with any degree of accuracy. A grid fine enough such that these effects could be seen, does not appear to be computationally feasible at this time.

The dispersion regime resulting from this analysis is presented in Figure 43. Its underlying features consist of lowering vertical dispersion in the summer to simulate stratification, lowering nearshore to mid-lake segments horizontal dispersion for a period in the spring to simulate thermal bar, and simulating stratification earlier in the nearshore segments than in the main lake segments. This is the dispersion regime which is used in Lake 3 for the full biological and chemical systems verification runs.

Though this analysis has many shortcomings, it does serve to give some basis in theory for coupling of flow transport and dispersion to the kinetics of the Lake 3 model and it appears that this approach of treating temperature as a conservative tracer is a reasonable method of analysis.

8.3 PRELIMINARY PHYTOPLANKTON COMPUTATIONS

Several runs have been made of the Lake 3 model using the transport and dispersion regime discussed previously and the system kinetics given in Chapter 5. The purpose of these runs is to determine the general direction of the output with special reference to spatial differences in phytoplankton biomass. Considerably more work remains to be done on Lake 3 including detailed verification analyses and simulation of effects of nutrient reduction.

The primary data source at this point in the analysis is the results from the IFYGL effort. The cruise stations are mapped onto the Lake 3 grid and only those stations for which a reasonably complete set of data were available

are included in the mapping. Figure 47 shows the location of the data stations and the Lake 3 grid. Some segments have only one station for comparison while other segments (primarily nearshore stations) may have three stations for comparison. Data retrievals have been completed from the STORET system and "segment depth" averages (and other statistics) by month and record length have been completed. This data set will then form the basis for the detailed verification analysis.

Figure 48 shows very early preliminary results of phytoplankton biomass at three segments across the lake. This run did not include any vertical settling velocity. Segment 17 represents the Rochester embayment and as seen reaches peak values of almost 15 µg chlorophyll/l at the end of May while the more open lake area (segment 16) lags by about one-half month. Peak values at the open lake segment are about half of the Rochester segment. At the end of May, therefore, at day 150, a lateral gradient of chlorophyll of about 10 µg/l is computed. This results primarily from the thermal bar effect simulated by variations in the horizontal dispersion (see Figure 43). Gradients across the lake in the fall are not pronounced and reflect the general well-mixed character of the lake at that time.

Figure 49 explores the vertical variation for two segments during the month of June and compares the results to data collected during IFYGL. Maximum biomass occurs in the upper layer and then decreases with depth. The mean values and range of the computed values agree quite well with the observed chlorophyll data. In fact, the agreement is so surprisingly good that further investigation is warranted to determine why the agreement was obtained so rapidly. This is especially important when it is recognized that the run shown in Figures 48 and 49 is for zero phytoplankton settling velocity.

8.3.1 Output Data Display

The Lake 3 model generates a substantial output totaling thousands of numbers that represent the time variable response of each variable at each segment. In addition, output on the growth and death kinetics, nutrient recycle and nutrient fluxes are also obtained. The size of Lake 3 makes it difficult to fully comprehend the output so some effort is being devoted to further analysis and display of the output. In this way, it is hoped that further understanding and insight can be obtained on the behavior of the solutions that are generated.

Figure 50 shows the output flow diagram that is presently being utilized. Output from the model is written on tape in addition to hard copy and digital overplots. The latter plots are for general screening by the analyst. Plotting software is then employed on the tape output from a model run. Paper contour plots and three-dimensional plotting routines are employed to provide further perspective on the output. Figure 51 shows a three-dimensional plot of output of phytoplankton biomass in the 0-4 meter layer from a view looking down the lake from east to west. Plots such as these reveal the structure of the solution in a meaningful way and also permit scanning of the output to determine any strange or anomalous results that may indicate a flaw in the numerical computations.

Returning to Figure 51, the three-dimensional plots are also displayed on a cathode ray tube, microfilmed and prepared for a motion picture of the complete output over time. A screening of this film then reveals the dynamic and spatial behavior of the solution in a very unique way. At this stage, a film has been prepared of a preliminary run for a full year of the surface phytoplankton chlorophyll.
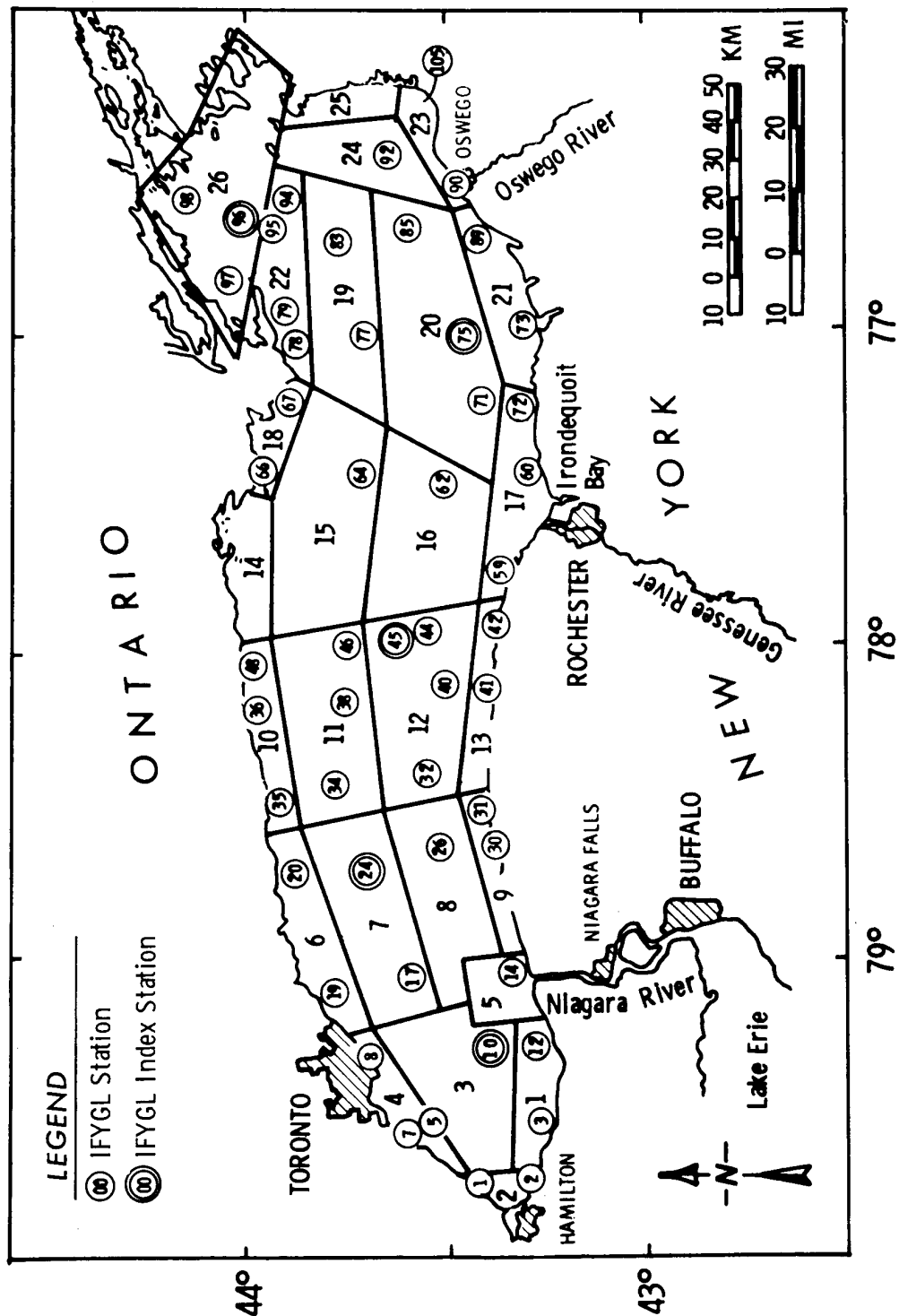
Figure 47. Principal IFYGL stations and the Lake 3 grid.
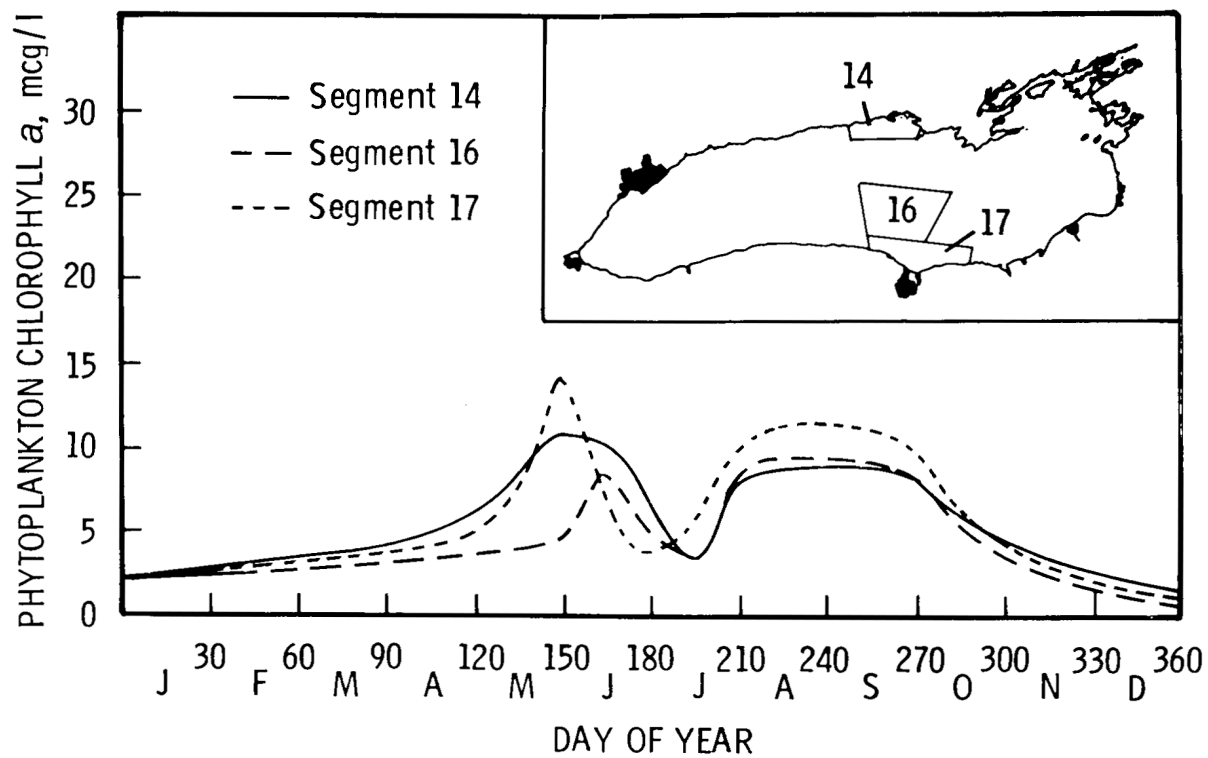
Figure 48. Preliminary results of Lake 3 model, 0-4 meters.
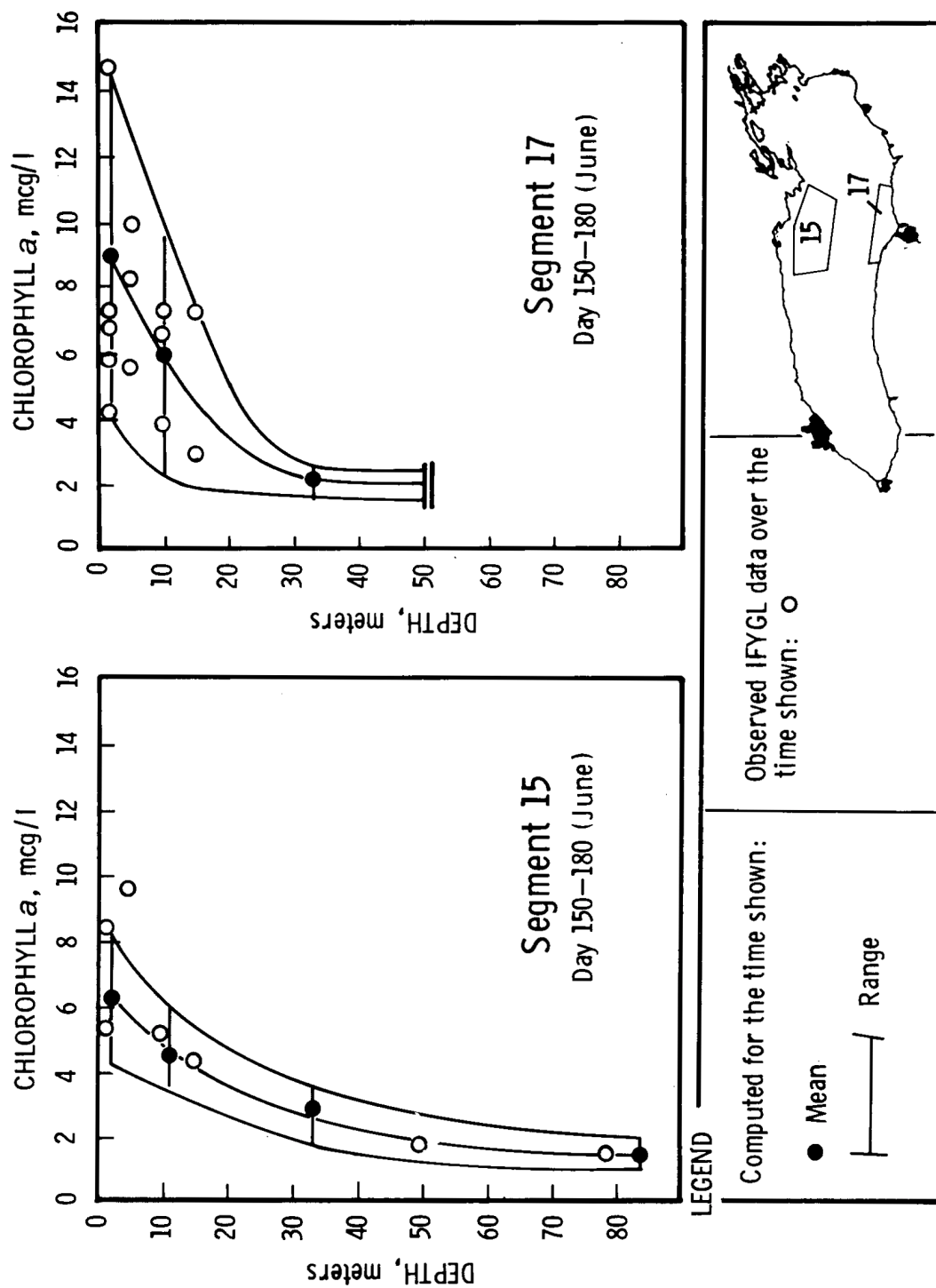
Figure 49. Preliminary comparison of Lake 3 model output to observed data at two segments for June.
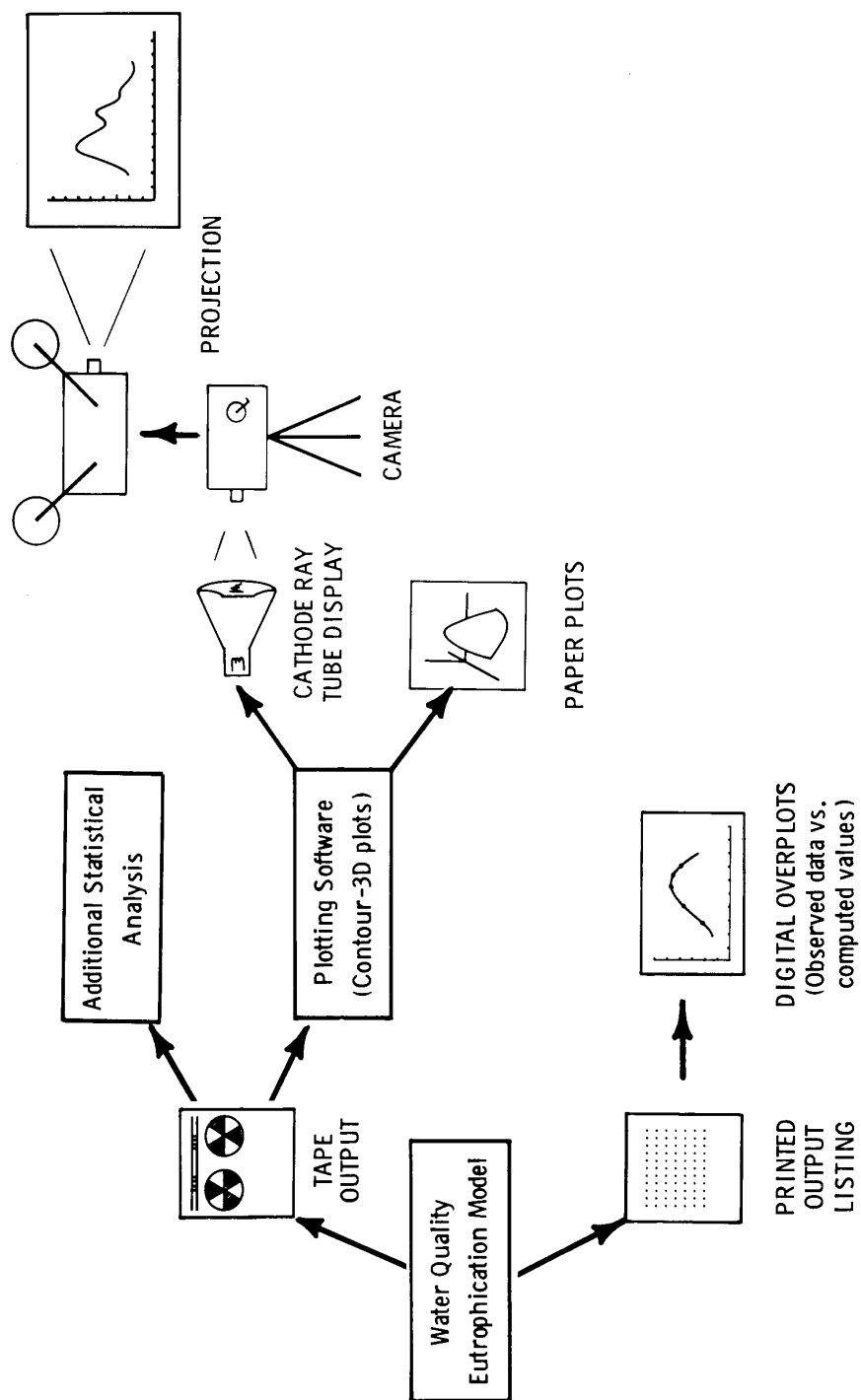
Figure 50. Data output flow diagram used for verification and display purposes.

LAKE ONTARIO—LAKE 3 MODEL
LAYER 1 (0—4 METERS)
JUNE

NIAGARA RIVER

TORONTO

ROCHESTER

N

OSWEGO RIVER

ST. LAWRENCE RIVER

PHYTOPLANKTON CHLOROPHYLL a Maximum, 8.2 µg/l

Figure 51. Three-dimensional plot of phytoplankton chlorophyll calculated from Lake 3 model in June, 0-4 meters.

LAKE 1 - INPUT AND PROGRAM LISTING

A.1 INPUT INFORMATION

Lake 1 is a kinetic interactive model spatially defined by three vertical mixed layers representing the epilimnion, hypolimnion and benthos of Lake Ontario as shown in Figure 9. The purpose of this appendix is to sumarize the input information needed to run the model and to present, where available, the background information from which this information was drawn. Units for the information given are consistent with those required by the computational software used, which is named Water Analysis Simulation (WASP). A listing of WASP and sample output are included.

A.2 MORPHOMETRY AND HYDRODYNAMIC REGIME

The information required to describe the morphometry of Lake Ontario for the Lake 1 model is presented in Table A-1, with the associated hydrodynamic regime.

The bulk of the morphometric data was generated using data supplied by the CCIW (personal communication). The bathymetric data, supplied on punched cards, were depth averages for a square grid laid o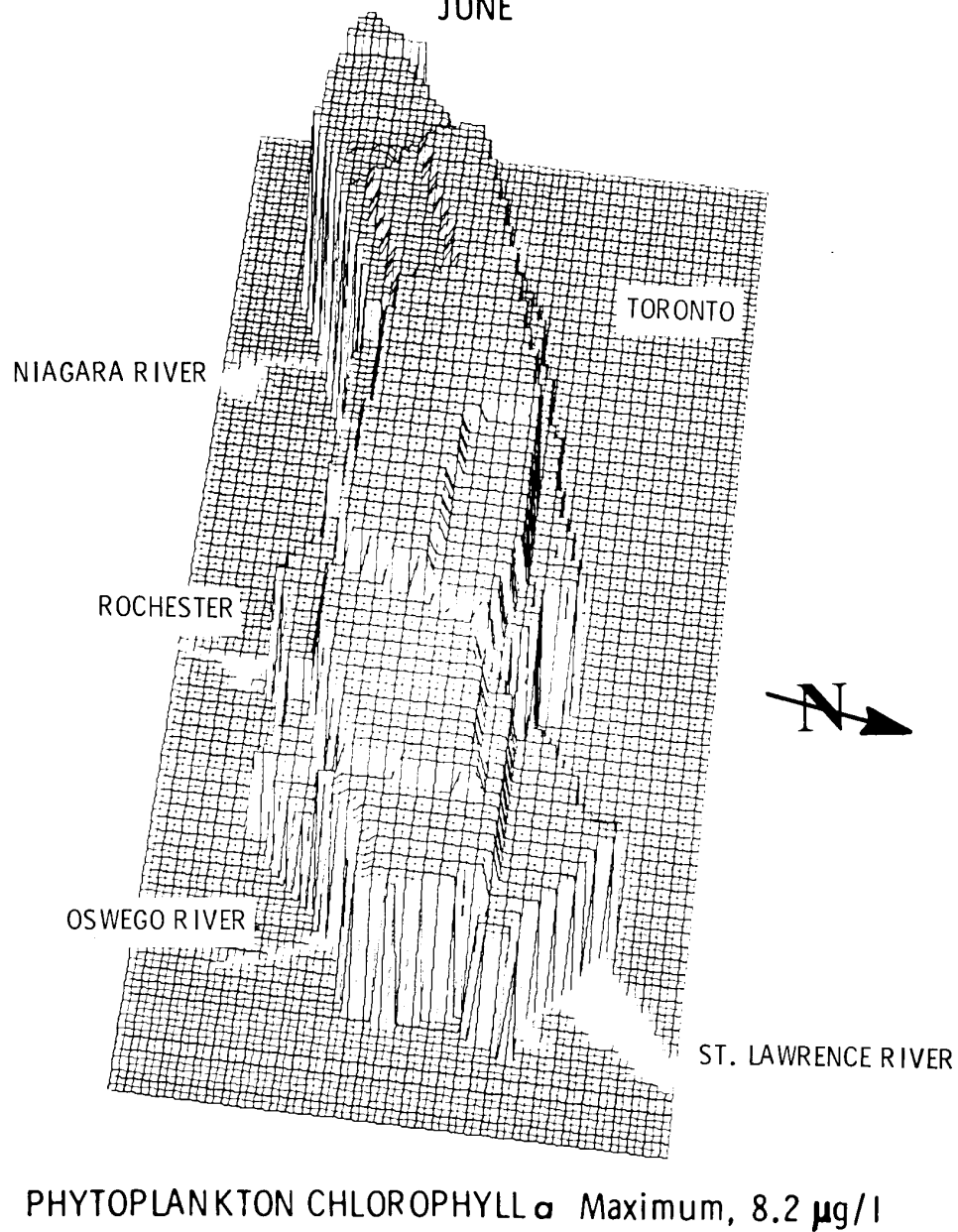n a polyconic projection of Lake Ontario, with geographical areas of 4 km (IJC, 1969). These surface areas were defined by sides which were actually curves on the earth's surface. These data were processed to yield the necessary information. The average depth of Lake Ontario is 396 feet (90 meters). The IJC (1969) reports the average depth of the developed thermocline is 55.8 feet (17 meters). This depth is used in the representation of the epilimnion. The remainder of the volume is placed in the hypolimnion. The benthos, which is currently used only to track accumulation of depositions, was given an arbitrary depth of 0.5 feet. Figures A-1 and A-2 which show the variation of volume and surface area with depth were generated with the CCIW supplied data.

Table A-1. Physical Parameters

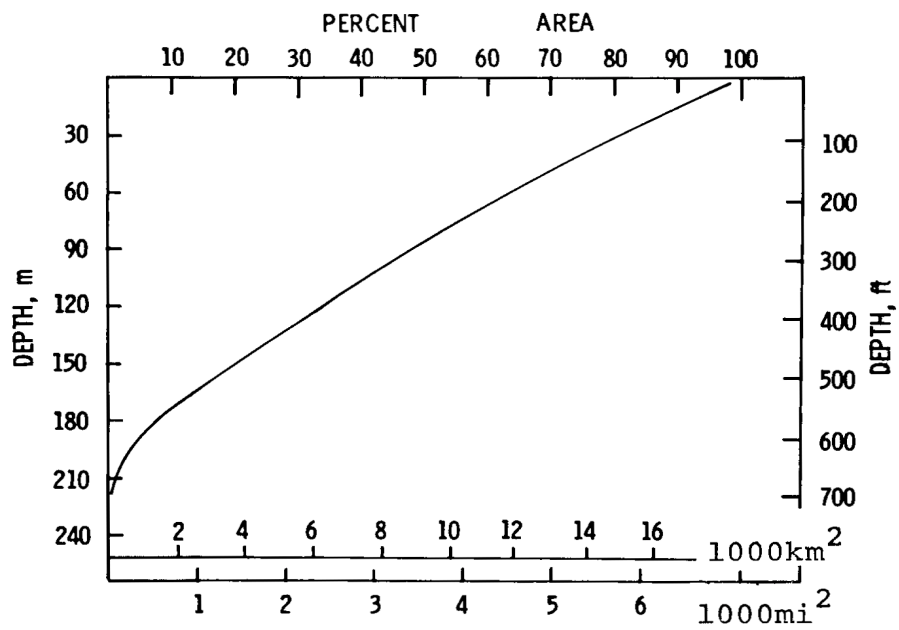| Seg-ment	Inter-Segment	Represent-ation	Volume (10^6 cf)	Depth (ft)	Inter-segment Areas (ft^2)	Inflow (cfs)	Outflow (cfs)	Dispersion Coefficient (mi^2/day)
1		Epilimnion	1.05×10^7	55.8		43,.500.	43,500.	
	1-2				1.76×10^{11}			See Figure A-4
2		Hypolimnion	4.85×10^7	240.5		188,400.	188,500.	
	2-3				0.959×10^{11}			0.0
3		Benthos	4.80×10^4	0.5		0.0	0.0	
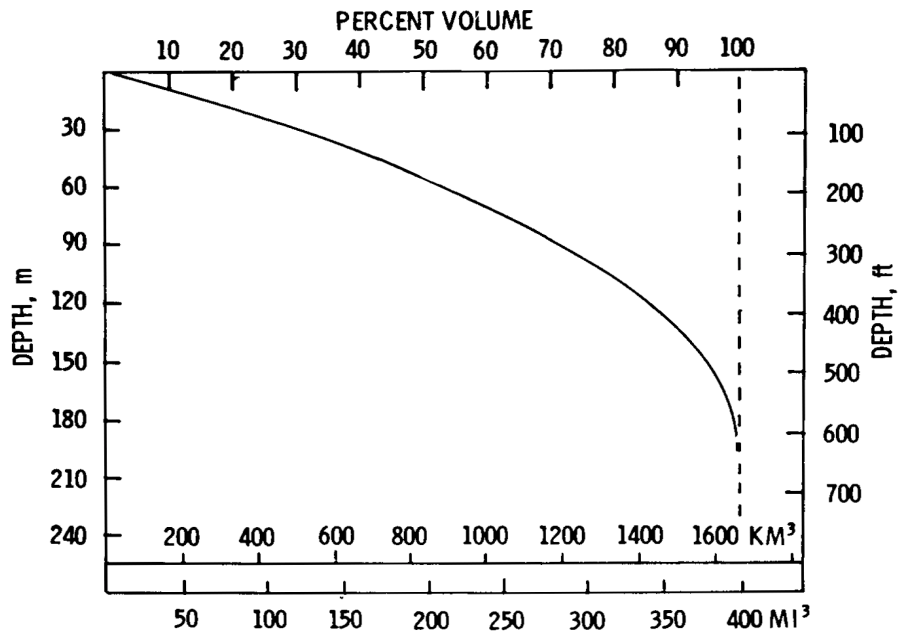
Figure A-1. Variation of volume with depth.

Figure A-2. Variation of area with depth.

100

The hydrodynamic regime is inputted into WASP, as opposed to a modeling configuration which would incorporate a hydrodynamic submodel internally. This differentiation is most significant for more spatially defined models than Lake 1. The hydrodynamics must, therefore, be obtained from a database, the literature, or an external hydrodynamic submodel. The mean annual outflow for Lake Ontario is 232,000 cfs (IJC, 1969). Inflow was set equal to outflow and was split proportionally to the segment depths, as shown in Table A-1.

The development of the thermocline was simulated by temporally varying the vertical dispersion coefficient as shown in Figure A-3. The establishment of the thermocline prevents exchange between the epilimnion and hypolimnion. This phenomena was incorporated by setting the vertical dispersion between segments 1 and 2 to zero during the period of stratification. For the remainder of the year, exchange takes place between segment 1 and segment 2. The vertical dispersion coefficient was set at 0.0003 mi^2/day (90 cm^2/sec) for periods of non-stratification, which is in the range reported in Hydroscience, Inc. (1973).

A.3 PHYSICAL EXOGENOUS VARIABLES

Water Temperature - The temporal variation of water temperature used in Lake 1 is shown in Figure A-4. Since the segments represent completely mixed volumes, representative temperatures were chosen. Data averaged from CCIW (1969) were used as temperature input. Only stations with depths over 50 meters were considered. These were viewed as representative of main lake conditions.

Solar Radiation - Data recorded at Brockport, New York and at Toronto-Scarborough, Ontario were available. The Toronto-Scarborough data were used as this comprised the longest period of record. The Toronto-Scarborough data were adjusted using an overland radiation to overlake radiation ratio proposed by Richards and Lowen (1965). The overland radiation data, lake-to-land

ratio and adjusted temporal lake radiation function used is shown in Figure A-5.

Photoperiod - That fraction of the day from sunrise to sunset is variable during the year, and is a function of latitudinal position. Sunset-sunrise data from Newspaper Enterprise Association (1974) were used to obtain the functions shown in Figure A-6. The Lake Ontario photoperiod function was obtained by interpolating to the equivalent of 43°40'N latitude.

Background Water Clarity - The variation of the extinction coefficient with time is a function of the phytoplankton concentration in the water body. Given no phytoplankton, there would still be extinction of light as it passes through the water column attributable to other factors. This fraction of the extinction coefficient, which is a function of background water clarity, was determined by plotting chlorophyll and extinction coefficient as shown in Figure A-7. The extinction coefficient was taken to be:

$$K_e = \frac{1.9}{Secchi\ depth}$$

after Beeton (1958).

A.4 BIOLOGICAL AND CHEMICAL EXOGENOUS VARIABLES

Mass Loadings and Boundary Concentrations - Sources of nutrient input into Lake Ontario are varied. Tributary runoff, direct municipal and industrial discharges comprise the principal sources of nutrients. Mass loadings (mass/unit time) are normally thought of as direct inputs to a water body. Boundary concentration conditions (mass/unit volume) are usually thought to be associated with tributary inflow or in dispersive situations with the "downstream" portion of the water body. Boundary conditions, since they are always associated with a flow regime (volume/unit time), can also be viewed as mass loadings into the water body. WASP has
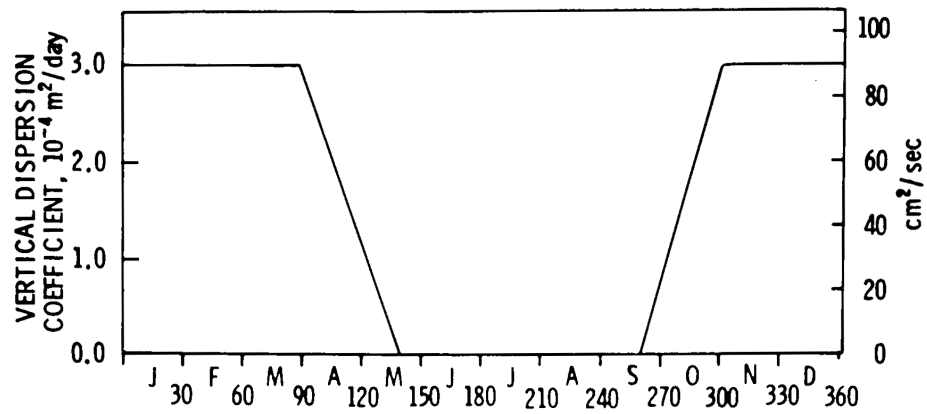
Figure A-3. Temporal variation of vertical dispersion coefficient--
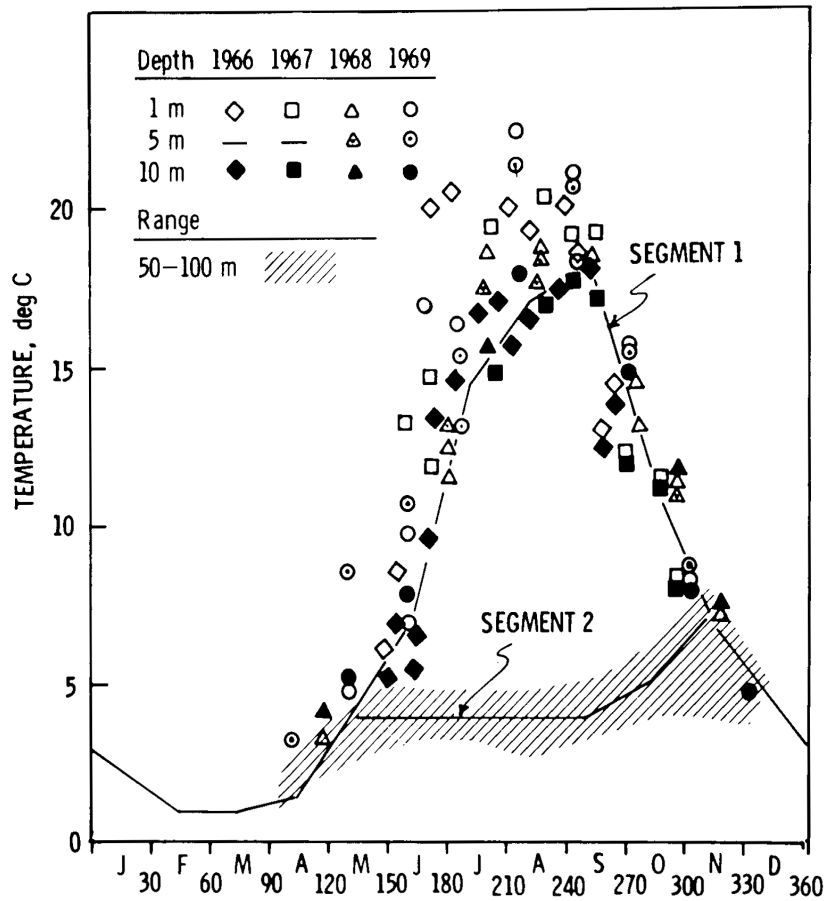interface 1-2

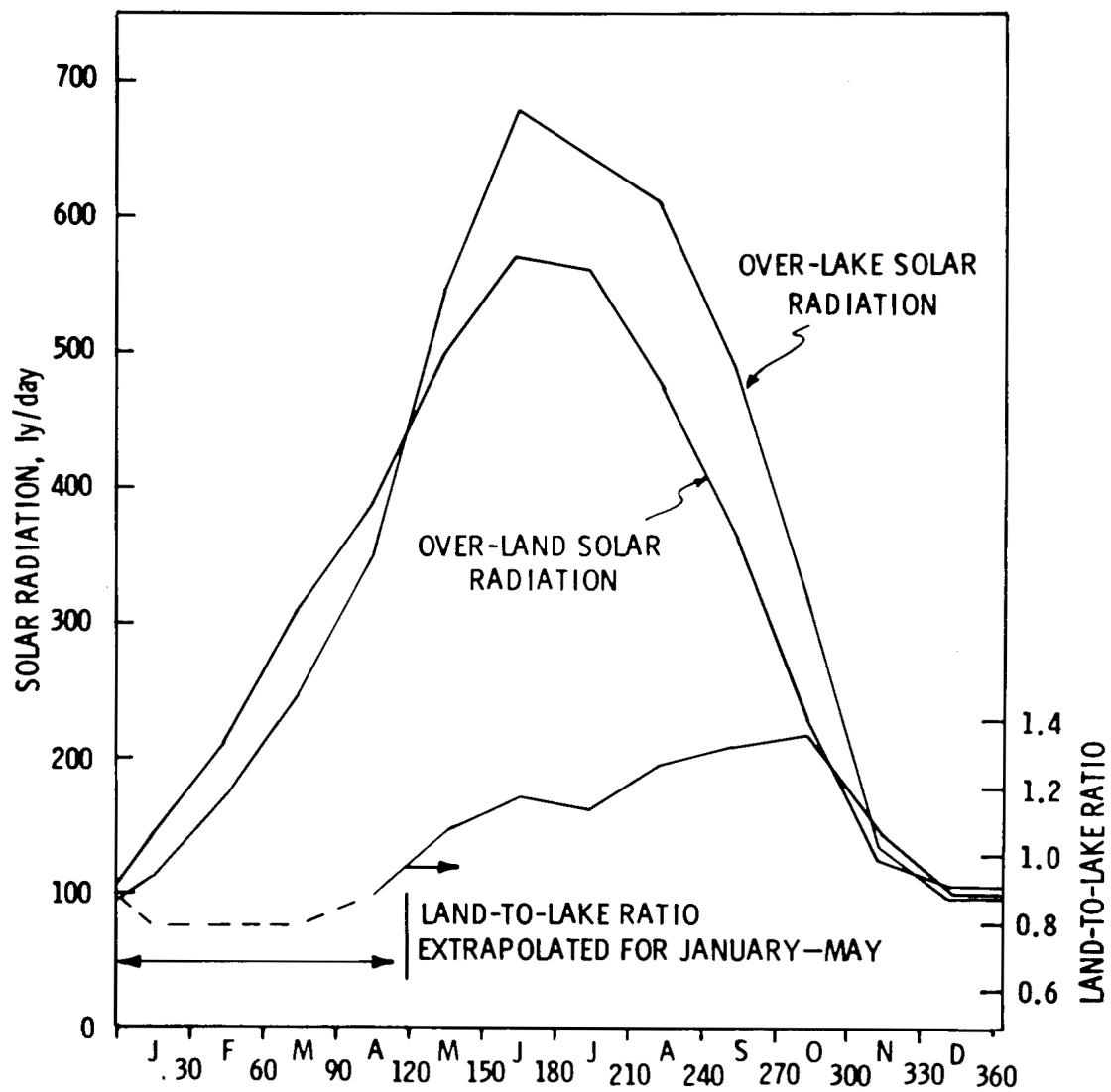Figure A-4. Temporal variation of water temperature

102

Figure A-5. Temporal variation of solar radiation.
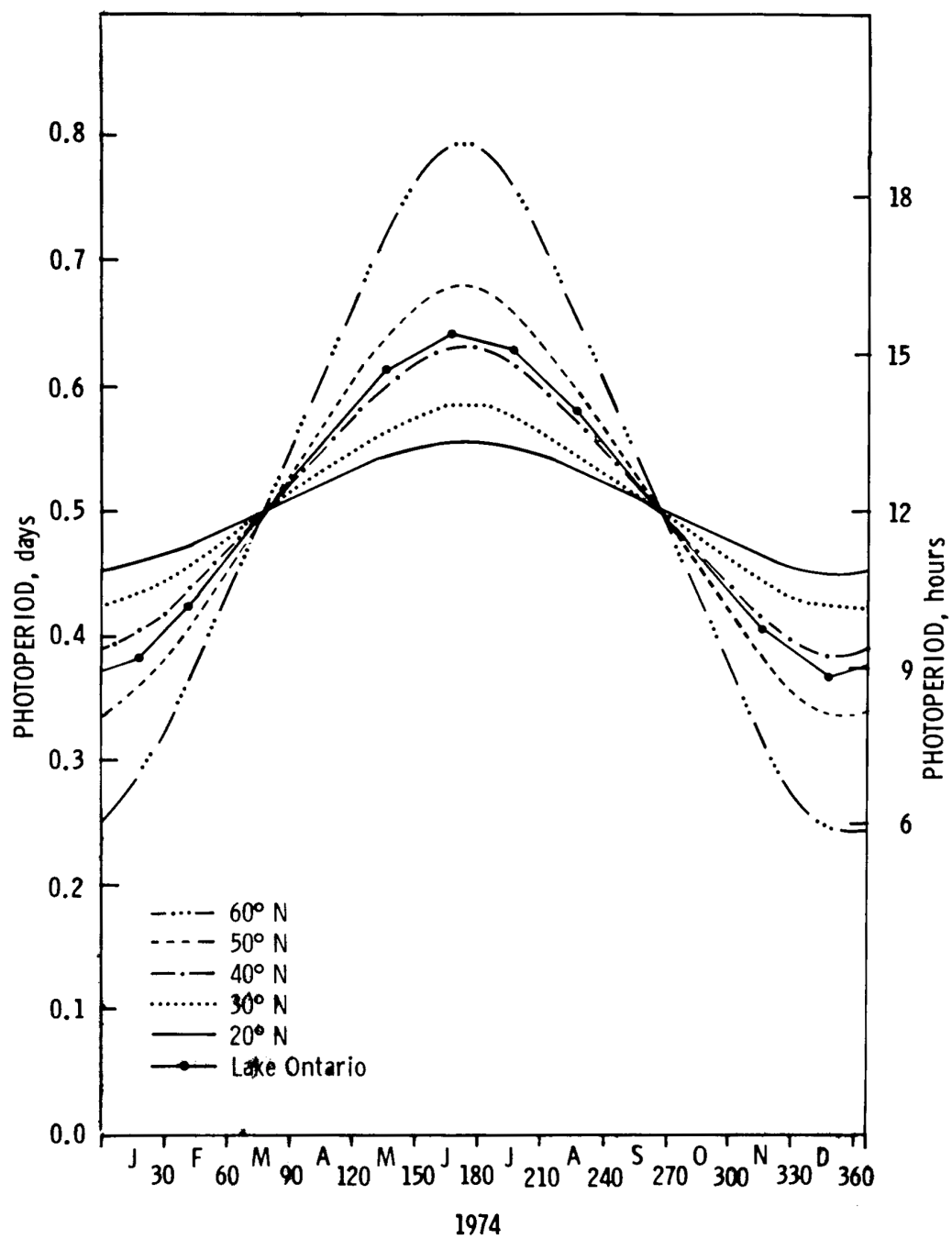
Figure A-6. Temporal variation of photoperiod

Figure A-6. Temporal variation of photoperiod.
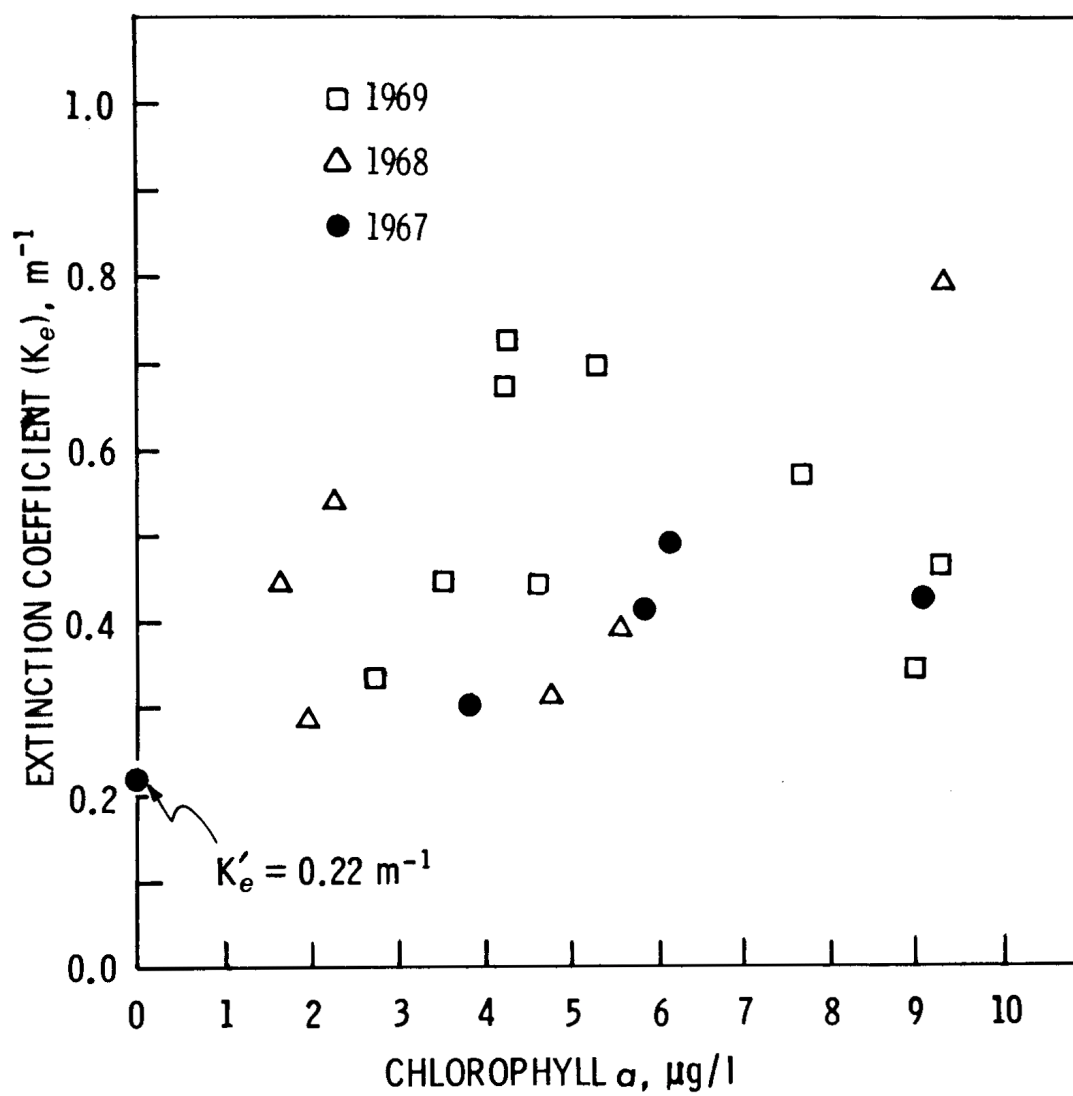
Figure A-7. Determination of background water clarity - K_e.

capabilities to input nutrients using either mass loadings or boundary conditions, with the associated flow regime. Lake 1 in its present configuration just utilizes the boundary condition form of mass input. The loading information used for the various nitrogen and phosphorus species used in the nutrient systems (non-living organic, ammonia and nitrate, nitrogen, non-living organic and available phosphorus) was not available. Only total nutrient information was given. Species loads were set at initial conditions for the inorganic nutrients with the remainder placed in the respective non-living organic system. Loading information and breakdown is shown in Table A-2.

nitial Conditions - The initial conditions for Lake 1 are shown in Table A-2. The integration starts the first of January and these values reflect the measured values for this part of the year.

A.5 CHEMICAL AND BIOLOGICAL ENDOGENOUS VARIABLES

System Parameters - The various constants and parameters which define the interaction between the various biological and chemical systems are listed in Table A-3. Units are those required by the present configuration of Lake 1.

NOTE:

Source listings for Lake 2 model and sample input and output are available from USEPA, Grosse Ile Laboratory, Grosse Ile, Michigan.

This program is currently operational on the Control Data Corporation 6600 at Courant Institute of New York University.

A version will be available on Optimal systems, Incorporated, in the near future.

Table A-2. Lake 1 - Mass Loadings and Initial Conditions

System	Boundary Concentration (mg/L)	Initial Conditions (mg/l)
Phytoplankton	1.0	2.0
Zooplankton - Herbivorous	.05	.005
Nitrogen		
Non-Living Organic	.443	.090
Ammonia-N	.0150	.0150
Nitrate-N	.250	.250
Phosphorus		
Non-Living Organic	.0454	.005
Available P	.0143	.0143
Zooplankton - Carnivorous	.01	.005
Zooplankton - Upper Trophic Level 1	By-passed system	
Zooplankton - Upper Trophic Level 2	By-passed system	

I

Table A-3. System Parameters

System - Parameter	Symbol	Value	Units
Phytoplankton Chlorophyll *a*			
1. Saturated Growth Rate (θ_o)	K1T	1.066	None
	K1C	0.580	day^{-1}
2. Saturating Light Intensity	IS	350.	ly/day
3. Michaelis Constant for Nitrogen	KMN	0.025	mg N/l
4. Michaelis Constant for Phosphorus	KMP	0.002	mg P/l
	K2T	1.08	None
5. Endogenous Respiration Rate (θ_{20})	K2C	0.10	day^{-1}
6. Carbon-to-Chlorophyll Ratio	CCHL	0.05	mg C/µg Chl *a*
7. Sink Velocity	SVEL	0.10	m/day
8. Preference Structure for Inorganic Nitrogen	PNH$_3$	0.5	None
Non-Living Organic Nitrogen			
1. Organic N-NH$_3$ Hydrolysis Rate	K34T	0.00175	day °C^{-1}
	K34C	0	day^{-1}
2. Nitrogen-to-Chlorophyll *a* Ratio	NCHL	0.010	mg N/mg Chl *a*
3. Sink Coefficient	K33	0.001	day^{-1}
Ammonia Nitrogen			
1. NH$_3$-NO$_3$ Nitrification Rate	K45T	0.002	day °C^{-1}
	K45C	0	day^{-1}
Nitrate-Nitrogen			
None			
Non-Living Organic Phosphorus			
1. Organic P-Inorganic P Conversion Rate	K67T	0.007	day °C^{-1}
	K67C	0	day^{-1}
2. Phosphorus-to-Chlorophyll *a* Ratio	PCHL	0.001	mg P/µg Chl *a*
3. Sink Coefficient	K66	0.001	day^{-1}

Table A-3. System Parameters (Continued)

System - Parameter	Symbol	Value	Units
Available Phosphorus			
1. Sinking Coefficient	K77	0	day^{-1}
Herbivorous Zooplankton-Carbon			
1. Grazing Rate	CGC	0	l/mg C/day °C
	CGT	0.06	l/mg C/day
2. Michaelis Constant for Phytoplankton	KMP	10	µg Chl *a*/l
3. Conversion Efficiency	AZP	0.60	None
4. Endogenous Respiration Rate	K4T	0.001	day °C^{-1}
	K4C	0.0	day^{-1}
Carnivorous Zooplankton-Carbon			
1. Grazing Rate	CGT8	0.06	l/mg C/day °C
	CGC8	0	l/mg C/day
2. Conversion Efficiency	A8Z	0.60	None
3. Endogenous Respiration Rate	K8T	0.001	day °C^{-1}
	K8	0	day^{-1}
Upper Trophic Level 1 - Carbon			
1. Grazing Rate	CGT9	0.01	l/mg C/day °C
	CGC9	0	l/mg C/day
2. Conversion Efficiency	A98	0.60	None
3. Endogenous Respiration Rate	K9T	0.00	day °C^{-1}
	K9	0.0	day^{-1}
Upper Trophic Level 2 - Carbon			
1. Grazing Rate	CGT0	0.06	1/mg C/day °C
	CGC0	0	1 mg C/day °C
2. Conversion Efficiency	A109	0.60	None
3. Endogenous Respiration Rate	K10T	0.002	day °C^{-1}
	K10	0	day^{-1}
	K9		

REFERENCES

Beeton, A.M. 1958. Relationship Between Secchi Disc Readings and Light Penetration in Lake Huron. Amer. Fish. Soc. Transac., 87:73-79.

Beeton, A.M. and D.C. Chandler. 1963. The St. Lawrence Great Lakes. In: D.C. Frey (Ed.), Limnology in North America. University of Wisconsin Press, Milwaukee, Wisconsin.

Bellman, R. 1960. Introduction to Matrix Analysis. McGraw-Hill Book Company, Incorporated, New York, New York.

Birkhoff, G. and R.S. Varga. 1958. Reactor Criticability and Nonnegative Matrices. J. SIAM, 6(4):354-377.

Bonham, Carter, G., J.H. Thomas, and D. Lackner. 1973. A Numerical Model of Steady Wind-Driven Currents in Lake Ontario and the Rochester Embayment Based on Shallow-Lake Theory, International Field Year for the Great Lakes Report Number 7, Rochester Embayment Project. Department of Geological Sciences, University of Rochester, Rochester, New York.

Burns, N.M. and C. Ross. 1972. Project Hypo. Canada Centre for Inland Waters Publication Number 6. Report to the U.S. Environmental Protection Agency, Washington, D.C. EPA-TS-05-71-208-24.

Burns, N.M. and A.E. Pashley. 1974. In Situ Measurements of the Settling Velocity Profile of Particulate Organic Carbon in Lake Ontario. J. Fish. Res. Bd. Canada, 31(3):291-297.

Canada Centre for Inland Waters (CCIW). Personal Communication on Descriptive Limnology. Burlington, Ontario, Canada.

Canada Centre for Inland Waters (CCIW). 1969. Limnological Data Reports, Lake Ontario, 1966-1969. Canadian Oceanographic Data Centre, Burlington, Ontario, Canada.

Canadian Hydrographic Service. 1970. Bathymetric Chart (881) of Lake Ontario. Department of Energy, Mines and Resources, Ottawa, Ontario, Canada.

Canale, R.P., S. Nachiappan, D.J. Hineman, and H.E. Allen. 1973. A Dynamic Model for Phytoplankton Production in Grand Traverse Bay. In: N.A. Rukavina, J.S. Seddon, and P. Casey (Eds.), Proceedings of the 16th Conference on Great Lakes Research, pp. 21-23. Braun-Brumfield Publishers, Ann Arbor, Michigan.

Caperon, J. and J. Meyer. 1972. Nitrogen-Limited Growth of Marine Phytoplankton. II. Uptake Kinetics and Their Role in Nutrient-Limited Growth of Phytoplankton. Deep Sea Res., 19:619-632.

Casey, D.J. 1965. Lake Ontario Environmental Summary. Report to the Lake Ontario Basin Office, U.S. Environmental Protection Agency, Rochester, New York.

Di Toro, D.M., D.J. O'Connor, and R. Thomann. 1971. A Dynamic Model of the Phytoplankton Population in the Sacramento-San Joaquin Delta. In: Advances in Chemistry, Number 106, pp. 131-180. American Chemical Society, Washington, D.C.

Di Toro, D.M., D.J. O'Connor, R.V. Thomann, and J.L. Mancini. 1973. Preliminary Phytoplankton, Zooplankton Nutrient Model of Western Lake Erie. In: B.C. Patten (Ed.), Systems Analysis and Simulation in Ecology, Volume 3. Academic Press, Incorporated, New York, New York.

Di Toro, D.M. 1974a. An Evaluation of Phytoplankton Kinetic Behavior in Flask Experiments. In preparation.

Di Toro, D.M. 1974b. Combining Chemical Equilibrium and Water Quality Models. Manhattan College, Riverdale, New York.

Epply, R.W. 1972. Temperature and Phytoplankton Growth in the Sea. Fish. Bullet., 70(4):1063-1085.

Glooschenko, W., J.E. Moore, and R.A. Vollenweider. 1972. The Seasonal Cycle of Pheo-Pigments in Lake Ontario With Particular Emphasis on the Role of Zooplankton Grazing. Limnol. Oceanogr., 17(4):597-605.

Glooschenko, W.A., J.E. Moore, M. Munawar, and R.A. Vollenweider. 1974. Primary Production in Lakes Ontario and Erie: A Comparative Study. J. Fish. Res. Bd. Canada, 31(3):253-263.

Goering, J.J., D.N. Nelson, and J.A. Carter. 1973. Silicic Acid Uptake by Natural Populations of Marine Phytoplankton. Deep Sea Res., 20(9):777-789.

Great Lakes Basin Commission. 1971. Appendix II - Levels and Flows. In: Great Lakes Framework Study, Draft Number 3. Great Lakes Basin Commission, Ann Arbor, Michigan.

Helgeson, H.C. 1967. Thermodynamics of Complex Dissociation in Aqueous Solution at Elevated Temperatures. J. Phys. Chem., 71:3121-3136.

Hendrey, G.R. and E. Welch. 1973. The Effects of Nutrient Availability and Light Intensity on the Growth Kinetics of Natural Phytoplankton Communities. Presented at the 36th Conference of the American Society of Limnology and Oceanography, Salt Lake City, Utah. June 1973.

Hubbard, J.E. Personal communication. Department of Geology and Earth Science, State University College, Brockport, New York.

Hutchinson, G.E. 1957. A Treatise on Limnology, Volume 1 - Geography, Pysics and Chemistry. John Wiley and Sons, Incorporated, New York, New York.

Hutchinson, G.E. 1967. A Treatise on Limnology, Volume 2 - Introduction to Lake Biology and the Limnoplankton. John Wiley and Sons, Incorporated, New York, New York.

Hydroscience, Incorporated. 1973. Limnological Systems Analysis of the Great Lakes. Report to the Great Lakes Basin Commission, Westwood, New Jersey. 474 pp.

International Joint Commission. 1969. International Lake Erie and International Lake Ontario - St. Lawrence River Water Pollution Control Boards Report to the International Joint Commission on the Pollution of Lake Ontario and the International Section of the St. Lawrence Rivers, Volumes 1, 2, and 3. Windsor, Ontario, Canada.

Kern, D.M. 1960. The Hydration of Carbon Dioxide. J. Chem., 37(1):14-22.

Kibby, N.V. 1971. Effects of Temperature on the Feeding Behavior of *Daphnia rosea*. Limnol. Oceanogr., 16(3):580-581.

Kierstead, H. and L.B. Slobodkin. 1953. The Size of Water Masses Containing Plankton Blooms. J. Mar. Res., 12:141-147.

Kramer, J.R. 1964. Theoretical Model for the Chemical Composition of Fresh Water With Application to the Great Lakes. Great Lakes Research Division, Publication Number 11, pp. 149-160. The University of Michigan, Ann Arbor, Michigan.

Kramer, J.R. 1967. Equilibrium Models and Composition of the Great Lakes. In: Equilibrium Concepts in Natural Water Systems, Advances in Chemistry, Series Number 67, pp. 243-254. American Chemical Society, Washington, D.C.

Lee, A.H. 1972. Regional Characterizations of the Thermal Properties of Lake Ontario. In: D.V. Anderson and J.S. Seddon (Eds.), Proceedings of the 15th Conference on Great Lakes Research, pp. 625-634. Braun-Brumfield Publishers, Ann Arbor, Michigan.

McNaught, D.C. and M. Buzzard. 1973. Zooplankton Production in Lake Ontario as Influenced by Environmental Perturbations. In: First Annual Reports of the EPA/IFYGL Projects, pp. 28-70. National Environmental Research Center, Office of Research and Development, U.S. Environmental Protection Agency, Corvallis, Oregon. EPA-600/3-73-021, 336 pp.

Murphy, G.M. 1960. Ordinary, Differential Equations and Their Solutions. D. Van Nostrand Corporation, Princeton, New Jersey.

Murthy, C.R., G. Kullenberg, H. Westerberg, and K.C. Miners. 1974. Large Scale Diffusion Studies. In: International Field Year for the Great Lakes Bulletin Number 10, pp. 22-49. U.S. Department of Commerce, National Oceanic and Atmospheric Administration, Rockville, Maryland.

Newspaper Enterprise Association. 1974. The World Almanac and Book of Facts. Newspaper Enterprise Association, New York, New York.

O'Brien and Gere Engineers, Incorporated. 1971. Onondaga Lake Study. Water Quality Office, U.S. Environmental Protection Agency, Washington, D.C. 11060 FAE 04/71, 460 pp.

Paasche, E. 1973. Silicon and the Ecology of Marine Plankton Diatoms. I. *Thalassiosira pseudomona* (*Cyclotella nana*) Grown in a Chemostat With Silicate as Limiting Nutrient. Marine Biol., 19:117-126.

Patalas, K. 1969. Composition and Horizontal Distribution of Crustacean Plankton in Lake Ontario. J. Fish. Res. Bd. Canada, 26(8):2135-2164.

Phillips, D.W. and J.A.W. McCulloch. 1972. The Climate of the Great Lakes Basin. Climatological Study Number 20, Environment Canada, Toronto, Ontario, Canada.

Platt, T. and B. Irwin. 1973. Preliminary Productivity Measurements in St. Margaret's Bay. Technical Report Number 203. Fisheries Research Board of Canada, Ontario, Canada.

Porter, K.G. 1973. Selective Grazing and Differential Digestion of Algae by Zooplankton. Nature, 244(5412)179-180.

Richards, T.L. and P. Lowen. 1965. A Preliminary Investigation of Solar Radiation Over the Great Lakes as Compared to Adjacent Land Areas. In: Proceedings of the 8th Conference on Great Lakes Research, pp. 278-282. Braun-Brumfield Publishers, Ann Arbor, Michigan.

Riley, G.A.; H. Stommel, and D.F. Bumpus. 1949. Quantitative Ecology of the Plankton of the Western North Atlantic. Bull. Bingham Oceanogr. Coll., 12(3):1-169.

Rodgers, G.K. and G.K. Sato. 1971. Energy Budget for Lake Ontario. Canadian Meteorological Research Report, Atmospheric Environment Service, Ontario, Canada.

Shapiro, N. 1962. Analysis by Migration in the Presence of Chemical Reaction. Report Number P-2596, Rand Corporation, Santa Monica, California.

Shapley, M. and L. Cutler. 1970. Rand's Chemical Composition Program: A Manual. Report Number R-495-PR, Rand Corporation, Santa Monica, California.

Simons, T.J. 1971. Development of Numerical Models of Lake Ontario. In: D.V. Anderson and J.S. Seddon (Eds.), Proceedings of the 14th Conference on Great Lakes Research, pp. 654-669. Braun-Brumfield Publishers, Ann Arbor, Michigan.

Simons, T.J. 1972. Development of Numerical Models of Lake Ontario, Part 2. In: D.V. Anderson and J.S. Seddon (Eds.), Proceedings of the 15th Conference on Great Lakes Research, pp. 655-672. Braun-Brumfield Publishers, Ann Arbor, Michigan.

Simons, T.J. 1973. Development of a Three-Dimensional Numerical Model of the Great Lakes. Scientific Series Number 12. Canada Centre for Inland Waters, Burlington, Ontario, Canada. 26 pp.

Steele, J.H. 1956. Plant Production on Fladen Ground. J. Mar. Biol. Assoc., 35:1-33.

Stumm, W. and J.J. Morgan. 1970. Aquatic Chemistry. John Wiley and Sons, Incorporated, New York, New York.

Thomann, R.V., D.M. Di Toro, D.J. O'Connor, and R.P. Winfield. 1973. Mathematical Modeling of Eutrophication of Large Lakes. In: N.A. Thomas (Ed.), First Annual Report of the EPA IFYGL Projects. U.S. Environmental Protection Agency, National Environmental Research Center, Corvallis, Oregon. EPA-660/3-73-024. 336 pp.

Thomann, R.V., D.M. Di Toro, and D.J. O'Connor. 1974. Preliminary Model of Potomac Estuary Phytoplankton. J. Environ. Eng., ASCE, 100(SA3):699-715.

Trussell, R.R. and J.F. Thomas. 1971. A Discussion of the Chemical Character of Water Mixtures. J. Amer. Water Works Assoc., 63(1):49-51.

Wagman, D.C., W.H. Evans, V.B. Parker, I. Halow, S.M. Bailey, and R.H. Schumm. 1968. Selected Values of Chemical Thermodynamic Properties. Technical Note 270-3, National Bureau of Standards, Washington, D.C.

Watson, N.H.F. and G.F. Carpenter. 1974. Seasonal Abundance of Crustacean Zooplankton and Net Plankton Biomass of Lake Huron, Erie and Ontario. J. Fish. Res. Bd. Canada, 31(3):309-317.

Yentsch, C.S. 1962. Marine Plankton. In: R.A. Lewin (Ed.), Physiology and Biochemistry of Algae, pp. 771-797. Academic Press, New York, New York.

TECHNICAL REPORT DATA
(Please read Instructions on the reverse before completing)

1. REPORT NO. EPA-660/3-75-005	2.	3. RECIPIENT'S ACCESSION NO.

4. TITLE AND SUBTITLE	5. REPORT DATE
Mathematical Modeling of Phytoplankton in Lake Ontario 1. Model Development and Verification	October 1974
	6. PERFORMING ORGANIZATION CODE

7. AUTHOR(S)	8. PERFORMING ORGANIZATION REPORT NO.
Robert V. Thomann Richard P. Winfield Dominick M. DiToro Donald J. O'Connor	EPA-660/3-75-005

9. PERFORMING ORGANIZATION NAME AND ADDRESS	10. PROGRAM ELEMENT NO.
Manhattan College Environmental Engineering and Science Program Bronx, N.Y. 10471	1BA026
	11. CONTRACT/GRANT NO. R800610

12. SPONSORING AGENCY NAME AND ADDRESS	13. TYPE OF REPORT AND PERIOD COVERED
U.S. Environmental Protection Agency National Environmental Research Center Grosse Ile Laboratory 9311 Groh Rd., Grosse Ile, Michigan 48138	Final, Part 1
	14. SPONSORING AGENCY CODE

15. SUPPLEMENTARY NOTES

16. ABSTRACT

The basic mathematical structure for describing the dynamics of phytoplankton in Lake Ontario is presented in this report. Data on chlorophyll and principle nutrients are reviewed and summarized and the mathematical modeling strategy is detailed. The modeling strategy begins with the construction of a horizontally completely mixed lake with vertical layers, LAKE 1. This spatially simplified model is used to develop the interactions and kinetic behavior of the various components of each subsystem. A more detailed 3-dimensional model is then used to describe open lake and near shore variations in phytoplankton biomass. Ten biological and chemical variables are used in both models and include four trophic levels above the phytoplankton, chlorophyll a as a measure of phytoplankton biomass two phosphorus components and three nitrogen components. Under reasonable sets of model parameters as reported in the literature, the Lake 1 model output compared favorably with observed data on the dependent variables. Spring growth and peak chlorophyll concentrations are related primarily to increasing light and temperature. The model indicates that growth ceases due to phosphorus limitation. The results to date indicate that the mathematical model of phytoplankton in Lake Ontario as developed herein is a reasonable first approximation to observed data. As such, the model can form a basis for preliminary estimates of the effects of nutrient reduction programs on Lake Ontario.

17.	KEY WORDS AND DOCUMENT ANALYSIS		
a. DESCRIPTORS	b. IDENTIFIERS/OPEN ENDED TERMS	c. COSATI Field/Group	
Mathematical Models, Computer Models, Eutrophication, Water Quality, Nutrients Cycling Nutrients, Dispersion, Mass Transfer, Simulation Analysis	Great Lakes, Lake Ontario		

18. DISTRIBUTION STATEMENT	19. SECURITY CLASS *(This Report)*	21. NO. OF PAGES
	20. SECURITY CLASS *(This page)*	22. PRICE

EPA Form 2220-1 (9-73)

☆ U. S. GOVERNMENT PRINTING OFFICE: 1975—698-182/III REGION 10